TÉCNICO LISBOA

Estimation of exclusion regions in LTE base stations co-located with GSM/UMTS

Marco Gonçalo da Cruz Antunes

Dissertation submitted for obtaining the degree of
Master in Electrical and Computer Engineering

Jury

President: Prof. Fernando Duarte Nunes
Supervisor: Prof. Luís Manuel de Jesus Sousa Correia
Co-Supervisor: Mr. Pompeu João Almeida Leão Ferraz da Costa
Members: Prof. Custódio José de Oliveira Peixeiro

October 2012

To Joana, my parents, brother and sister.

Acknowledgements

In the first place, I would like to express my deep gratitude to Professor Luís Correia for giving me the opportunity to write this thesis, and for the constant knowledge sharing and advising. Without his support, orientation, experience, discipline, patience, guidelines and opinion, this work would not have been possible. A great thank you for all.

To Optimus, especially to Pompeu Costa, for all technical support and for his precious time to answer all my doubts. His contribution has been very helpful to improve this work.

To all GROW members, for the opinions and suggestions given during the presentations performed, as well as for opportunity to learn more about telecommunications during GROWing meetings. In particular, I want to thank to Daniel Sebastião, who always showed his availability when I requested his help.

A special thanks to Professor Custódio Peixeiro, for his availability and for the information supplied, which allowed me to better understand some antenna concepts.

I want to express my gratitude to my IST friends, especially to André Grilo, Bruno Marta, Bruno Ribeiro, Diogo Lucas, Joana Rosa, João Gomes, João Sousa, Martim Camacho and Tiago Oliveira. I want to thank them for the friendship, good company, and help throughout my academic journey. I also want like to thank Duarte Gameiro and Pedro Silva for all their contributions, which were important in the final phase of this work.

To a unique person, Joana Grande, I would like to thank for her love, care, support, patience, friendship, and all the motivational words and advices when everything seemed impossible.

Finally, to the persons responsible for who I am, I would like to thank to my parents, my brother and my sister for their unconditional and constant support, encouragement, belief and everything that they have done for me.

Abstract

This work aims to develop an exclusion region estimation model for base station antennas with co-location of GSM, UMTS and LTE mobile communication systems. A model for estimating the electromagnetic field as a function of the distance to the base station antenna was developed, using the far-field and gain-based theoretical models. The model allows estimating the exclusion region in the direction of maximum radiation, considering that the antennas are fully loaded in a worst case perspective; the cylindrical exclusion region model is used for other propagation directions. Possible scenarios of co-located antennas are analysed, before and after the installation of LTE base stations, these scenarios being related to typical installation infrastructures. For the typical urban scenarios, the maximum difference between the estimated exclusion region after and before the LTE implementation is equal to 73%, while it is 53% in rural environments. In the indoor case, the maximum result is 66 cm for an omnidirectional antenna with MIMO. It is concluded that the developed model overestimates the real value of an exclusion region, always considering the worst-case perspective of exposure to electromagnetic radiation.

Keywords

Electromagnetic field, Antenna, Exclusion Region, GSM, UMTS, LTE.

Resumo

Este trabalho tem como objetivo desenvolver um modelo de estimação das regiões de exclusão de antenas de estações base com co-localização dos sistemas de comunicações móveis GSM, UMTS e LTE. Para esse efeito, um modelo de estimação do campo eletromagnético em função da distância à antena da estação base foi desenvolvido, recorrendo aos modelos teóricos do campo na zona distante e *gain-based*. O modelo permite estimar a região de exclusão na direção da máxima radiação, considerando que as antenas estão em carga máxima, numa perspetiva do pior caso; para as outras direções de propagação utiliza-se a abordagem do modelo da região de exclusão cilíndrica. Os cenários prováveis de antenas co-localizadas são analisados, antes e depois da instalação das estações base LTE, e estes cenários são relacionados com as infraestruturas de instalação típicas. Para os cenários urbanos típicos, a diferença máxima entre a região de exclusão estimada antes e após a implementação do LTE é igual a 73%, enquanto que para o ambiente rural é de 53%. No caso de ambientes indoor, o resultado máximo obtido é 66 cm para uma antena ominidirecional com MIMO. Conclui-se que o modelo desenvolvido sobrestima o real valor da região da exclusão, considerando sempre a perspetiva de pior caso em termos de exposição à radiação eletromagnética.

Palavras-chave

Campo Eletromagnético, Antena, Região de Exclusão, GSM, UMTS, LTE.

Table of Contents

List of Figures

List of Tables

List of Acronyms

1G	First-Generation mobile systems
2G	Second-generation mobile systems
3G	Third-generation mobile systems
3GPP	Third-generation Partnership Project
4G	Fourth-generation mobile systems
ANACOM	*Autoridade Nacional de Comunicações*
ARPA	Agenzia Regionale Prevenzione e Ambiente dell'Emilia-Romagna
BS	Base Station
BSS	Base Station Subsystem
CDMA	Code Division Multiple Access
CENELEC	European Committee for Electrotechnical Standardisation
CEPT	European Conference of Postal and Telecommunications Administrations
CF	Correction factor
CP	Cyclic prefix
DL	DownLink
DS-CDMA	Direct-Sequence Code Division Multiple Access
EC	European Council
ECC	Electronic Communications Committee
EDGE	Enhanced Data rates for GSM Evolution
EIRP	Equivalent Isotropic Radiated Power
EM	Electromagnetic
EMF	Electromagnetic Field
ETSI	European Telecommunications Standards Institute
E-UTRA	Evolved Universal Terrestrial Radio Access
E-UTRAN	Evolved Universal Terrestrial Radio Access Network
FDD	Frequency Division Duplex
FDMA	Frequency Division Multiple Access
FDTD	Finite-difference time-domain
FFT	Fast Fourier Transform
GSM	Global Systems for Mobile Communications
H	Horizontal

HSDPA	High Speed Downlink Packet Access
HSPA	High Speed Packet Access
HSUPA	High Speed Uplink Packet Access
ICNIRP	International Commission on Non-Ionising Radiation Protection
IEEE	Institute of Electrical and Electronics Engineers
IEGMP	Independent Expert Group on Mobile Phones
IFFT	Inverse Fast Fourier Transform
LTE	Long Term Evolution
LTE800	Long Term Evolution system in the 800 MHz band
LTE1800	Long Term Evolution system in the 1800 MHz band
LTE2600	Long Term Evolution system in the 2600 MHz band
MIMO	Multiple Input Multiple Output
monIT	Electromagnetic Radiation Monitoring in Mobile Communications
MT	Mobile Terminal
NRPB	National Radiological Protection Board
OFDMA	Orthogonal Frequency Division Multiple Access
Omni	Omnidirectional
PA	Power Amplifier
PN	PseudoNoise
PRAT	Rated Output Power
RB	Resource Block
RE	Resource Element
RF	Radio Frequency
RMS	Root-Mean-Square
RMSE	Root-Mean-Square Error
Rx	Receiver
SAR	Specific Absorption Rate
SC-FDMA	Single Carrier Frequency Division Multiple Access
SMS	Short Message Service
TDD	Time Division Duplex
TDMA	Time Division Multiple Access
TRX	Transceiver
TTI	Transmission Time Interval
Tx	Transmitter
UK	United Kingdom
UL	UpLink
UMTS	Universal Mobile Telecommunications Systems
V	Vertical
VoIP	Voice over IP
W	With

W/O	Without
WCDMA	Wideband Code Division Multiple Access
WHO	World Health Organisation

List of Symbols

Δ_{da}	Spacing between elements of the array antenna normalised to the wavelength
Δ_{sp}	Length between samples (sampling interval)
Δ_{max}	Largest difference of the values between $E_{fit}(d)$ and $\lvert E(d) \rvert$
ε_r	Dielectric constant of the substrate
ε_{ref}	Effective dielectric constant
θ_{dt}	Downtilt angle
θ_i	Elevation angle of the i-th element of the array antenna
ψ_i	Associated phase shift of the i-th element of the array antenna
ϕ_i	Azimuth angle of the i-th element of the array antenna
ΔL	Extension of the patch length due to fringing effects
θ	Elevation angle
λ	Wavelength of the electromagnetic wave
σ_{GSM}	Standard deviation of the measurement point in GSM
σ_{LTE}	Standard deviation of the measurement point in LTE
σ_{UMTS}	Standard deviation of the measurement point in UMTS
ϕ	Azimuth angle
A	Polynomial coefficient of the term d^{-2}
A'	Polynomial coefficient of the term d^{-2}
B	Polynomial coefficient of the term d^{-1}
B'	Polynomial coefficient of the term d^{-1}
B_m	Magnetic flux density
C	Polynomial coefficient of the term d^{-0}
C'	Polynomial coefficient of the term d^{-0}
D	Largest geometrical dimension of the antenna
d	Distance from the antenna to observation point
d_a	Spacing between elements of the array antenna
D_{back}	Back border of an exclusion zone
D_{bottom}	Border for the bottom of an exclusion zone
$D_{bottom}{}'$	Bottom border of the exclusion zone when it is used antenna tilt.
D_{front}	Front border of an exclusion zone
D'_{front}	Front border of the exclusion zone when it is used antenna tilt.

d_i	Distance from the i-th antenna element to the observation point
D_{max}	Maximum distance of an exclusion zone
d_{max}	Upper bound for the range simulation
d_{min}	Lower bound for the range simulation
d_{Pa}	Abscissa ordinate of point P_a
D_{side}	Side border of an exclusion zone
D_{top}	Border for the top of an exclusion zone
$D_{top}{}'$	Top border of the exclusion zone when it is used antenna tilt.
E	Electric field strength
E_θ	Transverse component of the electric field
E_ϕ	Longitudinal component of the electric field
$E\ d,\theta,\phi$	Root-Mean-Square electric field
$E_{fit}(d)$	Interpolation function of the maxima points of $\lvert E(d)\rvert$
E_i	Electric field strength at frequency i
E_r	Radial component of the electric field
$E_{ref,i}$	Electric field reference level from ICNIRP guidelines at frequency i
$E_{upper}\ d$	Upper bound of the electric field $E\ d$
f	Frequency
$f_p\ d$	Polynomial function
G	Antenna gain
$G\ \theta,\phi$	Antenna gain in function of θ,ϕ
G_{el}	Array element gain in the direction of maximum radiation
$G_{el}\ \theta_i,\phi_i$	Generalised gain of the i-th array element
H	Magnetic field strength
h	Thickness of the substrate
h_a	Downtilt influence in the height
h_{ant}	Antenna height
h_{el}	Height of the array element
H_j	Magnetic field strength at frequency j
h_{min}	Base Station minimum height to ensure acceptable levels of exposure
$H_{ref,j}$	Magnetic field reference level from ICNIRP guidelines at frequency j
I_o	Maximum electric current that crosses the monopole
k	Propagation constant
L	Patch length of the microstrip antenna
l	Length of the monopole
L_{ef}	Effective length of the patch
$L_{el,i}$	Length from the midpoint of the array antenna to the center of the i-th element
N_c	Carrier number

$N_{M,i}$	MIMO antennas number of the BS in the communication system i
$N_{c,GSM1800}$	Carrier number of GSM1800
$N_{c,GSM900}$	Carrier number of GSM900
$N_{c,i}$	Carrier number of the communication system i
$N_{c,UMTS}$	Carrier number of UMTS
N_{el}	Number of elements of the collinear array antenna
N_s	Number of communication systems installed in the site
N_{sp}	Number of samples
P_a	Interpolation point of the near-field model
P_b	Interpolation point of the far-field model
P_{el}	Element input power of a collinear and uniform array antenna
$P_{in\ i}$	Input power to the i-th unit element of the array antenna
P_{in}	Input power of the antenna
$power\ ratio_i$	Power ratio of the i mobile system
$R\ d$	Exposure function
R_{in}	Input resistance of the antenna
$RMSE_{max}$	Maximum permissible RMSE for the interpolation function
S	Power density
$S_{far}(d)$	Power density using the far-field model
$S_i(d)$	Power density at frequency i as a function of the distance
$S_{nupper}(d)$	Upper bound of the $S\ d$ in the near-field model
$S_{ref,i}$	Power density reference level from ICNIRP guidelines at frequency i.
$S_{total,i}$	Power density of the system i obtained with the global model
S_{total}	Global model of the radiated field levels
TM_{010}^{x}	Transverse Magnetic mode 010
$\boldsymbol{u}(\theta_i, \phi_i)$	Co-polar vector of the i-th element of the array antenna
V_o	Voltage across the microstrip slot
W	Patch width of the microstrip antenna
y_o	Physical notch introduced by inset feed
Z_0	Free space characteristic impedance

List of Software

Adobe Photoshop ©

Matlab ©

Microsoft Excel ©

Microsoft Word ©

Microsoft Powerpoint ©

Narda SRM – Tools ©

Chapter 1

Introduction

This chapter gives a brief overview of the work performed. The scope and the motivations of the thesis are presented. At the end of the chapter, the layout of the work is presented.

.

1.1 Overview and Motivation

The need for communication and mobility has always followed our society. From the conjunction of these two factors appear solutions of wireless systems that are crucial to realize bidirectional communications and also to access information anytime and anywhere. Although the industry had consciousness of this reality, the mobile communication systems only experienced a revolution of number of subscribers with the introduction of second-generation (2G) systems. The fast growth of this segment was achieved by the constant evolution of products and standards, following the trends and the growing desires of the customers. It was precisely the use of different technologies for different countries and high prices of Mobile Terminals (MT) that doomed the popularity of First Generation (1G) Systems. Nowadays, the cellular technology is an indispensable tool in the business world, but also for the general public as an interface for personal/social interaction with other users and as an access point of entertainment contents.

The implementation of 2G systems allowed changing the analogue to digital transmission, providing the necessary spectral efficiency according to the expectations of the operators. The European Telecommunications Standards Institute (ETSI) was responsible for developing the 2G cellular standard that was majority adopted throughout the world: Global System for Mobile communications (GSM) [Moli11]. The publication and launch of this specification happened in the early 90s, initially designed to offer voice communications and other services of low rate, 14.4 kbps, as the popular Short Message Service (SMS) [HoTo04]. The development of GSM extensions, the 2.5th generation, were finalized in 1995, which included the introduction of General Packet Radio Service (GPRS) and the more efficient modulation of Enhanced Data rates for GSM Evolution (EDGE). The introduction of these upgrades favored increased packet data transfer rates over the air interface, nevertheless, the data-handling capabilities were still limited [Moli11].

Third-generation (3G) mobile systems were designed to provide the high bit-rate services that enable high-quality images and video to be transmitted and received, and to provide access to the Web with higher data rates, following the growing popularity of the Internet [Hoto07]. One of the 3G systems is the Universal Mobile Telecommunication System (UMTS), with its first version, Release 99, presented by the 3rd Generation Partnership Project (3GPP) in 1999. UMTS provided initially a data rate up to 384 kbps for the Downlink (DL) and Uplink (UL), despite a theoretical bit rate up to 2 Mbps. In 2002, the 3GPP launched important evolution steps on top of Release 99, called Release 5, introducing the High Speed Downlink Packet Access (HSDPA), deployed on top existing networks and minimising equipment upgrade, with a peak data rate of 14.4 Mbps. UL packet-data enhancements were presented in Release 6, also known as High Speed Uplink Packet Access (HSUPA), with data rates up to 5.7 Mbps [HoTo06]. The set of HSDPA and HSUPA updates are referred to as High-Speed Packet Access (HSPA), with attractive features for Voice over IP (VoIP) and other packet-based applications that require low latency.

In 2004, the 3GPP started to develop the fourth-generation (4G) system, called Long Term Evolution (LTE), in parallel with solutions for HSPA evolution (Release 7 and 8), since it was predicted that the spectral efficiencies and data rates of 3G technology would not meet the demand of future applications. In fact, mobile data traffic has increased exponentially, being expected to increase 30 times between 2011 and 2015 [Vile12]. LTE specifications propose a complete change in both the core network and the air interface, supporting new major features to increase its performance and capability, such as Multiple Input Multiple Output (MIMO) antenna technology. This new standard provides peak data rates of 100 Mbps in DL and 50 Mbps in UL with a 20 MHz spectrum allocation for each of the DL and UL. Release 10 admits data rates up to 1Gbps, known as LTE-Advanced [Moli11].

The contents and services, which until then had been confined to the use of the fixed network, are gaining a new breath with its access from mobile devices due to this increasing technological evolution. The general public concern about potential health risks caused by radiation from mobile communication systems is motivated by its popularity and this technological evolution, accompanied by the increase of terminals and Base Station (BS) antennas. BSs are installed in increasingly smaller cells, and thus closer to the general public, alerting people to their existence.

The concern in investigating the impact that electromagnetic (EM) radiation causes in living tissues started in other sectors, such as military radar systems in World War II or the emergence of the first high-voltage lines. The study of different knowledge areas, such as physics, biology, medicine and engineering, are crucial to establish the limits of the electromagnetic field (EMF) strength above which may cause adverse effects to health. Several international organizations and entities were responsible for the advances in this area, working on recommendations for radiation exposure limits from the quantification of the thermal effects [OlCa02]. However this topic continues to generate a great deal of controversy regarding the non-thermal effects of EM radiation. Over the past years, studies with contradictory results were published, where many deficiencies were found in these works, as regards the number of insufficient samples or results that are not replicated in real environments [ICNI98], [COST00], [WoHO02], [ICNI11].

Measurements or estimation of the field intensity may be performed to verify if the EMF levels around a BS are in accordance with the recommended limits. Another useful quantity is the exclusion region, which is defined as the zone around antennas or BSs where the limits of radiation exposure may be exceeded inside it. The exclusion regions are suitable for defining physical barriers in areas of public access, protecting the public from potentially dangerous levels of radiation. In Figure 1.1, the exclusion region is represented as one imaginary semi sphere limited by physical barriers and adequate signage, since the public has access to this area.

Operators usually know the exclusion regions, and defined the physical barriers necessary for BSs with 2G and 3G systems. LTE antennas tend to be placed/replaced in existing BSs, since this scenario simplifies the network and is more financially favourable. With the introduction of more radiation sources in the same infrastructure of installation of GSM and UMTS antennas, EM levels will be changed and consequently the existing exclusion region and physical barriers may no longer be applicable.

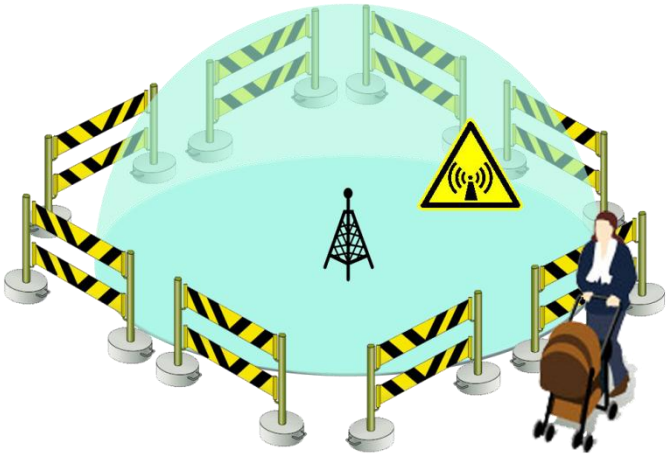

Figure 1.1 - Exclusion region limited by physical barriers.

This work has the objective to estimate the impact on exclusion regions after the implementation of LTE, and to verify in which situations the exclusion regions suffer significant changes, being necessary to define new physical barriers. Knowledge of the radiated EMF by the antenna and the analysis of the environment around the BS are required in the evaluation/establishment of limits for EM exposure and estimation of the exclusion regions. Therefore, in the vicinity of a BS antenna, the level of exposure to EM radiation is associated the antenna characteristics that describe its performance. The infrastructure that supports the antenna also influences the EMF, since it is chosen according to the requirements for coverage and capacity, and also in accordance to the restrictions imposed by the environment surrounding the BS.

Several works on EM exposure assessment or estimation of exclusion regions can be found in the literature. The far-field or the far-field approximation models are a simple way for exclusion region estimation, but they always over-predict the real value of exposure levels and the exclusion region is usually smaller than the validity distance of these models [CENE02], [OFRC05], [MFRL02], [MNMV02]. Martínez-González et al. [MFRL02] defined also basic rules for the exclusion region estimation for different directions of the maximum radiation direction, considering a cylindrical exclusion region around the radiation sources. In [BiGi99] and [ABDK02], accurate models in the areas close to the antenna were published, though its complexity is greater than the far-field models and are applicable only to panel antennas.

Hybrid models, such as those described in [BCFF99], [BCDF02], and [Sche43], can use various propagation models and allow estimating the radiation levels taking into account the effect of the surrounding environment. Moreover, these algorithms make use of ray tracing techniques, therefore being significantly more complex, but on the other hand are more accurate in areas near the antenna. In [Oliv06], an approach to exclusion region estimation is presented, considering the EM influence of the installation structures of the BS antennas.

1.2 Structure of the Dissertation

This work is composed of 5 Chapters, followed by a set of annexes.

Chapter 2 starts by presenting the radio interface of the mobile communication systems, concerning the techniques of multiple access, BS output powers and frequency bands. Following this, the EMF behaviour, as well as the description of the relevant parameters that influence the antenna performance is presented. Then, a classification of BS installations is studied according to its characteristics. The EM exposure is presented, by examining the reference levels and guidelines for EMF assessment and measurement established by several international entities. Finally, the estimation models of the EMF levels and the exclusion regions are described.

All issues related to the implementation of the models can be found in Chapter 3. At the beginning, the assumptions regarding typical BS antennas and their installations are presented, since they influence the development of the model. The theoretical models in the EMF estimation used in this work are described, concerning far-field and the gain-based models. Then, the development of the estimation model of the EMF radiation levels at any distance to the antenna is presented, by considering three possible scenarios: outdoor array antennas, omnidirectional (monopole element) and sectorial (microstrip element) indoor antennas. Finally, these models are developed to estimate the exclusion region of a BS antenna in the direction of maximum radiation (the frontal border), presenting also a practical approach to determine all exclusion region dimensions from the frontal border of the exclusion region. A detailed description of the different program modules is also given, as well as the discussion of the assessment of the program.

In Chapter 4, the analysis scenarios are identified, according to characteristics of the typical BS antennas. The studied scenarios take into account the site before and after the introduction of LTE, in order to verify the changes undergone by the exclusion region. The model results for the exclusion region are analysed for each scenario, and a set of simulations is discussed in order to understand the dependence of the exclusion region with the variation of some model parameters. The power contribution that each mobile communication system triggers over EM exposure, and the analysis of the need for change/install physical barriers of EM protection, are also analysed. The chapter ends with the presentation and analysis of the measurements performed.

The Chapter 5 finalizes this thesis, drawing conclusions and suggestions for future work. A set of annexes with auxiliary information and results is also included. Annex A presents the technical characteristics of used BS antennas in this work, while the simulation parameters resulting from EMF estimation for each of these antennas are provided in Annex B. The additional information that supports the study results is shown in Annex C. The model results in the direction of maximum radiation are presented in Annex D, and the results for other radiation directions are described in Annex E. Finally, the Annex F presents the measurement data and characteristics of the analysed BSs and the surrounding environment.

Chapter 2

Fundamental Concepts

This chapter provides an overview of the GSM, UMTS and LTE, on the radio interface. Antenna performance, the basic aspects of coverage, and a classification of BS installations are also discussed. Then, the reference levels and guidelines for EMF assessment and measurement established by international entities are presented. Afterwards, the EMF estimation models around antennas are studied, by analysing also the methodologies of exclusion region estimation adopted by other entities.

2.1 Radio Interface

The basic concepts of radio interface are presented in this section concerning GSM [Moli11], the UMTS [HoTo04], [WaSe03], as well as the LTE [3GPP09a], [HoTo09], namely techniques of multiple access, duplex, BS output powers, and bands of frequency assigned to each system.

2.1.1 Global Systems for Mobile Communications

Frequency Division Duplex (FDD) is used as duplex procedure in GSM. In the first GSM version, the band assigned to UL was [870,915] MHz and to DL [935,960] MHz. The 1800 MHz band uses [1710, 1785] MHz for UL and [1805, 1880] MHz for DL.

GSM employs a Frequency Division Multiple Access (FDMA) combination with Time Division Multiple Access (TDMA) for multiple access. FDMA is characterised by dividing the frequency range of UL and DL sub-bands in a channels with a bandwidth of 200 kHz. To obtain a biggest capacity of users, TDMA is used for multiple access in each sub-band: due to the timeslot structure, a 200 kHz channel supports 8 TDMA's conversation channels, each time slots with 576.92 μs. Timeslots in the UL are shifted by 3 timeslots from the DL ones for simplifying the transmitter and receiver's duplex design.

The GSM standard defines 8 classes for the BS Transmitter maximum output power measured at the input of the BS Subsystem (BSS) Transmission (Tx) combiner. For the micro-BS, the maximum output power per carrier is measured at the antenna connector after all stages of combining. The range of these values are presented in Table 2.1. The typical values for MT nominal maximum output power are in between [22, 39] dBm [ETSI00]. Note that GSM, as well the recent systems, performs power control in the BS and the MT so that the transmitted power is not always the maximum one, but only the necessary level for the desired quality in transmission.

Table 2.1 - GSM Base Station maximum output power classes [ETSI00].

GSM BS maximum output power [dBm]		
Macro-cell	**Micro-cell**	**Pico-cell**
[34,58]	[9,32]	[13 23]

2.1.2 Universal Mobile Telecommunications Systems

The air interface technology used by UMTS, Wideband Code Division Multiple Access (WCDMA), is a wideband Direct-Sequence Code Division Multiple Access (DS-CDMA) system that spreads the

spectrum of the transmitted signal of user data by a chips sequence derived from CDMA spreading codes (PN binary-value sequence). The codes are orthogonal to each other to reduce interference between users. However, with the increasing number of users in the same band, the quality of the channel decreases. This is due to the limited orthogonal code numbers and the influence of signal propagation with the increase of users, enlarging the interference between users. WCDMA has two operation modes: FDD and Time Division Duplex (TDD). Nowadays the TDD mode is not used, and only the FDD mode is implemented.

In Portugal, as well as in the rest of Europe and Japan, UMTS-FDD uses frequencies in [1920, 1980] MHz for UL and [2110, 2170] for DL. The chip rate of 3.84 Mcps provides a regular carrier spacing of 5 MHz, with a bandwidth of 4.4 MHz. The network operator can implement a carrier spacing for any multiple of 200 kHz to increase capacity. UMTS supports highly variable data rates, although user data rate is kept constant during each frame for 10 ms, and the each user's data rate can change from frame to frame. UMTS has typical values for the BS transmitter maximum output power, Table 2.2. Typical values for the MT nominal maximum output power range in [21, 33] dBm [ETSI06].

Table 2.2 - UMTS Base Station maximum output power [Bena02], [Opti12].

UMTS BS maximum output power [dBm]	
Macro-cell	**Micro-cell**
[40,46]	[30,33]

2.1.3 Long Term Evolution

In LTE, the radio interface is described in both frequency and time domains, thus, the resources are assigned in a flexible manner to users, and different users can have different data rates. Regarding the time domain, the structure defines frames, slots and symbols. There are two frame structure types: type 1 uses FDD/TDD, whereas type 2 uses TDD mode. This thesis only considers type 1, because this structure is optimised to co-exist with UMTS.

ETSI and 3GPP specified together frequency bands that can be allocated to fourth-generation systems: 17 bands for the FDD mode, and 7 bands for the TDD one. In Europe, it is foreseen that some operators will migrate from GSM to LTE, for the FDD mode, assigning the bands [880, 915] MHz to UL and [925, 960] MHz to DL; [1710, 1785] MHz (UL) and [1805, 1880] MHz (DL). It is also foreseen that LTE operation in the FDD mode in Europe will use the bands [815, 830] MHz (UL) and [860, 875] MHz (DL), [1920, 1980] MHz (UL) and [2110, 2170] MHz (DL), [2500, 2570] MHz (UL) and [2620, 2690] MHz (DL).

In Portugal, the regulatory authority for the communications sector, ANACOM, auctioned the assignment of rights of use of the bands 450 MHz, 800 MHz, 900 MHz, 1800 MHz, 2.1 GHz and 2.6

GHz. For the three winner operators were assigned a total of 60 MHz, 84 MHz and 145 MHz respectively in the bands of 800 MHz (LTE800), 1800 MHz (LTE1800) and 2.6 GHz (LTE 2600). According to the statement issued by an operator, the spectrum in the 800 MHz band ensures a better coverage in areas of lower population density, while the higher frequency bands will ensure high network capacity in urban areas [OPTI11].

The physical layer supports the following multiple access schemes: Single Carrier Frequency Division Multiple Access (SC-FDMA) on the UL, and Orthogonal Frequency Division Multiple Access (OFDMA) on the DL.

OFDMA consists of achieving the orthogonality between the different sub-carriers, therefore the transform between time and frequency domains is necessary, which is implemented with the Fast Fourier Transform (FFT) and the Inverse Fast Fourier Transform (IFFT). The sub-carriers spacing is 15 kHz independently of the total transmission bandwidth. LTE resorts to the concept of cyclic prefix (CP) to combat inter-symbol interference and reduce the complexity of the equaliser. The CP is the final part copy of the symbol which is copied and attached to the beginning of the symbol. The biggest time unit used for transmitting information is a 10 ms frame that is divided into 20 slots of 0.5 ms, and the smallest unit for transmission in DL is designated as Resource Element (RE), which is one symbol on one sub-carrier. To allow the access of several users to the available bandwidth, minimum units of allocation are distributed among users: Resource Blocks (RBs). For a normal CP, an RB is composed of 12 contiguous sub-carriers and 7 consecutive OFDMA symbols in the slot duration. Therefore, a RB has 84 REs (12 sub-carriers x 7 symbols) per slot in the time domain and 180 kHz (12 sub-carriers x 15 kHz sub-carriers spacing) in the frequency one. Using extended CP is analogous to the previous case, but instead of 7 OFDMA symbols in a slot, an RB has a 6 consecutive OFDMA symbols.

The amplification techniques used in OFDMA systems cause an excessive energy consumption, which makes its use difficult in mobile terminals coming from battery constraints, essentially due to power back-off requirements. This is one of the main reasons that the SC-FDMA is used in UL. SC-FDMA signal generation is similar to OFDMA, but the information is modulated only on to one carrier, i.e., each data symbol is represented by one wide signal. The CP is also added periodically in UL. For a normal CP, in a slot there are 7 SC-FDMA symbols, whereas for extended CP there are 6 SC-FDMA symbols per slot.

The adopted packet-based transmission scheme has maximum efficiency, since there are only shared channels. The system bandwidth is scalable, with values from 1.4 up to 20 MHz, with change the parameters FFT length, sampling rates sub-carrier spacing, among others.

LTE specifies the BS maximum rated output power (PRAT), Table 2.3. PRAT is the mean power level per carrier that the manufacturer has declared to be available at the antenna connector [ETSI11a]. The Typical values for MT nominal maximum output power are in [21, 33] dBm [ETSI11b].

Table 2.3 - LTE BS maximum rated output power [ETSI11a].

Cell type		Maximum PRAT [dBm]
Macro-cell		-[1]
Micro-cell		38
Pico-cell		24
Femto-cell	**without transmit diversity or MIMO**	20
	with transmit diversity or MIMO	17

[1]There is no upper limit required for the rated output power of the Wide Area Base Station like for the base station for General Purpose application in Release 99, 4, and 5.

2.2 Base Stations

This section gives a brief interpretation of the EMF behaviour with the distance to the BS, as well as the description of the relevant parameters that influence the performance of an antenna. Finally, a study is presented concerning the classification of BS installations according to their characteristics, based on [OFRC05].

2.2.1 Radiation Regions

According to the behaviour of EMF, the space surrounding an antenna may be divided into three regions: reactive near-field, radiating near-field (or Fresnel), and far-field (or Fraunhofer) regions, Figure 2.1. Although the boundaries between regions are established, abrupt changes do not occur in the field configurations when these boundaries are crossed. These limits are not unique, using various criteria to establish its value, in accordance with the perspective and tolerance necessary for the project [Bala05], [Capp01].

The expressions that delimit these regions suggested by [CENE02] are the following:

- Reactive near-field region: $d \leq \lambda/4$;
- Radiating near-field region: $\lambda/4 < d \leq 2D^2/\lambda$;
- Far-field region: $d > 2D^2/\lambda$;

where:

- d: Distance from the antenna to the point of investigation;
- λ: Wavelength of the EM wave;
- D: Largest dimension of the antenna.

The reactive near-field region is the region closest to the transmitting antenna; the reactive characteristic of the field is predominant with a field decay of d^{-3} [Bala05], where a certain amount of

oscillating energy flow is trapped near the antenna due to the reflector effect of the imaginary surface of this field region [Krau88].

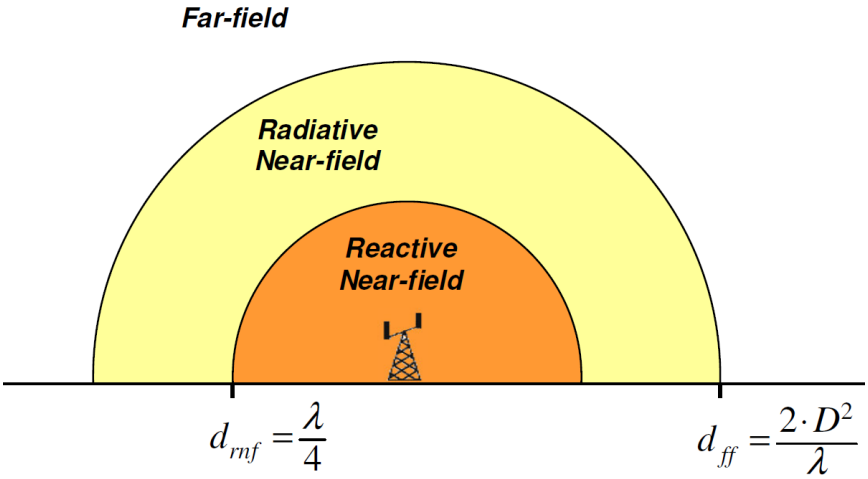

Figure 2.1 - Boundary regions of the radiation fields existing around an antenna [OFRC05].

In the radiating near-field region, also entitled Fresnel region, radiation fields are predominant with a field decay of d^{-2}. The radial field component may be significant and the angular distribution of the field depends on the distance from the antenna. In this region, the shape of the field pattern is a function of the radial distance for most antennas. The radiating near-field region may not exist if the maximum dimension of the antenna is not larger than the wavelength [Bala05].

The Far-field region is sometimes referred to as the Fraunhofer region, where the plane-wave model is a good approximation, the measurable field components being transverse to the radial direction from the antenna and all energy flow being directed radially outward [Krau88]. In the expressions that describe the field, the dominant term is d^{-1}. The field pattern of the antenna in this region is independent of the radial distance.

The field strength in this region may be described by simple expressions from Maxwell's equations, in which the Magnetic (H) and the Electric (E) field strength may be related by the characteristic impedance of free space (120π) or by Power density (S) [Chen89]. Thus, it is necessary to make only a measurement to know the two components of the EM fields, E and H. For the radiating near-field region, E- and H-field measurements are directly interrelated by the free space characteristic impedance, while in reactive near-field region, electric and magnetic fields should be separately estimated to determine the field impedance and power density [OFRC05].

2.2.2 Coverage Types

Most of the main antenna characteristics can be taken from the antenna radiation pattern, which is a graphical representation of the spatial distribution of field's strength (or the power) as a function of

space coordinates. The important characteristics that can be taken are bandwidths, power flux density, phase, directivity, radiation intensity, polarisation, among others [Bala05]. Manufacturers of antennas usually provide only the vertical and the horizontal planes of the radiation pattern.

In the structure of an antenna pattern, the major lobe is the part of energy radiated in direction of maximum radiation, typically being the desired direction for communication [Krau88]. There are also a series of lobes smaller than the main one, the minor lobes, which should be minimised since they represent radiation in undesired directions [Bala05]. As the radiation pattern is often determined in the far field region, changes may occur when analysed outside this region. The radiation pattern begins to smooth and form lobes when the distance between the antenna and the observation point decreases [Bala05]. The infrastructure where the antenna is installed can also influence the radiation pattern [OFRC05].

BS antennas may be divided into two types: omnidirectional (Omni) and sectorial antennas. The omnidirectional antennas radiate horizontally in every direction, while sectorial ones are directional antennas with a sector-shaped radiation pattern, Figure 2.2. These antennas allow the reduction of interference and its transmitted power is many times stronger in the intended directions compared to an Omni antenna, being ideal to cover high traffic density areas. In the vertical direction, the antenna lobe tends to be fairly narrow, using the downward tilt for greater area coverage, [BFHM02].

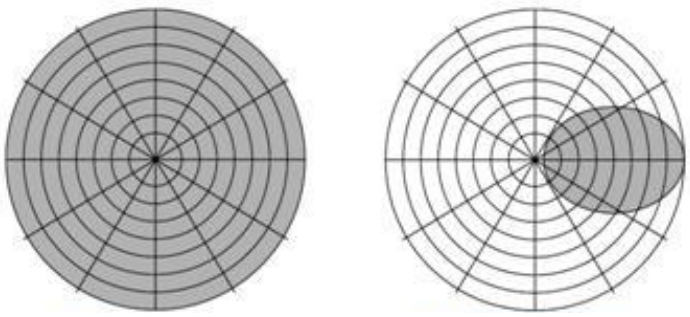

(a) Omni antenna. (b) Sectorial antenna.

Figure 2.2 - Omnidirectional and Sectorial antenna radiation patterns based on [BFHM02].

Directivity is another parameter that can be obtained from the analysis of the antenna radiation pattern. The gain of the antenna is closely related to the directivity, being an important measure of the performance of an antenna, since it indicates how efficiently the antenna converts the power available at its input terminals to radiated power, taking its directional capabilities into account [StuT98]. In Table 2.4, typical gain values used in mobile communication systems and for typical bands used in Portugal are presented, in accordance to [Andr12], [Allg12], [JAYB12] and [KATH12a]. For LTE, the values of the gain are only shown in the bands of 800 and 2600 MHz, because these bands are the assigned in Portugal.

The polarisation of an antenna is an important property, since it describes the orientation of the

electric field of the wave radiated by the antenna in a given direction of propagation. The direction of interest is typically the one with maximum gain, in which the polarisation is determined in the far-field region, where plane wave behaviour exists [StuT98]. The polarisation may be classified as linear, circular or elliptical. In cellular communications, the antennas are usually vertically or double (±45º) polarised, getting the best polarisation diversity gain results [KATH12b], [KATH12c].

Table 2.4 - Typical antenna gain values based on [Andr12], [Allg12], [JAYB12] and [KATH12a].

Gain [dBi]	Antenna type	GSM		UMTS	LTE	
		900 MHz	1800 MHz		800 MHz	2600 MHz
Indoor	Omni	[2, 7]	[2, 7]	[2,7]	[2,7]	[2,7]
	Directional	[5, 7]	[5, 7]	[5,7]	[5,7]	[5,7]
Outdoor	Omni	[2, 11]	[2, 11.8]	[2, 11.8]	[2, 11]	[2, 11]
	Directional	[5, 22]	[5, 24.2]	[2.9, 24.2]	[2.9, 19.3]	[8, 19.5]

The polarisation characteristics of an antenna remain relatively constant over its main beam, but not over its side lobes. Another important feature of an antenna polarisation is its reciprocity: an antenna responds best, with maximum output, if the incident wave has the same polarisation than receiving antenna, as regards the axial ratio, sense and spatial orientation, i.e., if there is polarisation matching [StuT98].

LTE supports MIMO, which allows significant improvements in the performance of the antenna/system. MIMO takes advantage of OFDM and multipath propagation, using multiple antennas for a single user, providing higher data rate, and spectral efficiency improvement, since MIMO does not consume extra radio frequency [Moli11]. From the viewpoint of EM exposure, as an LTE antenna can have several “MIMO elements”, these elements cause an additional increase in the levels of the radiated field.

2.2.3 Classification of Base Station Installations

The surrounding environment influences the installation of antennas in such a way that in deployment of the cellular network has to take into account the factors that influence the choice of the site and the infrastructure that supports the antenna. Some of these factors are the requirements of the coverage and capacity, interference, terrain type, rural or urban environment, building structure and existence of obstacles, among others.

For the purpose of the study of human exposure to EMF from BS antennas, it is advantageous to classify installations with the same characteristics, and to identify the typical parameters of these typologies as antenna characteristics, technologies, number of carriers and transmitter maximum

output levels. Table 2.5 presents a common classification of BS antennas installations according to the coverage range, since low traffic density areas, like rural environments, are served by large cells, while areas with high traffic density (urban environments) are covered by small ones, [OFRC05].

In [OFRC05], another classification is suggested, according to the type of infrastructure supporting the antenna and the involving environment, Table 2.6. This classification allows a more precise characterisation of each configuration, being more suited for the estimation of exclusion zones around BS antennas.

Table 2.5 - Classification of BS antennas installations according to coverage range [Oliv06].

Cell type		Coverage range	Description
Macro	**Large**	3 – 30 km	Used to serve either rural or suburban environments, where the density of BSs is small due to low traffic density; antennas are typically installed on high masts, top of high buildings or other structures, using high-radiated power levels to allow a wide coverage area. Propagation is typically over rooftops.
	Small	0.5 – 3 km	
Micro		50 – 500 m	Provide coverage in urban areas, where requirements in terms of capacity are rigorous due to high traffic demand; antennas are strategically installed in small towers, top of lower buildings or façades. Characterised by radiating medium power levels in order to satisfy the capacity demand in a restricted coverage area, and to avoid interference with neighboring cells. Propagation is typically below rooftops.
Pico		Few tens of meters	Used to increase Indoor coverage, where demand is very high; antennas are typically installed on walls and ceilings inside buildings for the coverage of small areas, requiring lower power levels.

Table 2.6 - Classification of BS antennas installations according to coverage range extracted from [OFRC05] and [Opti12].

Denomination	Cell type	Environment	Installation type	Antenna height [m]
Rtower	Macro-cell	Rural, Suburban	Tower, Mast, Water sump, “Tree”	20-50
Uroof	Micro/Macro-cell*	Urban	Roof-top	2-5**
Utower			Tower	20-40
Ufaçade	Micro-cell		Building façade	3-10
Upole			Light pole or other	3-5
Iceil	Pico-cell	In-building	Ceiling	2-3
Iwall			Walls	

** The cell type will depend on the coverage area*
*** Height from the roof top*

Regarding the number of transmitter (Tx) and receiver (Rx) antennas, in regions with a relatively low

number of users, an Omni BS is typically used, requiring one Tx/Rx antenna (or even two in case of diversity in RX) per communication system. The usual configuration of BS antennas in high traffic density areas consists of three sectors of 120º. A sector is interpreted as a cell and consists of one Tx/Rx antenna (or two diversity case) per system. For the study of human exposure to EMF, one must take into account the cumulative impact of these co-location systems, as well as the energy radiated by BS antennas of other operators that share the same installation infrastructure. The sharing of sites and infrastructures is a common practice used by operators, due to the difficulty in finding new available sites, to reduce costs and to minimize the visual impact. Due to the need for higher bit rates, cells tend to have smaller diameters and with very directional antennas.

2.3 Electromagnetic Radiation Exposure

The increasing number of users of mobile communication systems, and the consequent densification of mobile networks has caused anxiety among general public about the biological effects of radiated EMF in humans. The potential EMF effects on health are related to the levels of energy of the field source, i.e., frequency. In this section, are presented a discussion on biological effects of EMFs and an overview on the guidelines established by international entities for EMF assessment and protection against harmful radiation levels for health.

Mobile communications use part of the EM spectrum corresponding to the radio frequency (RF) band, 3 kHz to 300 GHz, i.e., non-ionising radiation. Despite the non-existence of molecular changes as the genetic effects associated with exposure of Ionising Radiation (frequency radiation above 2.4 THz), other biological effects may occur when non-ionising radiation interacts directly with living tissues. Note that the biological effect may or may not cause a potential harmful effect in the health.

Two potential types of biological effects are associated to RF: thermal and non-thermal effects. Thermal effects consist of the increase of tissue temperature resulting from the absorption of energy of the radiated field. Damage can occur if the level of heating exceeds the natural capacity of the body to dissipate this excessive energy. This short-term biological effect is well-understood and quantifiable, so it is possible to make measurements and studies aiming to determine the relation between the RF energy absorbed by all or a part of the human body and the corresponding increase of temperature. The restrictions for exposure may be established from thermal effects to ensure human safety [OFRC05].

Regarding to the non-thermal effects, in 1998, the publication of the International Commission on Non-Ionising Radiation Protection (ICNIRP) guidelines for limiting exposure to EM fields, [ICNI98], referred that the works presented in the relevant literature on human reproductive effects, tumors and cancer risk, minor reduction in heart rate or retinal damages as potential health effects associated with EM exposure, are inconclusive. The studies provided no evidence of these adverse effects, since the results are based on a small number of samples, and due to the inability to reproduce satisfactory

results of the in-vitro experiments obtained in laboratory.

Several scientific reviews and health hazard assessments in the following years have been undertaken, such as [COST00], [ICNI01] and [WoHO02], which strengthen the idea about the lack of scientific evidence of such effects, although the technology can be too recent to rule out possible long-term effects. Some scientific data suggests minor effects of mobile phone usage including disturbance on the sleeping cycle, changes in brain activity and reaction times. However, these results are quickly refused, because they appear to lie within the normal bounds of human variation. In 2004, new epidemiologic studies did not provide a consistent evidence of a causal relation between EM exposure and any harmful effect in health, due to the deficiencies presented by these works [ICNI04].

In 2009, ICNIRP published a statement on the guidelines presented in 1998, [ICNI09], where they conclude that the guidelines do not need an immediate revision and they reaffirm the lack of evidence for relationship between non-thermal effects and EM exposure. However, new scientific data of recent research programs need to be assessed with respect to possible health risks. The in vitro and animal studies are rather consistent overall and show that such effects are unlikely at low exposure levels. The analysed epidemiological studies indicate that the risk of head cancer after exposure does not increase with the use of cell phones during 10 years after the first use. Regarding the effects associated to the use of mobile phones, the review [ICNI11] presented the same conclusions, although there are few data on risk of childhood tumors or for other periods of exposure duration. Therefore, the performed researches cannot in principle prove the complete absence of any non-thermal effect, so more data are needed to overcome several gaps found in these studies.

Protection should be afforded to anyone exposed to radiation from mobile communication systems, in particular, from BS antennas, since in this case exposure is involuntary. Although RF exposure is far higher for mobile phone users than for those who are near BSs, the BSs are continuously transmitting signals [WoHO02]. International and national entities have established safety thresholds that define the maximum allowed values for the levels of the radiation exposure of the human body. Mobile operators have to comply with these restrictions, established in the respective country.

As seen previously, safety levels may be defined according to thermal effects, since these are quantifiable, being based directly on established health effects. The parameter that quantifies the radiation absorbed by the body in RF frequencies is the Specific Absorption Rate (SAR), which is the rate at which EM energy is absorbed by unit of tissue mass, being expressed in units of Watt per kilogram of exposed tissue [W/kg]. The values of SAR depend of the incident field parameters, the characteristics of the exposed body, ground effects and reflector effects. The measurement of SAR implies making measurements inside the body, so it is not an easy procedure.

Two classes of guidelines are defined: basic restrictions or safety levels, and reference thresholds [ICNI98]. Basic restrictions are established from thermal effects caused by exposure to EM radiation, using SAR as physical quantity. Reference thresholds are a practical exposure assessment, since they are specified from the basic quantities that can be easily measured outside the body, such as electric field strength (E), magnetic field strength (H), magnetic flux density (B_m), power density (S), and currents flowing through the limbs. Whenever a measured or calculated value does not exceed

the reference threshold the safety level has not been exceeded. On the other hand, it does not necessarily follow that the safety level will be exceeded if the reference threshold is exceeded. This situation requires additional measurements to verify the compliance with the safety levels.

The basic restrictions and the reference thresholds are established for two distinct population groups: occupational and general public. The occupational population is the group of adults exposed under known conditions, typically in professional situations, which are trained to be aware of potential risk and to take appropriate precautions to minimize or avoid exposure. The general public consists of individuals of all ages and of varying health status, including sensitive groups as children or elderly people. Exposure restrictions are more stringent for the general public than for the occupational one.

Most European countries, as Portugal, adopted the exposure thresholds established by the European Union Recommendation for general public [CoEU99] and occupational exposure [CoEU04], based on ICNIRP guidelines [ICNI98]. These guidelines have been developed from immediate health effects hence long-term effects are poorly assessed. These short-term effects are stimulation of peripheral nerves or muscles, shocks and burns indirectly induced in metal objects exposed to radiation, and elevated tissue temperature due to absorption of energy of the EMF exposure. The Institute of Electrical and Electronics Engineers (IEEE) also issued a recommendation [IEEE05] to prevent harmful effects due to exposure of EMFs in the frequency range from 3 kHz to 300 GHz, in which the maximum exposure limits are also based on prevention of short-term effects. The recommendation presents a basic restriction for particular areas of the body and for whole body, and maximum permissible exposure values, which are the limits derived from the basic restrictions.

For the frequency ranges of interest in this work, reference thresholds for general public are presented in Table 2.7 in accordance with ICNIRP guidelines. Basic restrictions were applied to reference thresholds for occupational exposure with the objective of obtaining reference thresholds for exposure of the general public. For the analysed frequencies, the E, H, B and S values are evaluated over the entire body, and these values must be measured, averaged over any 6-minutes period.

Table 2.7 - Reference levels for general public exposure (unperturbed RMS) [ICNI98].

Reference levels	Frequency range, f [GHz]	E [V/m]	H [A/m]	B_m [μT]	S [W/m^2]
General public exposure	0.4-2	$1.375 f_{[MHz]}^{1/2}$	$0.0037 f_{[MHz]}^{1/2}$	$0.0046 f_{[MHz]}^{1/2}$	$f_{[MHz]}/200$
	2-300	61	0.16	0.20	10

ICNIRP guidelines also establish peak power limits: for frequencies exceeding 10 MHz, the field strength should not exceed 32 times the value given in the table, or S should not exceed 1,000 times the restrictions.

In circumstances of simultaneous exposure to fields of different frequencies, these exposures are

additive in their effects, so it is possible to analyze separately each radiated exposure for different frequencies. For the relevant frequencies in this work, the following requirements should be applied to the field levels:

$$\sum_{i>400MHz}^{300GHz} \left(\frac{E_i}{E_{ref,i}}\right)^2 \leq 1 \tag{2.1}$$

and

$$\sum_{j>400MHz}^{300GHz} \left(\frac{H_j}{H_{ref,j}}\right)^2 \leq 1 \tag{2.2}$$

where:

- E_i: Electric field strength at frequency i;
- $E_{ref,i}$: Electric field reference level from ICNIRP guidelines at frequency i;
- H_i: Magnetic field strength at frequency j;
- $H_{ref,j}$: Magnetic field reference level from ICNIRP guidelines at frequency j;

2.4 Exclusion Zones

From the need to restrict public access to places where the levels of radiation can cause harmful effects to health derived to the concept of exclusion zone. It is defined as a region around radiating elements where the general public is prohibited to enter, since the reference levels may be exceeded inside it. With the aim of estimate the dimensions of the exclusion zones around BS antennas, the models to the assessment of EMF levels are described in this section. In addition, the methodologies taken by some entities for estimating exclusion zones are also presented.

In order to determine the dimensions that define an exclusion zone, the value of E, H, or S should be known in the vicinity of the BS antennas. One of the methods to obtain these electromagnetic quantities radiated by an antenna is through measurements, as shown in [CENE02] or [ECCC07]. The measure procedures has the particularity to depend on the used antennas, and consume too much time.

Complex simulations are also used to estimate the field strength by an antenna, and require a good knowledge of the software tools. Simulations also need powerful equipment and quite an extensive computation time, therefore not being effective to reach quick and precise results [OFRC05].

As an alternative to the measurement procedures and simulations, models may be used to obtain a prediction of the radiation levels. There are simple models in the literature that are very accurate, being a good way to estimate exclusion zones [OFRC05]. Next, a literature overview on these methods is presented.

As addressed in Section 2.2, the radiated EMF has a distinguished behaviour according to the distance to the antenna, and there are three EMF regions. The radiation levels of the far-field region may be estimated by a simple model, the far-field model [CENE02], which over-estimates the field strength if it is used in the radiating near-field region. It does not take into account the dimension of the antenna, and the influence of the environment is neglected. This model estimates the root-mean-square (RMS) value of S at a distance d, from the antenna to the observation point, depending on the values of the λ, input power, gain (G) and largest dimension of the antenna D.

A flexible and rigorous procedure to verify if the European Council (EC) recommendations thresholds are not exceeded in the vicinity of a BS is described in [MFRL02]. This model defines a set of simple formulas that are sufficient to estimate the exclusion zone and the S value near the BS antenna located in free-space areas, as a rural environment that has no obstacles within the exclusion zone, being valid for distances greater than $\lambda\ \ 2$. For situations like a BS in an urban environment, with many scattered objects within the exclusion zone or where two or more BSs are located on the same site, additional measurements of radiation levels should be performed.

The previous model defines the concept of exclusion zone for a BS antenna (collinear array of half-wave dipoles) as the surface of an imaginary cylinder that extends from the bottom of the lowest element to the top of the highest one. Limits for the top and the bottom of the cylindrical exclusion zone ($D_{top}$and D_{bottom}, respectively) are defined at the expense of the maximum distance of the cylindrical exclusion zone D_{max}. When a downtilt $\theta_{dt}$is used, the exclusion zone accompanies this inclination and the expressions for these dimensions suffer a correction according to the downtilt.

For a BS with several sector antennas, the total exclusion zone may be defined by the added composition of truncates sector cylinders of the individual exclusion zones, being important to define the limit for the back of the cylinder D_{back}, Figure 2.3.

The far-field approximation model described in [MNMV02] allows a good prediction of the EMF levels very close to a BS antenna, where the far-field model can be typically over-estimated for these values. The results are presented in the finite-difference time-domain (FDTD) being compared to simple expressions based on cylindrical and far-field approximations for the determination of the exclusion zones. The approximate average value expression near the array formulated by the model is valid for $d \geq\ D^2\ \ 4\lambda$.

Although this model is applicable to a smaller distance from the antenna than the far-field model, for distances above $2D^2/\lambda$, the far-field approximation model always over-predicts the real value of exposure levels. In this case, the far-field model gets more accurate results, since it is applied to the given distance [OFRC05].

Another possible way to estimate the EMF radiated around BSs is the far-field-gain-based model proposed in [BiGi99] which is applicable in near and far regions of antennas, for distances above 3λ. To obtain a good estimate of the radiated near-field, this method adopts the gain function of the antenna from the far-field pattern. The method considers the BS as a uniform array antenna, and the radiated EMF in the near field region is a combination of the far-field radiated by each element of the

array.

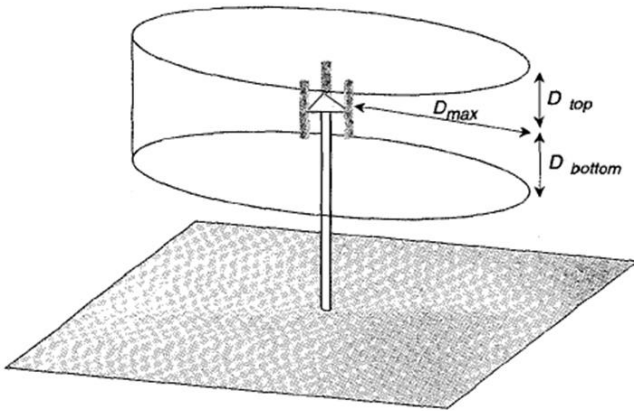

(a) Side view.

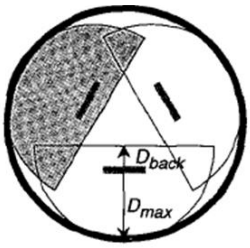

(b) Top view.

Figure 2.3 - Cylindrical exclusion zone for a sectored base station [MFRL02].

The obtained field level values with this model were compared with results of Numerical Electromagnetic Code (NEC) simulations and with measured data, and a good agreement among them has been shown. The method is fast and efficient, but does not consider the influence of environment topology, e.g., the effect of buildings in the urban environment, on the radiation levels.

In [ABDK02], two accurate models for analysing BS panel antennas are presented, which may be adapted for human exposure assessment and for verification of compliance with recommended threshold values: the synthetic and the gain-based models.

The synthetic model describes the radiated near field of the full array antenna by way of the superposition of contributions of the radiated field of unit cells of the panel antenna. The model revealed to be very accurate for distances above λ from the antenna, compared with a full-wave analysis of the antenna.

The gain-based model is derived from the synthetic model, by computing and storing the gain pattern of one single cell for all angles and avoiding a full-wave analysis of the entire antenna. So the radiated near-field of the antenna is approximated to the sum of the far-field contributions, in amplitude and phase. The model requires a short computation and a small memory storage, allowing a reasonable

approximation of the near field at a distance of about 2λ.

Due to the limitations and complexity found in most of the full-vectorial EM algorithms, a rigorous hybrid prediction model is described in [BCFF99] and [BCDF02]. It offers a fast evaluation of field strength and takes into account the effect of the surrounding environment, combining three different propagation models to be used in different spatial regions around the antenna. These regions correspond to the near-field region of a single antenna element, the intersection between near-field region of the whole antenna and the far-field region of each element, and finally, the far-field region of the whole antenna. This algorithm defines the exclusion zone as a parallelepiped volume around the antenna, symmetrical with respect to the maximum radiation direction.

The near-field region of a single antenna element is defined by $d \ll \lambda$, the spherical waves triples model [Sche43] being chosen as prediction model. This rigorous method consists of evaluating the exact value of the electrical field radiated by a dipole as the sum of the fields radiated from three different point-sources of spherical non-uniform waves located in the middle and at the extremes of the dipole. Although this model is applicable in the far-field region, the hybrid prediction model does not account for the influence of surrounding objects, so it is limited to receiving points very close to the antenna.

For the region corresponding to the intersection between the near-field region of the whole antenna and the far-field region of each element, $d \gg \lambda$ and $d < 2D^2 \ \lambda$, the combination of the sub-element radiation pattern antenna model with a ray-tracing propagation tool is used [CGLM99]. The ray-tracing algorithm defines propagation as “rays”, thus, allowing the reproduction of the multipath effect due to obstacles near the antenna. The total field radiated is obtained as the sum of all different contributions (transmission, reflection and diffraction) originated from each single antenna element, assuming that these elements are independent non-uniform spherical sources.

The ray-tracing propagation tool is also used in the far-field region ($d > 2D^2 \ \lambda$) with the purpose of taking into account the effect of the reflections and diffractions due to the presence of surrounding buildings or other objects near the antenna. Assuming that the antenna is seen as a single source, the total field is given by the vectorial sum of all the contributions of the transmitted, reflected and diffracted rays. It is necessary to describe obstacles by its EM properties, and consider that these properties are homogeneous on the whole volume of the obstacle. If the antenna is located in an open area where the influence of buildings can be neglected (distances greater than 60 m), a simple free-space propagation formula established in [Gree90] and [Pars92] describes the electrical field level according to the hybrid prediction model. This approach used in the far-field region can be used for lower distances when the aim is to analyze the worst-case.

After the comparison of the model results with measurements, it is concluded that environment factors can affect the field strength levels: the value in real cases can be quite higher than the field intensity obtained with the free space approach. The relationship between EM exposure and the radius of the cell is another interesting conclusion: in micro-cellular deployments, the reduction of cell size usually translates into a better distribution of field intensity, and consequently, in to a reduction of the exposure peaks and of the safety limit problem.

When it is intended to analyze field exposure levels at a certain distance from the antenna, or more specifically, identify a precautionary volume around BS antennas, the definition of a methodology based on the models found in the literature is convenient, as the previously presented ones.

In [OFRC05], a simple and precautionary approach to the estimation of exclusion zones around typical GSM and UMTS BS antennas installations is suggested. According to the classification used in Table 2.9, three different scenarios were considered to find agreement in the results in similar types of antennas. The installation scenarios chosen were Rtower/Utower, Uroof and Iceil. Also there was the concern of gathering antennas parameters from different sources with the purpose of obtaining typical results.

As in the cylindrical exclusion zone model [MFRL02], the exclusion zone is interpreted as an imaginary surface with a cylindrical shape around BS antennas, Figure 2.4. Using a simple model, the distance value of the exclusion zone is determined in the direction of the main lobe of the antenna, for the worst case scenario, D_{front}. This distance can be determined by estimating the distance from antennas where the power density or field strength value equals the reference thresholds.

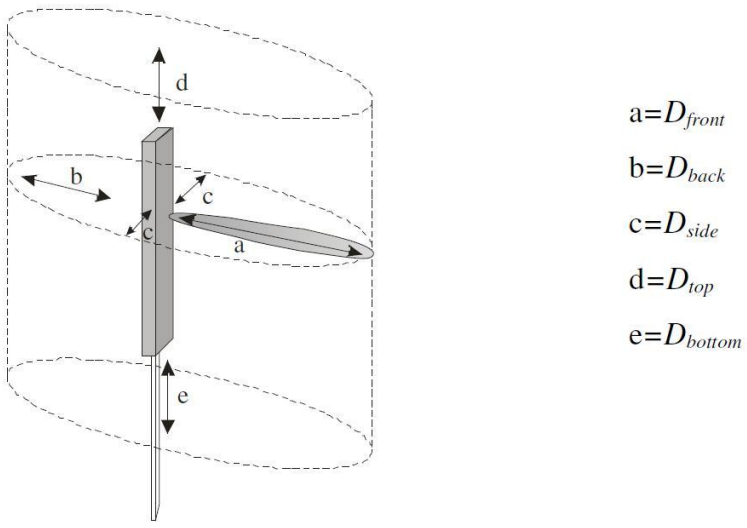

Figure 2.4 - Representation of an antenna exclusion region (extracted from [OFRC05]).

For the antennas that are not omnidirectional, the distance values for the other directions of the exclusion zone are calculated based on the D_{front} value, applying correction factors. For the limits for the side and back of the exclusion zone (D_{side} and D_{back}, respectively), the correction factors are determined from the typical antennas characteristics found in the antennas catalogues. The correction factor value for the antenna sides is -10 dB, since this value is the typical one for a 130º beam width. The value of -15 dB is used as the correction factor for the back, because it corresponds to the relative value of the second biggest radiation lobe. For the top and bottom (D_{top} and D_{bottom}, respectively), the used value is the correction factor presented in [MFRL02]: 0.3 (in linear units). The use of downtilt θ_{dt} is also taken into account, using the expressions proposed by [MFRL02].

The far-field approximation model is used, [MNMV02], to ensure the simplicity of the method. Although the far-field model [CENE02] is relatively simpler, the validity distance of $d > 2D^2/\lambda$ limits the calculation of exclusion zones, since the power density for $d = 2D^2/\lambda$, assuming the worst case, is around 20 times below the threshold values established by ICNIRP [ICNI98], so the exclusion zone will be smaller than $2D^2/\lambda$. Thus, the far-field approximation model gets results at a much closer distance from the antennas, with minimum valid distance equal to $D^2 \quad 4\lambda$, 8 times smaller than the far-field model.

The results obtained for the Iceil scenario show that for the minimum valid distance of the far-field approximation model, the results are above the threshold values, while for Rtower/Utower and Uroof scenarios, the results are still below them. Therefore, this methodology takes a preventive attitude: the exclusion zone value is given by this model, or if the obtained distance value is not valid, the exclusion zone is given by the model minimum valid distance, $D^2 \quad 4\lambda$.

In typical situations, for the Iceil scenario, front borders obtained of an exclusion zone (D_{front}) are around 0.2 m for GSM 900 antennas and 0.1 m for GSM 1800 and UMTS. For Rtower/Utower and Uroof scenarios, the results obtained are around 3 m for GSM 900 and UMTS, while for GSM 1800, the results are around 5.8 m, Table 2.8.

Table 2.8 - Exclusion zone front borders for various scenarios [OFRC05].

D_{front} [m]	Rtower/Utower		Uroof		Iceil	
	1 carrier	4 carriers	1 carrier	4 carriers	1 carrier	4 carriers
GSM900	3.00	4.18	2.94	4.17	0.18	0.72
GSM1800	5.87	5.87	5.75	5.75	0.09	0.36
UMTS	3.07	3.07	3.07	3.07	0.08	0.32
GSM900/GSM1800	5.87	5.87	5.75	5.75	0.27	1.09
GSM900/UMTS	3.07	5.59	3.07	5.58	0.26	1.05
GSM900/GSM1800/UMTS	5.87	6.86	5.75	6.87	0.35	1.41

Scenarios with the cumulative of four carriers in each system were also studied, presenting a small increase in exclusion zones dimensions for the Iceil scenario and for GSM900. In the other scenarios, the results do not suffer practically variations, because the obtained distances remain smaller than the validity of the model.

For the co-location of networks with the existence of 1 and 4 carriers per system, the following scenarios were considered: GSM900/GSM1800, GSM900/UMTS and GSM900/GSM1800/UMTS. For

the Iceil scenario, exclusion zones obtained increased a bit, mainly for a case of co-location of three systems. The highest result is in co-location of three systems with 4 carriers in each one.

This methodology is adopted by Portuguese operators, but different procedures are taken in other countries and entities. The hybrid prediction ([BCFF99] and [BCDF02]) is adopted by ARPA, the regional agency for environment protection of Emilia-Romagna in Italy.

French operators follow the report published by the Ministry for Health and Social Security [MSPS01]. This guideline defines the security perimeter around BS antennas for different BS types, from its installation characteristics, type of cell, output power and numbers of antennas in same site. The front border of the exclusion zone varies between 0.3 and 4.5 m for typical antennas and radiated power. For sensitive areas, as hospitals, schools grounds or kindergartens, a specific exclusion zone is defined with a value of 100 m.

In the United Kingdom (UK), the National Radiological Protection Board (NRPB) issued the recommendation that defines the values for exclusion zones in the range 10 to 15 m for large macro-cell BSs, in the direction of the main lobe of the antenna. For micro-cell BSs with radiating power around 1 to 2 W, exclusion zones have values much smaller than macro-cells [OFRC05]. In [RaWh98], the Independent Expert Group on Mobile Phones (IEGMP) has an interesting opinion: most BSs are surrounded by perimeter fences, and exposures at the boundary of these fences are approximately 300-fold lower than the ICNIRP reference levels in GSM and UMTS. Masts often also carry line-of-sight microwave communication dishes, in which the exclusion zones typically do not extend beyond the mouth of the dish.

2.5 Measurement of Electromagnetic Radiation

In order to evaluate compliance with thresholds for human exposure, or to validate models of EMF strength estimation, measurements of the EMFs around BS antennas should be performed. The definition of measurement procedures is essential in such a way that the results are replicated, and it is possible to compare different measurement values. In this sense, the measurement recommendations issued by international entities are an important tool.

The CENELEC issued a reference and alternative methodologies for measurement of EMF strength and SAR in EN 50383 standard, [CENE02]. This basic norm is valid in the 110 MHz to 40 GHz frequency range and can be used to establish the compliance boundary, applicable to each antenna region. The field measurements can be obtained by surface or volume scanning. Table 2.9 shows the reference methodology which is the best evaluation technique, and two alternative techniques.

The recommendation ECC/REC (02)04, [ECCC07], from Electronic Communications Committee (ECC) within the European Conference of Postal and Telecommunications Administrations (CEPT) specifies a measurement method to assess non-ionising EMF levels with the view to compare against the limits for human exposure, in the frequency band from 9 kHz to 300 GHz. This recommendation

was applied by most European Telecommunications Administrations, as the ANACOM [ANAC07].

Table 2.9 - Methodologies established by EN 50383 standard [CENE02].

Methodology	Reactive near-field region	Radiating near-field region	Far-field region
Reference	SAR evaluation	SAR evaluation	E-field or H-field calculation
First alternative	E-field or H-field measurement	E-field or H-field measurement	E-field or H-field measurement
Second alternative	none	E-field or H-field calculation	none

As seen in Section 2.2.1, the magnetic and the electric field strengths may be related directly, indirectly or not, depending on the distance to the antenna. Thus, the method of measurement of E-field and/or H-field is chosen in accordance with the field region, Table 2.10. The measurements are usually performed in radiating near-field or far-field region [ANAC07].

The measurement method is based on three typical cases: quick overview (case 1), variable frequency band scan (case 2), and detailed investigation (case 3). Each case has its characteristic procedure, depending on the purpose of the measurement, and the complexity increases gradually. Case 3 is the only that allows to verify if exposure limits were exceeded due to the rigour of the used procedure.

Table 2.10 - Measurement procedure established by ECC recommendation [ECCC07].

	Reactive near-field region	Radiating near-field region	Far-field region
Component to be measured	E-field and H-field	E-field or H-field	E-field or H-field

The measurement point should represent the highest levels of exposure to which a person might be subjected, 1.5 m above the ground or at floor level. The measurement duration should be referenced to the exposure guidelines used. For ICNIRP guidelines, this value is equal to 6 minutes [ICNI99]. When the measured value exceeds the decision level (value below the threshold values, defined by telecommunications Administrations), a spatial average of three points shall be executed, matching the dimensions of the human body (1.1, 1.5 and 1.7 m). The value of the field strength is given by the mean square of these three values. The decision level established by ANACOM in [ANAC07] is 17 dB below the reference level.

A simple method to evaluate compliance with exposure to EM radiation thresholds based on the ECC recommendation is presented in [CoFe04], focusing on the importance of the selection of measurement points. The two factors that influence the beginning of the procedure are the installation topology and the number of BS antennas. With these factors, the most representative points of the measurement environment are selected. In the first step, the choice of measurement point(s) depends on the BS antenna installation and the number of antennas. This method uses the classification of BS installations presented in Table 2.9. After the choice of points, the measurement used procedure is based in [ECCC07].

Chapter 3

Model Development

This chapter presents the EMF models, as well as the exclusion region models used in this work. The description of the implemented models is also discussed.

3.1 Antenna Scenarios

The solutions provided by the manufacturers of antennas cover the largest number of possible situations, being clear the necessity to identify common characteristics among the various scenarios used by several operators to ensure an efficient design of the model. In this context, there can be two main types of BS antennas according to the environment where the antennas are inserted: indoor or outdoor.

The signal strength from a BS antenna outside the building may be typically insufficient to ensure an effective coverage inside the building, either by attenuation caused by the building construction or its size. In this case, the discrete antennas of small dimensions are placed in rooms and corridors, which are connected to the nearest BS or network node. There can be two typical indoor antennas: directional antennas, which are placed on walls or other surfaces, and ceiling antennas, typically omnidirectional and often a monopole. The directional antenna is usually composed of a rectangular metal plate mounted on a conductive plane, with the power lower than the outdoor case due to the reduced dimension of coverage areas [KATH12c].

To simplify the indoor network, the same antenna supports the service of several mobile communications systems, and in some cases several operators share the same BS antenna, being required to take into account the input power loss that arises due to the introduction of the multi-band (multi-operator) combiner: the typical value is equal to 6 dB [KATH12b], [Opti12]. The developed model takes into account that the antennas are shared by operators and technology (GSM, UMTS and LTE). Wi-Fi systems are not considered since operators do not usually install this system in their BS antennas. Operators may use 900 MHz band for both GSM and UMTS, and 1800 MHZ band for GSM and LTE, as was said above in Chapter 2.

With the introduction of LTE, operators tend to replace the old indoor antennas by antennas that support the new technology, such as antennas with MIMO and without MIMO, or antennas with higher bandwidths, depending on the requirements of the site coverage [Opti12]. From the viewpoint of EM exposure, it can consider that the MIMO elements contribute separately to the levels of radiation.

Outdoor antennas are usually installed in relatively high locals, as rooftops, building faces, posts, or towers, and are normally arrays of vertically stacked dipoles, to decrease the vertical half power beam width compared with a single element, and providing thereby the increase of the power radiated in the horizontal plane. In array antennas, half wavelength dipoles are used with the distance between dipoles not larger than one wavelength, corresponding to the optimal value that maximizes directivity [Corr12a], Figure C.1. For outdoor sector antennas, panel antennas are generally used to ensure isolation in undesirable directions through a metallic reflector placed behind the array. The arrangement for sectorial antennas is formed by one or two dipoles that are rotated +45º/-45º, resulting in horizontal half power beam widths of 90° and 65º, respectively [KATH12b], [KATH12c].

Concerning the type of infrastructure that supports the antennas, a possible classification of typical BS installations is shown in Table 2.6. It is assumed that in most typical installations masts or towers are

used to support the BS antennas (Rtower and Utower installation), or the antennas are placed on rooftops in urban environments (Uroof) or on the façades, where the field is influenced by buildings and other obstacles in the vicinity of the antennas (Ufaçade) [OFRC05].

Before the introduction of LTE, GSM and UMTS antennas were sharing the same infrastructure, being usually placed side by side, because it is the simplest configuration. With the implementation of LTE BSs, typically with MIMO technology, these are co-located with the existing systems and in many sites a multi-band antenna will support LTE well as other technologies, replacing the old antennas. The sharing of infrastructure and the variety of configuration choices for existing antennas is the result of the many variables involved as the licensing issues, the rental of the space where BS is installed, stability of the antenna supports, the simplification and optimisation of networks, etc.

3.2 Far-Field Model

According to [CENE02], the RMS value of $S(d,\theta,\phi)$, in the far-field region can be estimated by:

$$S\ d,\theta,\phi\ = \frac{P_{in}G(\theta,\phi)}{4\pi d^2}, \qquad d > \frac{2D^2}{\lambda} \tag{3.1}$$

where:

- d: Distance from the antenna to the observation point;
- θ,ϕ: Elevation and azimuth angles;
- P_{in}: Input power of the antenna;
- $G\ \theta,\phi$: Generalised antenna gain;
- D: Largest dimension of the antenna;
- λ: Wavelength of the electromagnetic wave.

Note that, as mentioned in Section 2.2.1, in the far-field region the radiated field has a decay of d^{-1}, since S is related to E and free space characteristic impedance, Z_0 (equal to 120π), as follows [Moli11]:

$$S = E^2\ Z_0 \tag{3.2}$$

To assume the worst case scenario in relation to EM exposure, the model estimates S for the lower frequency band, since the model is valid for distances closer to the antenna. As discussed in Section 2.4, the far-field model becomes less accurate when there are estimated values nearer the antenna, over-estimating the real value of EMF.

Table C.1 (Annex C) presents the typical distances of this far-field region, $2D^2\ \lambda$. For BS outdoor antennas, the model is valid for distances greater than 9.86 m (LTE800), which makes this model generally insufficient for the exclusion regions study. In indoor environments, due to the small size of the antennas, the distances are much lower than those obtained with outdoor antennas, with the typical largest dimension of indoor antennas between 0.18 m and 0.30 m, Table C.1. However, with

the increase of frequency and/or D, the distance of the far-field region has high values, taking into account the indoor environment, being also required in some cases to resort to valid models in the near-field region.

3.3 Near-Field Model of Outdoor Antennas

The radiating near-field region is the zone of interest for EMF estimation in areas closer to the antenna, since the reactive near-field region has very reduced dimensions and the exclusion zone is defined typically in the radiating near-field region [OFRC05], [SBCo12].

For an outdoor environment, the model chosen for the determination of the radiated field in the near-field region is the gain-based one, in which the near-field is approximated by the sum of the far-field contributions of each array element [ABDK02]:

$$E\ d,\theta,\phi \ \cong \ \sum_{i=1}^{N_{el}} \frac{\sqrt{30P_{in\,i}G_{el}\ \theta_i,\phi_i}}{d_i} e^{-j\ kd_i+\psi_i}\ \boldsymbol{u}\ \theta_i,\phi_i \quad , \qquad d > 2\lambda \tag{3.3}$$

where:

- $E\ d,\theta,\phi$: RMS electric field;
- d_i,θ_i,ϕ_i : Spherical co-ordinates centred at the i-th element of the array;
- N_{el}: Number of elements of the collinear array antenna;
- $P_{in\,i}$: Input power to the i-th unit element;
- $G_{el}\ \theta_i,\phi_i$: Generalised gain of the i-th element;
- k: Propagation constant equal to $2\pi\ \ \lambda$;
- ψ_i: Associated phase shift of the i-th element;
- $\boldsymbol{u}(\theta_i,\phi_i)$: Co-polar vector of the i-th element.

In Figure 3.1, the coordinates system is shown for the analysis of a panel antenna consisting of elements of two dipoles with orthogonal polarisation.

The phase shift ψ_i is associated to the feeding currents of each array element. Considering the direction of maximum radiation as the perpendicular direction to the axis of the antenna, $\theta = \pi\ \ 2$, and without considering the tilt angle, the phase shift should have the value zero in order that all antenna elements contribute positively to the antenna radiation [Moli11].

The collinear array antennas usually have 2, 4 or 8 elements, with uniform spacing between elements equal to the wavelength multiplied by a factor Δ_{da}= $[0.45\ \ 1]$, since the spacing is not always exactly equal to one wavelength:

$$d_a = \Delta_{da} \times \lambda \tag{3.4}$$

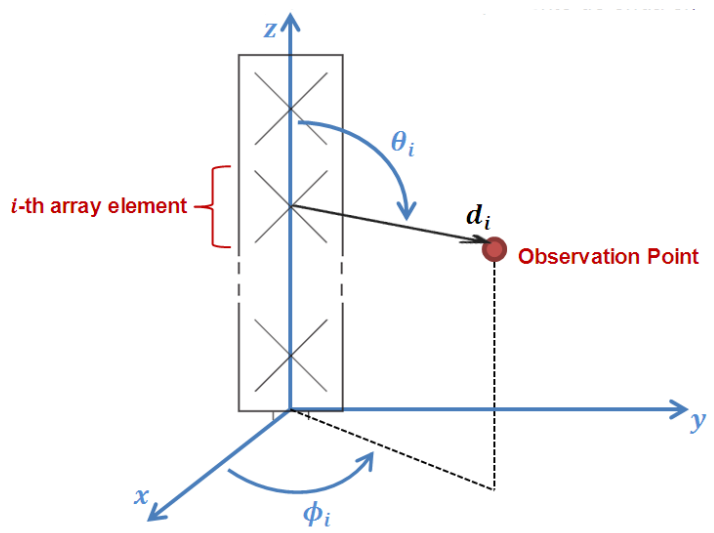

Figure 3.1 - Coordinates scheme of a panel antenna for gain-based model.

The value of d_a takes particular relevance when the aim is the estimation of EMF in areas close to the antenna, although this parameter is not generally provided by manufacturers in antennas datasheets. Considering the value of Δ_{da} always equal to 1, it can lead to values without any physical meaning, particularly if the total length of all the spacing elements is larger than the real height of the antenna. A study to determine the multiplicative factor Δ_{da} was conducted, analysing panel antennas with half wavelength dipoles inclined ±45º. For this purpose the definition of the antenna height is necessary, which can be determined by the analysis of Figure 3.2:

$$h_{ant} \simeq N_{el} - 1 \times d_a + h_{el} \tag{3.5}$$

where:

- h_{ant}: Height of the antenna array;
- h_{el}: Height of the element.

It is assumed that the contribution of the antenna extremities (i.e., from the end of element to the end of the antenna) is negligible. Dimension h_{el} is determined by trigonometric properties:

$$h_{el} = \frac{\lambda}{2} \sin 45^{\underline{o}} = \frac{\lambda \times \overline{2}}{4} \tag{3.6}$$

Note that h_{el} would be equal to the length of the dipole if its polarisation was vertical.

From (3.4), (3.5) and (3.6), one gets:

$$\Delta_{da} = \frac{h - h_{el}}{N_{el} - 1 \ \lambda} = \frac{h - \lambda \ \overline{2} \times 4^{-1}}{N_{el} - 1 \ \lambda} \tag{3.7}$$

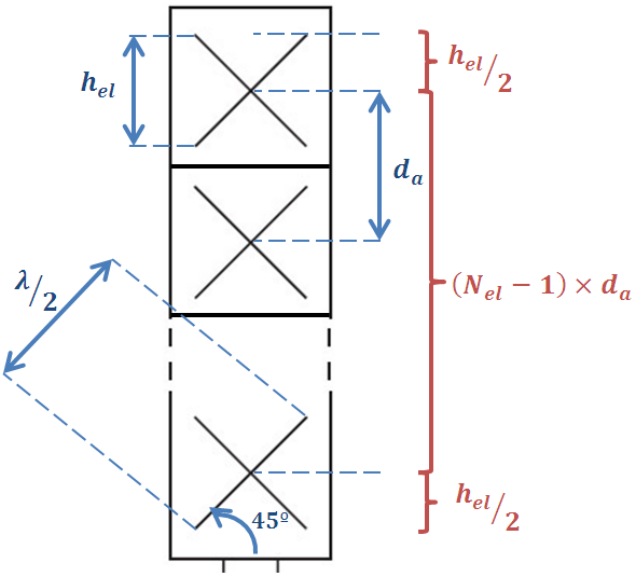

Figure 3.2 - Dimensions analysis of an array antenna.

Table 3.1 shows the values of Δ_{da} for the systems under study, by assuming the lower frequencies of the system bands (DL) that provide the worst-case of EM exposure and a greater spacing between elements. The bands corresponding to LTE at 900 MHz, 1800 MHz and 2100 MHz are not analysed, since they are very close to those used by GSM and UMTS.

The spacing between elements, d_a, cannot be much larger than a wavelength. Considering the typical height of outdoor antennas between 1.3 and 2.6 m, it is concluded that an array of two elements always leads to impracticable spacing, since the values are greater than 3.38 wavelengths. For GSM 900 and LTE 800 MHz ($N_{el} = 4$) only two results were obtained with values near one wavelength. The increased number of elements is reflected on the smaller spacing between elements to ensure the same height of the antenna. In LTE2600, there are no satisfactory results, but one should note that the LTE BS antennas are generally multiband ones.

For BS antennas that support various systems, the same antenna may be composed of several arrays, each one of a given band, that, by themselves, may not occupy the entire length of the total antenna. Thus, the following approach was taken: when the calculated value of Δ_{da} provides satisfactory results (Δ_{da} takes values less than approximately one), this value is used to determine d_a, for cases where the spacing calculated is higher than a wavelength, the value of one wavelength is used as the spacing between elements.

With $d_a = \lambda$, the gain of one element in the direction of maximum radiation G_{el} can be obtained by [ABDK02]:

$$G_{el} \approx G \;\; N_{el} \tag{3.8}$$

where G is given by the antenna gain in the direction of maximum radiation. This gain overestimation is valid for panel antennas, and is considered valid for any array regarding the objectives of the study. In panel antennas, the use of metallic barriers between elements is characterised by the radiation of all the input power, since the coupling between the unit elements can be neglected. It is assumed that the input power is equally distributed by all elements:

$$P_{in\,i} = P_{el} = P_{in} \;\; N_{el} \tag{3.9}$$

where P_{el} corresponds to the input power of an element.

Table 3.1 - Spacing between elements normalised to the wavelength.

Δ_{da}	$h\ [m]$	N_{el}		
		2	**4**	**8**
LTE 800 MHz (860 MHz)	1.30	3.38	1.13	0.48
	2.60	7.10	2.37	1.01
GSM 900 (935 MHz)	1.30	3.70	1.23	0.53
	2.60	7.76	2.59	1.11
GSM 1800 (1805 MHz)	1.30	7.47	2.49	1.07
	2.60	15.30	5.10	2.19
UMTS (2110 MHz)	1.30	8.80	2.93	1.26
	2.60	17.95	5.98	2.56
LTE 2600 MHz (2620 MHz)	1.30	11.01	3.67	1.57
	2.60	22.37	7.46	3.20

The d_i length can be described as a function of the distance d from the antenna that favours the simplification of the model. The observation point is then defined at a distance d of the antenna and at a height that corresponds to the midpoint of the antenna height ($h\ \ 2$), enabling to focus on half of the elements of the problem, due to the symmetric characteristic of the antenna and its radiation, Figure 3.3. This symmetry is verified both by the choice of the observation point and by the gain and input power with the same value to all elements.

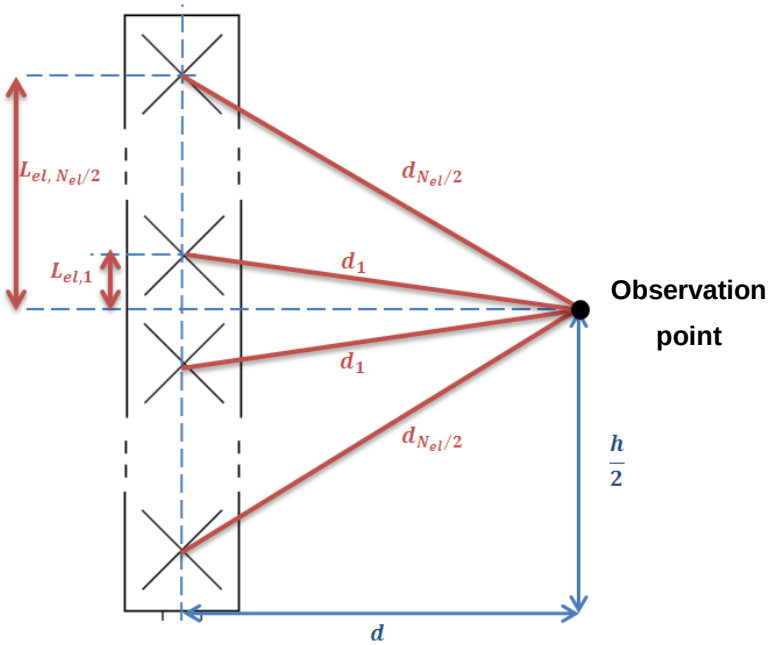

Figure 3.3 - Geometric approach for the determination of d_i.

According to the Figure 3.3, the expression that relates d_i with d is as follows:

$$d_i = \sqrt{d^2 + L_{el,i}^{\;2}} \tag{3.10}$$

where $L_{el,i}$ is the length from the midpoint of the antenna to the center of the i-th element, being a known value. For the two elements closer to the centre of the antenna, $L_{el,i}$ takes values of d_a 2 with the N_{el} pair, whereas for N_{el} odd, there is a single element in the centre of the antenna, where $L_{el,i}$ is equal to zero. The following elements have the value of $L_{el,i}$ equal to multiples of the d_a. From the considerations adopted above, (3.3) can be written as:

$$E\ d \cong \begin{cases} \sum_{i=1}^{\frac{N_{el}}{2}} 2\,\frac{\sqrt{30P_{el}G_{el}}}{d_i} e^{-j\,kd_i+\psi}, & N_{el}\ even \\ \frac{\sqrt{30P_{el}G_{el}}}{d_1} e^{-j\,kd_1+\psi} + \sum_{i=2}^{\frac{(N_{el}-1)}{2}+1} 2\,\frac{\sqrt{30P_{el}G_{el}}}{d_i} e^{-j\,kd_i+\psi}, & N_{el}\ odd \end{cases} \tag{3.11}$$

The fluxogram corresponding to the electric field computation of an array antenna in the near-field region is shown in Figure 3.4. Figure 3.5 shows the result of outdoor antennas for LTE2600, with the input power for each antenna of 40 W and N_{el} equal to 8 elements. The characteristics of the antenna are described in Annex A (*Kathrein* 80010622). Note that the graph relates to only one MIMO element, since these MIMO elements are usually equal, and from viewpoint of exposure to EM radiation, MIMO antennas can be analysed separately.

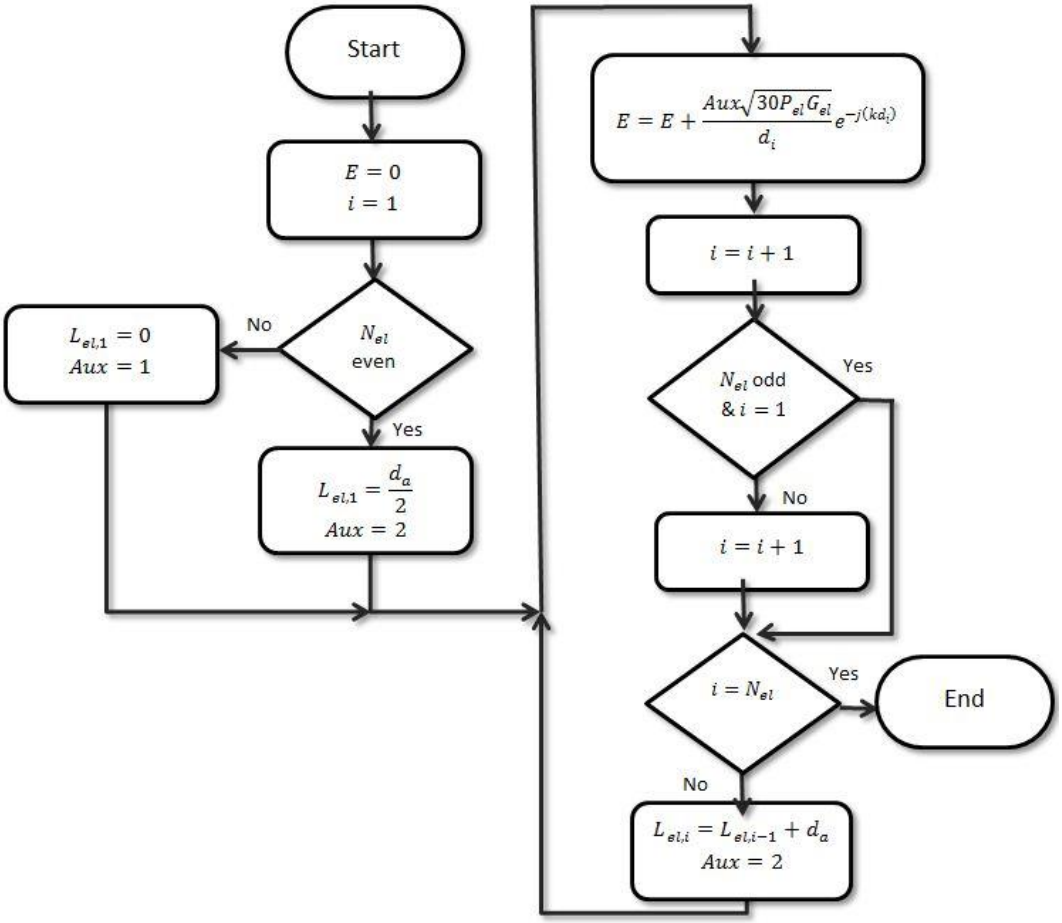

Figure 3.4 - Electric field computation of an array antenna in near-field for a distance d.

The phase differences among several possible scenarios are considered by applying an interpolation method with the type function:

$$f_p\ d\ = Ad^{-2} + Bd^{-1} + C \tag{3.12}$$

where A, B and C are the coefficients of the polynomial function $f_p\ d$. This function is chosen due to the fact that the electric field has a decay with the dominant term of the d^{-2} in the radiating near-field region. The values of these coefficients provide the best fit of the maxima points of $|E(d)|$ being obtained by using the computational capabilities.

To determine the maximum values, all field samples are analysed along d, where each sample $|E(d)|$ is compared with the following and previous one, $|E(d + \Delta_{sp})|$ and $|E(d - \Delta_{sp})|$, respectively, taking into account that Δ_{sp} is the length between samples. The value of $|E(d)|$ is maximum if it is greater than $E\ d + \Delta_{sp}$ and $E\ d - \Delta_{sp}$. The exception is the first sample that is only compared with the following one. In the interpolation process, the function responsible for determining A, B and C returns also the RMS error (RMSE). If this error is high, the interpolation function runs again up to determining

the most perfect possible interpolation. After some experiments, it was concluded that the value of 3 as maximum permissible RMSE leads to satisfactory results, although the acceptable RMSE is a program variable that can be changed. It was also noted that the results are better if the first maximum is neglected when is less than the second one.

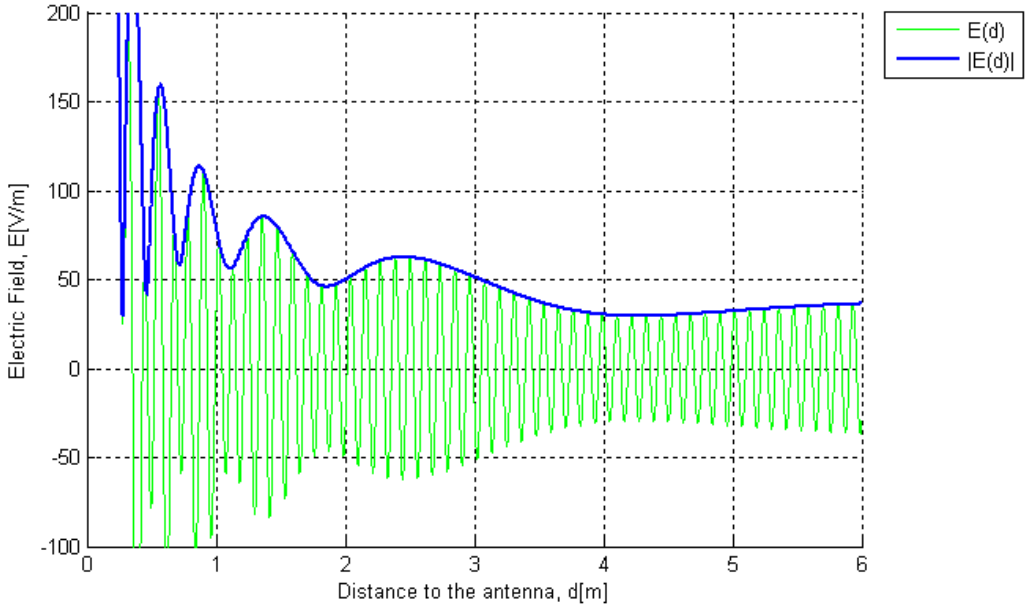

Figure 3.5 - E response with d for an LTE2600 outdoor antenna (gain-based model).

The obtained interpolation function, $E_{fit}(d)$, may have values for d that are less than $|E(d)|$, the worst case being ensured with the upper bound method: the largest difference between $E_{fit}(d)$ and $|E(d)|$, Δ_{max}, is determined and applied on the $E_{fit}(d)$, moving it vertically, Figure 3.6:

$$E_{upper}\ d\ = (1+\Delta_{max}) \times E_{fit}\ d\ = (1+\Delta_{max}) \times (Ad^{-2} + Bd^{-1} + C) \tag{3.13}$$

with:

$$\Delta_{max} = \max_{d} \frac{E\ d\ - E_{fit}(d)}{E_{fit}(d)} \tag{3.14}$$

where $E_{upper}\ d$ is the upper bound of the electric field $E\ d$.

The range defined for d for estimating $E_{fit}(d)$ and $E_{upper}\ d$, should have the lower bound equal to the limit imposed by the model, $d_{min=}2\lambda$, and should not have high values for the d_{max} upper limit. With the increase of the range dimension, the interpolation method has more points to analyze, then it is less accurate to make the adjustment of the maximum points in the zone closest to the antenna. The range upper limit with value of about 6 m (approximately half of the validity distance length of the far-

field model for LTE800 and GSM900 antennas) has acceptable results, although this limit is variable in the model. In Figure 3.7, a diagram illustrating the procedure for the near-field model is presented.

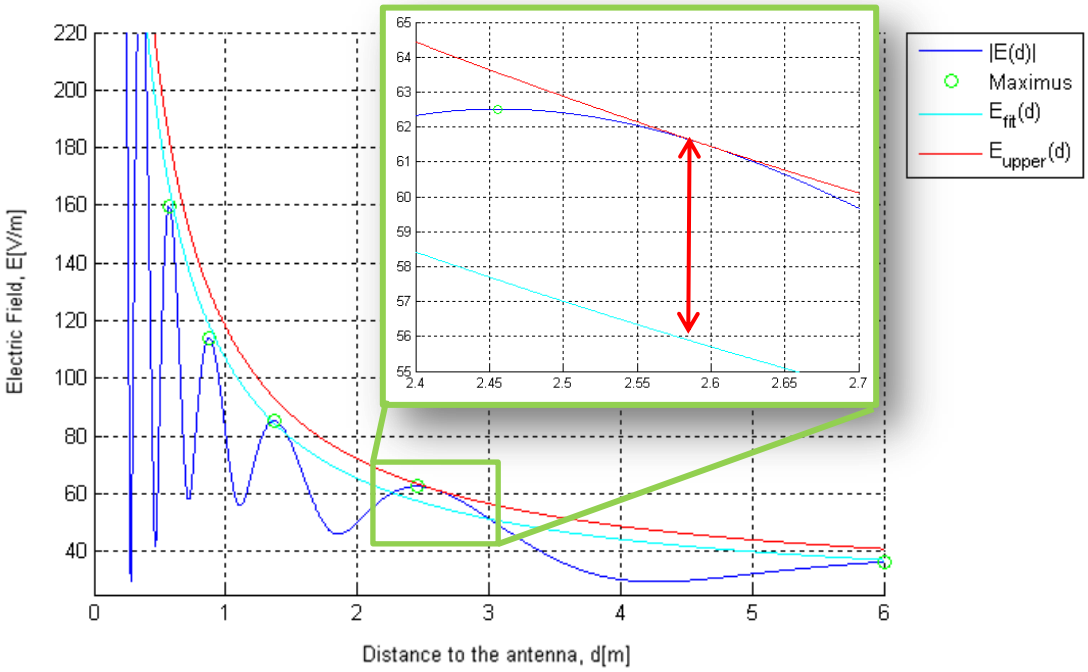

Figure 3.6- Field Interpolation for LTE2600 outdoor antenna by varying the d.

3.4 Field Model of Indoor Antennas

In an indoor environment, two methods are needed for the estimation of EMF, since two typical types of antennas must be considered: the microstrip antennas that are used in sectorial antennas, and the monopoles when an omnidirectional radiation pattern is intended.

A microstrip antenna with feeding by a microstrip line, as well as its important parameters are presented in Figure 3.8. Manufacturers do not provide the value of these parameters, so an analysis on these dimensions is necessary to find an approximation consistent with reality. According to [KATH12c] and [Bala05], the length of the patch, L, has typically a value close to $\lambda\ 2$. For the analysis of the other dimension of the patch, width W, the expression for theoretical design is:

$$W = \frac{\lambda}{2}\ \frac{2}{\varepsilon_r + 1} \tag{3.15}$$

where ε_r is the dielectric constant of the substrate, with values between 2.2 and 12. The antenna has a higher performance for lower values of ε_r: the antenna is more efficient, has a greater bandwidth

and less loss of radiated fields in space. However, the thickness of the dielectric substrate is higher for ε_r lower values. The FR-4 epoxy substrate is often used in multiband antennas for wireless systems, with ε_r equal to 4.4 and thickness h of 1.6 mm [PaPH12], [Tuan10], [ABOM09], [LeSu09]. The influence of the physical notch introduced by inset feed can be neglected, $y_o = 0$, although its corresponding junction capacitance has a slightly influence on the resonance frequency. The thickness of the patch can also be neglected [Bala05].

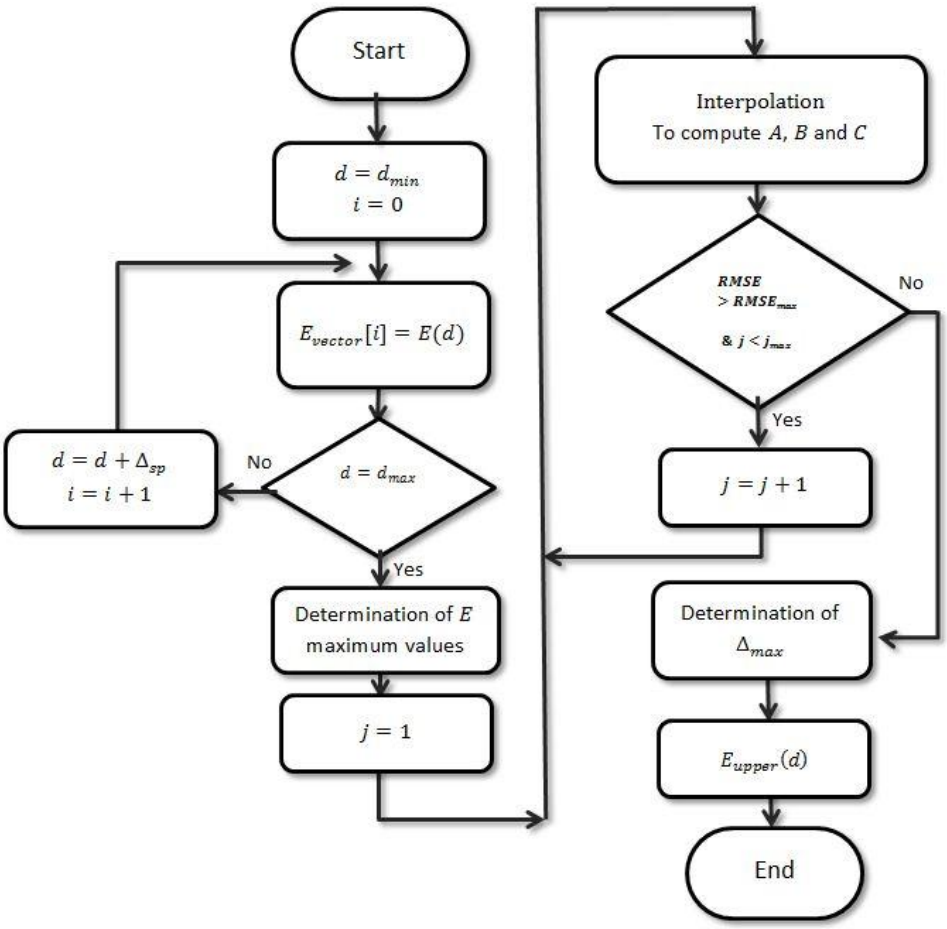

Figure 3.7 - Near-field model program overview for an array antenna.

In a multiband antenna, the dimensions calculated for L and W are different for each frequency, since the resonant frequencies affect different areas of the patch. The highest values of L and W are obtained with lower frequencies. It is verified that these values for LTE800 do not exceed the overall dimensions of typical antennas [KATH12a].

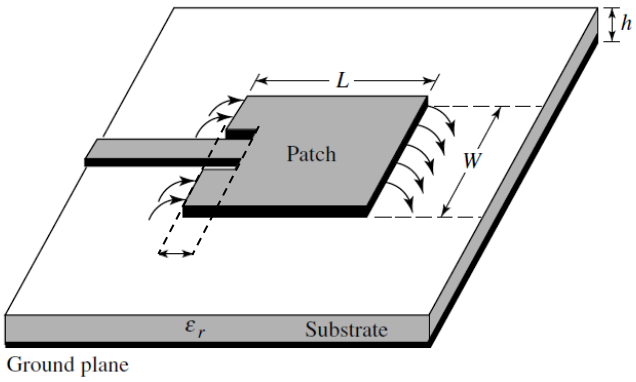

Figure 3.8 - Microstrip antenna (extracted from [Bala05]).

If the field configuration is the Transverse Magnetic mode TM_{010}^{x}, the radiated far-field according to the Cavity model, in the E-Plane ($\theta = \pi\ \ 2$), is given by:

$$\mathrm{E}_r \simeq \mathrm{E}_\theta \simeq 0 \tag{3.16}$$

$$\mathrm{E}_\phi(d) = j\frac{kWV_o e^{-jkd}}{\pi d}\frac{\sin(\frac{kh}{2}\cos\phi)}{\frac{kh}{2}\cos\phi}\cos(\frac{kL_{ef}}{2}\sin\phi) \tag{3.17}$$

where:

- V_o: Voltage across the slot;
- L_{ef}: Effective length of the patch.

TM_{010}^{x} is the dominant mode when $L = \lambda\ \ 2$ and $\mathrm{L} > \mathrm{W} > \mathrm{h}$. Figure 3.9 shows the coordinate system for a slot.

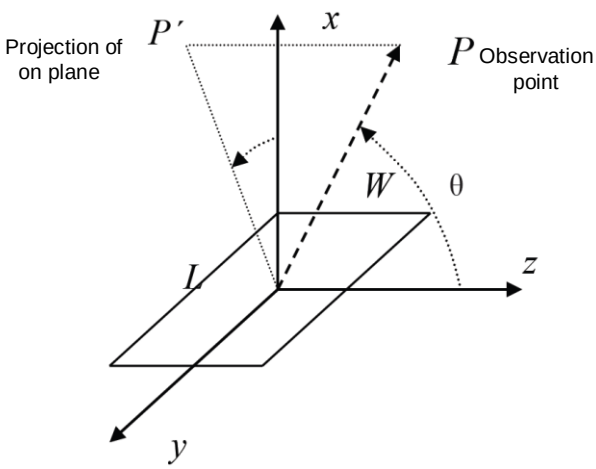

Figure 3.9 - Coordinate system for a microstrip antenna [More12].

The direction perpendicular to the microstrip, $\phi = 0$, corresponds to the direction of maximum radiation and is the goal for our estimation. The value of V_o is determined from the power input and the input

resistance of the antenna, R_{in}. The input resistance is provided by the manufacturer, with a typical value of $50\ \Omega$. The expression of V_o is the following:

$$V_o = \sqrt{P_{in} R_{in}} \tag{3.18}$$

From the electrical point of view, the patch looks greater than its physical dimensions, due to fringing effects, defining the effective length as well as the effective dielectric constant ε_{ref} due to the waves that travel in the substrate and some air. L_{ef} is given by:

$$L_{ef} = \frac{\lambda}{2\sqrt{\varepsilon_{ref}}} = L + \Delta L \tag{3.19}$$

with:

$$\varepsilon_{ref} = \frac{\varepsilon_r + 1}{2} + \frac{\varepsilon_r - 1}{2}\left(1 + 12\frac{h}{W}\right)^{-\frac{1}{2}}, \qquad W/h > 1 \tag{3.20}$$

and

$$\Delta L = h \times 0.412 \frac{(\varepsilon_{ref} + 0.3)(\frac{W}{h} + 0.264)}{(\varepsilon_{ref} - 0.258)(\frac{W}{h} + 0.8)} \tag{3.21}$$

where:

- ε_{ref}: Effective dielectric constant;
- ΔL: Extension of the length due to fringing effects.

In the case of omnidirectional radiation, the considered antenna is a monopole with a negligible diameter in order to minimize the complexity of the problem. The electric field radiated by a monopole is given by [Bala05]:

$$E_\theta(d) = j\frac{Z_o I_o e^{-jkd}}{2\pi d}\frac{\cos(kl\cos\theta) - \cos(kl)}{\sin\theta}, \qquad 0 \le \theta \le \frac{\pi}{2} \tag{3.22}$$

where:

- I_o: Maximum electric current that crosses the monopole;
- l: Length of the monopole.

When (3.22) is used in the near-field region, results may lead to a maximum phase error greater than $\pi/8$ rad.

In this case, it is also intended to determine the field in the direction of maximum radiation, with $\theta = \pi/2$. The most popular monopole length in Mobile Communication Systems is $\lambda/4$, being the value chosen in this work. I_o is obtained from:

$$I_o = \sqrt{\frac{P_{in}}{R_{in}}} \tag{3.23}$$

It is important to estimate the field in areas closer to the antenna, due to the value of powers involved in indoor environments. The CENELEC standard considers that at distances greater than $\lambda/4$ the

maximum difference between all field components and radiated field components is less than or equal to 10% [CENE02]. In [SBCo12], the perspective of worst-case corresponds to the minimum distance values of λ, since in this case the error is practically residual. Thus, in this study, the module of expression (3.17), $|\mathrm{E}_{\phi}\ d\ |$, and (3.22), $|\mathrm{E}_{\theta}\ d\ |$, is sufficient to estimate the electric field radiated for distances to the indoor antenna greater than λ.

3.5 Electric Field Global Model

From the analysis performed in the previous sections, two models were obtained to describe the EMF radiated by an antenna in outdoor environments, Figure 3.10. When the points farthest to the antenna are analysed, the near-field model loses accuracy, while the far-field model is more accurate. Thus, the choice of a single model is not sufficient to estimate the EMF for every value of d.

Choosing the far-field model distance as the limit of either model, in which for $d < 2D^2 / \lambda$ the near-field model is used and otherwise the far-field one, leads to an unrealistic approach, because EMF varies continuously as a function of distance. The solution is to create a method for linking two models, in order to determine an estimator of EMF continuous throughout the distance d.

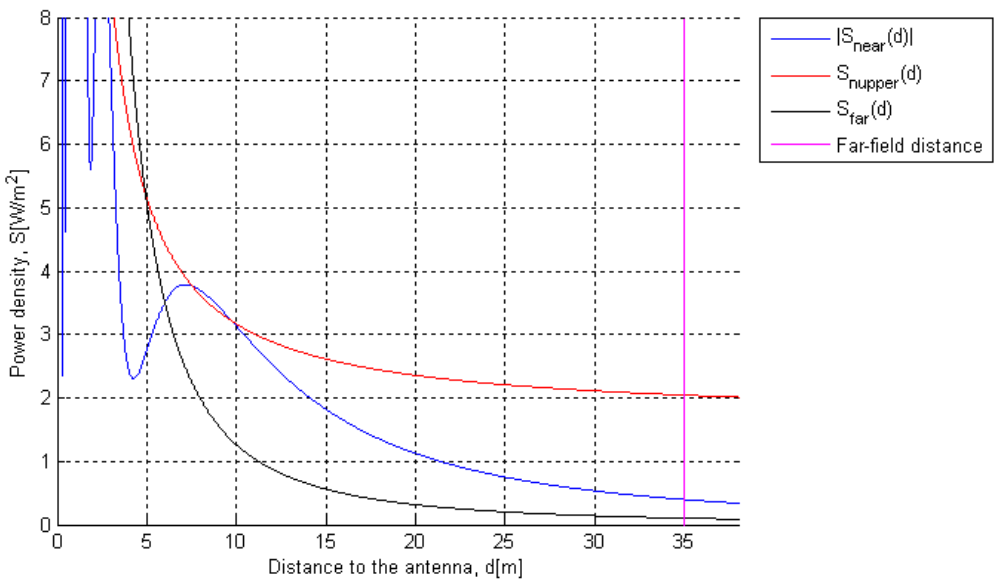

Figure 3.10 - Electric field Models of a LTE2600 outdoor antenna as a function of d.

The continuity can be performed by an interpolation between the two models, with the interpolation points carefully chosen for this purpose. The point where the far-field model begins to be valid, $S_{far}(d = 2D^2 / \lambda)$, is the logical choice for one of the points: interpolation point equal to $P_b =$

$(2D^2 \ \lambda, S_{far}\{2D^2 \ \lambda\})$. For the interpolation point that relates to the near-field model one has chosen an intersection point between the electric field estimated by the gain-based model $|S_{near}(d)|$ and its upper bound, $S_{nupper}(d)$, (interpolation point $P_a = (d_{Pa}, S_{nupper}\{d_{Pa}\})$).

The chosen strategy of the point P_a consists in the determination of all intersection points, giving preference to the most distant points of the antenna. For this purpose, an auxiliary variable is used which indicates which value of d the model uses to find a point of intersection. This value must be less than the far-field model distance. The value of 4 m is considered as acceptable, given the objectives of the study. If the program does not find an intersection point between this range of values, the farthest point of intersection from the antenna is used.

As this new interpolation is obtained in the radiating near-field region, the interpolation polynomial function is also given by (3.12). Thus, the same algorithm is used to determine new values for coefficients A', B' and C' . The expression of S_{total} of the global model is provided by a system of three equations:

$$S_{total} = \begin{cases} S_{nupper}(d), & 2\lambda \leq d < d_{Pa} \\ A'd^{-2} + B'd^{-1} + C', & d_{pa} \leq d < \dfrac{2D^2}{\lambda} \\ \dfrac{P_{in}G}{4\pi d^2}, & d \geq \dfrac{2D^2}{\lambda} \end{cases} \tag{3.24}$$

with

$$S_{nupper}(d) = Z_0^{-1} \times E_{upper}^{\ 2} \ d \tag{3.25}$$

The electric field of the global model coincides with the estimated one for the near-field region at a distance up to d_{Pa}, as shown in Figure 3.11. The global model is given by the interpolation explained in this section when the distance has values between d_{Pa} and far-field distance, and from this far-field model validity limit, the electric field of the global model coincides with the far-field model.

In indoor environments, the global model of the radiated field is given by (3.17) and (3.22) for sector antennas and omnidirectional antennas, respectively. As indicated above, this approach is considered satisfactory for the estimation of the field as a function of distance in accordance to the objectives of the work.

The relevant auxiliary variables are the simulation range and the number of samples N_{sp} contained in this range. The value of the lower bound d_{min} takes values of λ and 2λ for indoor and outdoor antennas, respectively. In the outdoor case, the upper bound d_{max} should always be greater than the far-field distance, $d = 2D^2 / \lambda$. The number of samples reflects the model accuracy, and it is considered acceptable when its value exceeds 60,000 samples. The sampling interval is obtained at:

$$\Delta_{sp} = \frac{d_{max} - d_{min}}{N_{sp}} \tag{3.26}$$

In conclusion, an estimation model of the electric field as a function of distance from the antenna was

developed for three types of antennas: outdoor array antennas, sectorial and omni indoor antennas. The obtained values are related to one MIMO element or one carrier of an antenna operating in a given band, in the direction of maximum radiation. The performed approaches have in mind the worst-case perspective of EM radiation exposure: the BS resources are being fully utilised at the lowest frequency of the used band. In contrast, the environment around the antenna is neglected. The main input parameters of the model are the antenna dimensions, input power, gain, mobile communication system, input resistance and environment (outdoor or indoor), but other parameters can be changed, as N_{sp}, d_{max}, d_{min} or N_{el}.

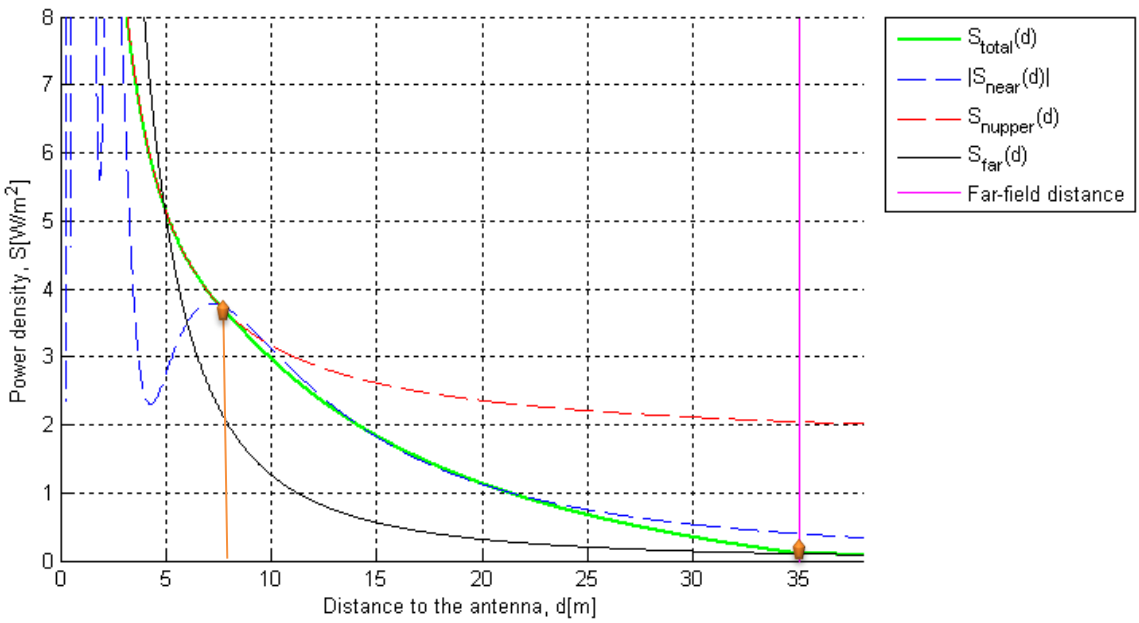

Figure 3.11 - Global model of the S by varying the d for a LTE2600 outdoor antenna.

3.6 Distance Evaluation Model

The intention is to determine the exclusion zone dimensions of a given BS from the global model described in the previous sections. Since the global model estimates for the direction of maximum radiation, the value of the front border of the exclusion zone, D_{front}, can be determined. The other dimensions of the exclusion region can be determined by applying correction factors to the value of D_{front}, as described in [MFRL02] for the model of the cylindrical exclusion zone. Thus, the proposed method is described below.

The formulation in (2.1) relates the reference levels with the electric field. Since this expression is a function of the distance d, D_{front} can be obtained:

$$\sum_{i>400MHz}^{300GHz} \frac{S_i(d)}{S_{ref,i}} \leq 1 \leftrightarrow (\ldots) \leftrightarrow d \geq D_{front} \tag{3.27}$$

where:

- $S_i(d)$: Power density at frequency i as a function of the distance;
- $S_{ref,i}$: Power density reference level from ICNIRP guidelines at frequency i.

One (2.1) can rewrite under the conditions of this problem, in particular regarding the number of carriers, number of MIMO antennas and communication systems installed in the same site (GSM900, GSM1800, UMTS, LTE800, LTE1800 and LTE2600):

$$R(d) \leq 1 \tag{3.28}$$

with:

$$R\ d = \sum_{i=1}^{N_s} N_{c,i} \times N_{M,i} \times \frac{S_{total,i}(d)}{S_{ref,i}} \tag{3.29}$$

where:

- N_s: Number of communication systems installed in the site;
- $N_{c,i}$: Carrier number of the communication system i;
- $N_{M,i}$: number of MIMO elements of the BS in the communication system i;
- $S_{total,i}(d)$: Power density of the system i obtained with the global model;
- $R\ d$: Exposure function.

The resolution of (3.29) as function of d has a significant computational complexity, since function $R(d)$ is the sum of N_s terms with a system of three equations to describe each term, in the outdoor case. Instead of manipulating the problem in this way, the iteration of d is proposed for determining which value of d is $R(d) \geq 1$, Figure 3.12. The value of D_{front} is given by the maximum value of d that verifies $R(d) = 1$. For the simulation range in an outdoor environment, d_{min} is equal to 2λ, where λ is the maximum wavelength of all the systems involved in the simulation; for indoor scenarios, d_{min} is equal to λ. In both cases, d_{max} should ensure that $d_{max} > D_{front}$.

When $D_{front} < d_{min}$, nothing can be concluded regarding the exact value of the region of exclusion, considering the limitations of the model. Note that in order to determine the value of D_{front}, it would be enough to use one of the methods presented in Chapter 2, which are valid for distances closer to the antenna, introducing excessive complexity to the work. The main input parameters of the Matlab program are $N_{c,i}$, $N_{M,i}$ and the input parameters of the electric field global model. Note that for an antenna/system without MIMO technology, $N_{M,i}$ is equal to one.

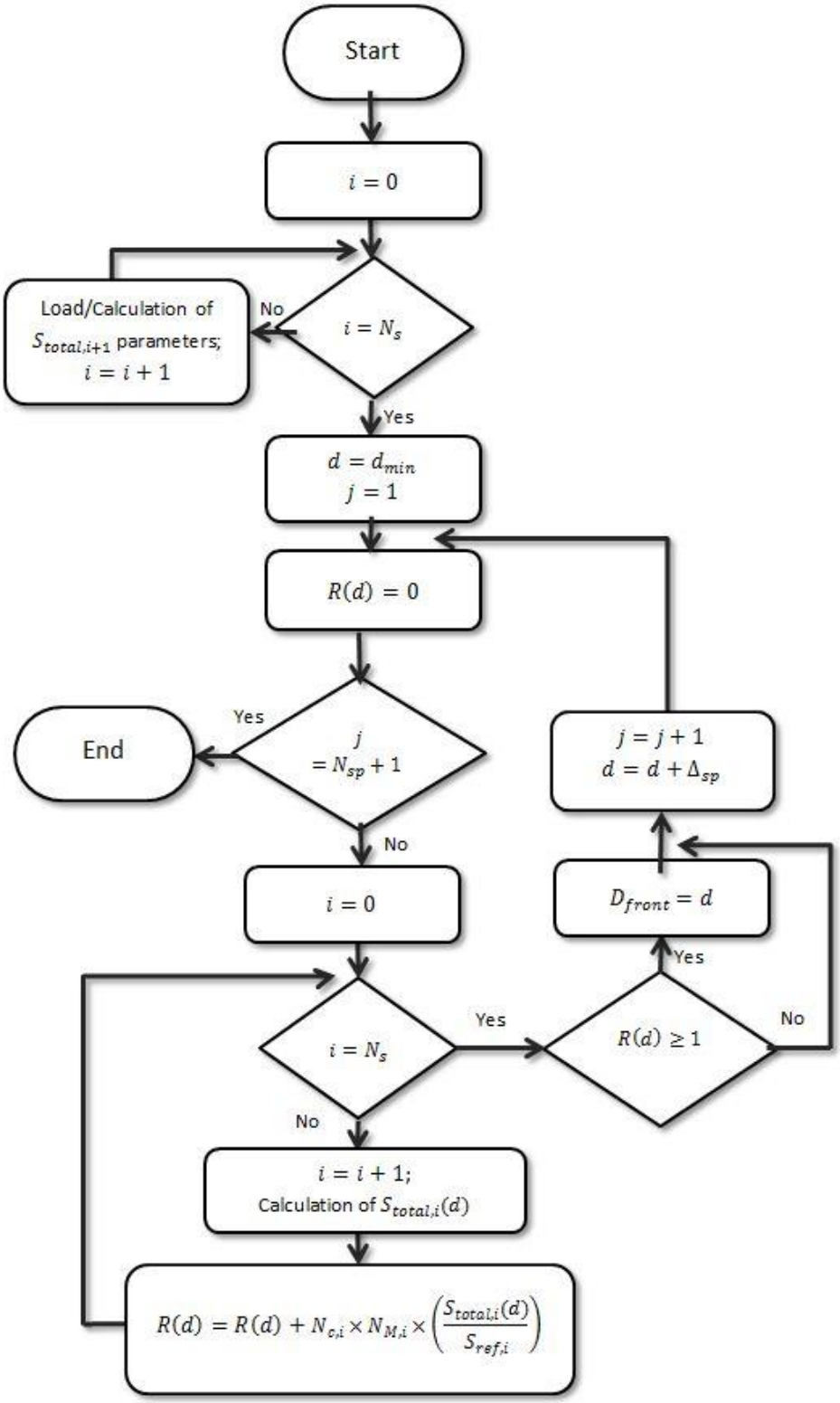

Figure 3.12 - Distance Evaluation Model program overview.

The power ratio is defined in order to analyze the power contribution that GSM, UMTS or LTE BS antennas have on the exclusion region of the total BS. This quantity has values between 0 and 1, being taken from (3.29):

$$power\ ratio_i = N_{c,i} \times N_{M,i} \times \frac{S_{total,i}(d = D_{front})}{S_{ref,i}} \quad (3.30)$$

The access to public areas close to a BS may require the definition of an exclusion region in other directions that are different from the maximum radiation, as shown in Figure 2.4. The model was developed for the direction of maximum radiation, perpendicular to the array alignment and with the axis in the mass centre of the antenna, so the values obtained for other directions are "extra" overestimated by the model.

In what follows a practical approach is presented: the back (D_{back}), bottom (D_{bottom}), top (D_{top}) and side (D_{side}) borders of the exclusion zone are determined by the method of cylindrical exclusion zone model [MFRL02]. From the analysis of the antenna radiation patterns, the normalised gains are determined as a function of the propagation direction, and these gains are then applied as correction factors (CF) to the D_{front} values obtained in the direction of maximum radiation. In multiband BSs, the normalised gain used corresponds to the smallest value found in bands/antennas (value that provides more gain). The directions analysed for each exclusion zone dimension are given in Table 3.2.

Table 3.2 - Directions analysed for the back, bottom, top and side border of the exclusion zone.

Bottom	Top	Back	Side
-90° (V plane)	90° (V plane)	-135°,180° and 135° (H plane)	-135°,-45°, -90°, 45°, 90° and 135° (H plane)

In order to take into account the tilt θ_{dt} used to maximize the coverage of a given antenna, the expressions of bottom and top border of the exclusion zone are the following [MFRL02]:

$$D_{bottom}{}' = D_{bottom}\ 1 + \sin\theta_{dt} \quad (3.31)$$

$$D_{top}{}' = D_{top} \cos\theta_{dt} \quad (3.32)$$

where:

- $D_{bottom}{}'$: Bottom border of the exclusion zone when BS downtilt is used.
- $D_{top}{}'$: Top border of the exclusion zone when the BS downtilt is used.

When the analysed BS radiates omnidirectionally, the horizontal plane has a circular exclusion region:

$$D_{side} = D_{back} = D_{front} \quad (3.33)$$

For BSs with omnidirectional and sectorial antennas, a distinct analysis to define D_{back} and D_{side} should be perform. The values of D_{back} and D_{side}, obtained by applying correction factors of sectorial antennas, are analysed and compared with D_{front} for omnidirectional antennas. D_{back} and D_{side} of

the BS are equal to the highest value found in these two results.

3.7 Program Assessment

In order to validate the developed model, evaluations were performed to the program using several tools and approaches. The results obtained with the model as well as all intermediate steps were confirmed performing calculations using Microsoft Excel and a calculator. Thus, different approaches were carefully chosen to cover all the calculations done by the program being concluded that the program works in accordance to the theoretical model.

The validation of the far-field model is performed by the calculation of the power density values: given the simplicity of (3.1), it was reversed and used to verify if the value of the power density estimated by the program led to the same value of distance with a calculator and Excel.

Excel capabilities are used to check if the estimated values of the field given by (3.3) led to satisfactory results of the program. Also the intermediate steps were verified, as the determination of element length and spacing between elements normalised to the λ. The results obtained from the program function in order to return the maximum of the near-field were analysed, with the aid of the graphical capabilities of Matlab. The interpolation process was also inspected, by performing several analyses with the same input parameters, with the aim of verifying that all the simulations returned the same values of the polynomial function coefficients. With Excel it was verified if the coefficients effectively performed a good fit to the field obtained by the near-field model. Similarly, the obtained results are analysed for the function $E_{upper}\ d$ ensuring that the worst case is provided in the vicinity of the antenna. Thus, one confirmed the results with the aid of Excel, and it was checked whether one of the points of intersection between $E_{upper}\ d$ and $|E_{env}(d)|$ coincide with the point which is verified as the largest difference of the values between $E_{fit}(d)$ and $|E_{env}(d)|$, Δ_{max}.

The global model was evaluated by the analysis to the obtained interpolation function, verifying that it intersects the near-field and far-field in points that are expected, by validating the continuity of the estimated global field. Also the intersection function of program that was developed to determine the intersection of $|S_{near}(d)|$ with $S_{nupper}(d)$ was tested, using several sets of mathematical functions and validating the results with the graphical capabilities of the calculator. Finally, it was checked whether the vector containing the total field was in accordance with the theoretical models, and several analysis were performed with the same parameters to verify if it led to the same results.

The program results for the estimation of exclusion zones were validated by the confirmation of the calculations, with Excel and a calculator. The robustness of the program was also analysed by checking if the cycles led to infinite loops, or if an unusual behaviour by the user could lead to critical scenarios.

Chapter 4

Result Analysis

Along this chapter, results are presented, analysed, and compared with data obtained from measurements and from the far-field approximation model.

4.1 Description of Scenarios

The divergence of the radiation levels between the sites without LTE (W/O LTE) and the same sites after the installation of this technology (W LTE) was evaluated by performing calculations that allow covering representative cases of BS antennas installations. The scenarios chosen for this purpose are presented below, characterising each site by typical antennas, powers delivered to antennas, and characteristics of communication systems.

The Table 4.1 describes the scenarios and the antennas used in each scenario (one cell sector), with the antenna characteristics presented in Annex A. Each scenario represents a given site, with the respective antennas topology before and after the introduction of LTE.

Table 4.1 - Description of antennas involved in each scenario.

Scenario	**Antennas**	
	W/O LTE	**W LTE**
SRural-1.a	• Sector GSM900 • Sector UMTS	• Sector GSM900/LTE800 • Sector UMTS
SRural-1.b	• Sector GSM900 • Sector UMTS • Sector GSM1800	• Sector GSM900/LTE800 • Sector UMTS/ LTE1800
ORural-1	• Omni GSM900/UMTS • Omni GSM1800	• Omni GSM900/UMTS • Sector LTE800/LTE1800
SUrban-1.a	• Sector GSM900 • Sector UMTS	• Sector GSM900 • Sector UMTS/LTE2600
SUrban-1.b	• Sector GSM900 • Sector GSM1800 • Sector UMTS	• Sector UMTS/LTE2600 • Sector GSM900/LTE1800
SUrban-2.a	• Sector GSM900/UMTS	• Sector GSM900/UMTS/LTE2600
SUrban-2.b	• Sector GSM900/UMTS • Sector GSM1800	• Sector GSM900/UMTS • Sector LTE1800/LTE2600
OUrban-1	• Omni GSM900/UMTS • Omni GSM1800	• Omni GSM900/UMTS • Sector LTE1800/LTE2600
IPanel-1	• Sector GSM900/GSM1800/ UMTS	• Sector GSM900/LTE1800/UMTS (both W and W/O MIMO)
IPanel-2	• Sector GSM900/GSM1800/ UMTS	• Sector GSM900/LTE1800/UMTS/LTE2600 (both W and W/O MIMO)
ICeiling-1	• Omini GSM900/GSM1800/ • UMTS	• Omni GSM900/LTE1800/UMTS (both W and W/O MIMO)
ICeiling-2	• Omini GSM900/GSM1800/ • UMTS	• Omini GSM900/LTE1800/UMTS/ • LTE2600MHz (both W and W/O MIMO)

It is assumed that the different antennas are installed side by side in the infrastructure that supports the BS, because this case is the most usual one. The case in which the antennas are installed vertically involves technical difficulties, as the need for a higher and more resistant mast. This study analyses three outdoor scenarios in rural environment (SRural-1.a, SRural-1.b and ORural-1), five urban outdoor scenarios (SUrban-1.a, SUrbnal-1.b, SUrban-2.a, SUrbnal-2.b and OUrban-1) and four indoor scenarios (IPanel-1, IPanel-2, ICeiling-1 and ICeiling-2). The LTE800 is typically associated to rural environments while LTE2600 is usually used in urban BSs, due to the band characteristics described in Chapter 2. Two of these outdoor scenarios have omni radiation: ORural-1 and OUrban-1. IPainel-1 and IPainel-2 scenarios represent the typical directional antennas that are installed on walls inside buildings, whereas ICeiling-1 and ICeiling-2 are Omni antennas installed on ceilings.

4.2 Scenario Results

The calculations were performed for the scenarios presented above, maintaining the same input parameters for each outdoor or indoor scenario. In the outdoor case, the antennas have 8 elements, with the typical maximum output power of the power amplifier (PA) presented in the Table 4.2. The input power of the antenna is obtained by subtracting 2 dB, the typical losses between the antenna and power amplifier.

Table 4.2 - Output power of the PA used in the simulation of outdoor scenarios.

System		Output power of the PA [W]
GSM	**900 MHz**	40
	1800 MHz	
UMTS		
LTE	**800 MHz**	2x40
	1800 MHz	
	2600 MHz	

The exclusion region values in the direction of maximum radiation, D_{front}, were obtained for different carriers typologies of GSM900 ($N_{c,GSM900}$), GSM1800 ($N_{c,GSM1800}$) and UMTS ($N_{c,UMTS}$): 1/1 ($N_{c,GSM900}/N_{c,UMTS}$) or 1/1/1 ($N_{c,GSM900}/N_{c,GSM1800}/N_{c,UMTS}$), 2/1 or 2/2/1 and 4/2 or 4/4/2. The results for each outdoor scenario are presented from Table D.1 to Table D.8 (Annex D, Section D.1). These results are also shown in Figure 4.1 to Figure 4.3. The power ratio of the mobile communication systems, which

allows analysing the influence of each system on the D_{front} distance, is presented from Figure D.4 to Figure D.11 (Annex D, Section D.2). The model results of the electric field estimation of each antenna and exclusion zone of the individual antennas/systems are shown in Annex B.

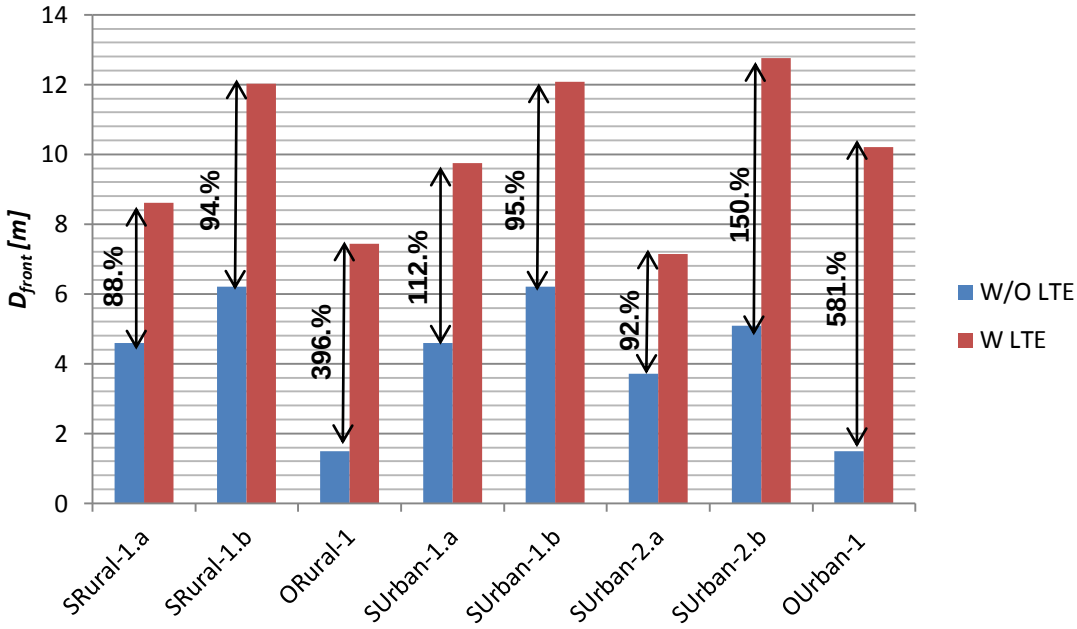

Figure 4.1 - Exclusion region results with the carrier configuration of 1/1 (or 1/1/1).

As it can be seen in the power ratio obtained for each outdoor scenario (Section D.2), GSM is the main responsible for the levels of EM exposure for the W/O LTE case, with radiated power greater than 48.3% of the transmitted total radiation, Figure D.9. LTE is the technology that contributes most to the distance of the exclusion zone after the introduction of this system in the BS (W LTE), since it presents higher values of radiated power, mainly due to the two MIMO elements. The exceptions found were scenarios SRural-1.a and SUrban-1.a with carrier configuration of 4/2 ($N_{c,GSM900}/N_{c,UMTS}$), where the power associated to GSM900 is significantly higher than LTE2600, Figure D.4 and Figure D.7. The influence that LTE has on the D_{front} value decreases with the increasing number of GSM and UMTS carriers.

According to the behaviour of the far-field model, it is expected that the low frequency systems contribute more to the D_{front}. In scenarios SUrban-2.a, SUrban-2.b, ORural-1 and OUrban-1, W/O LTE and one carrier for GSM and UMTS, the opposite occurs: GSM1800 or UMTS contributes more than GSM900, see Figure D.9, Figure D.10, Figure D.6 and Figure D.11. With the increase of frequency, array elements are closer to each other, and so the radiation levels are higher in the zone near the antenna compared to the systems of lower frequencies.

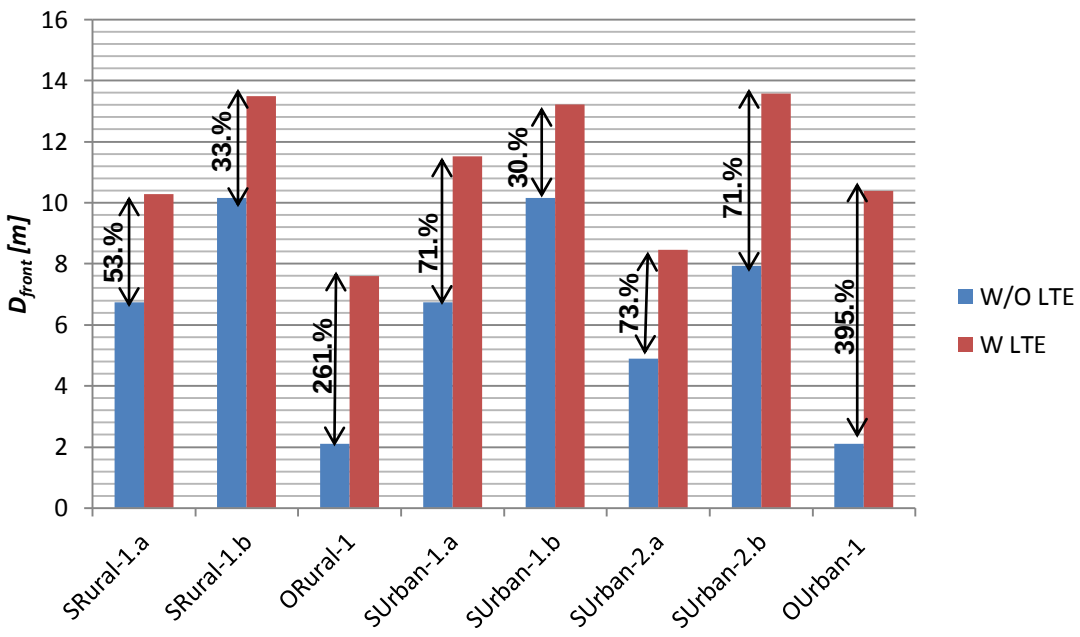

Figure 4.2 - Exclusion region results with the carrier configuration of 2/1 (or 2/2/1).

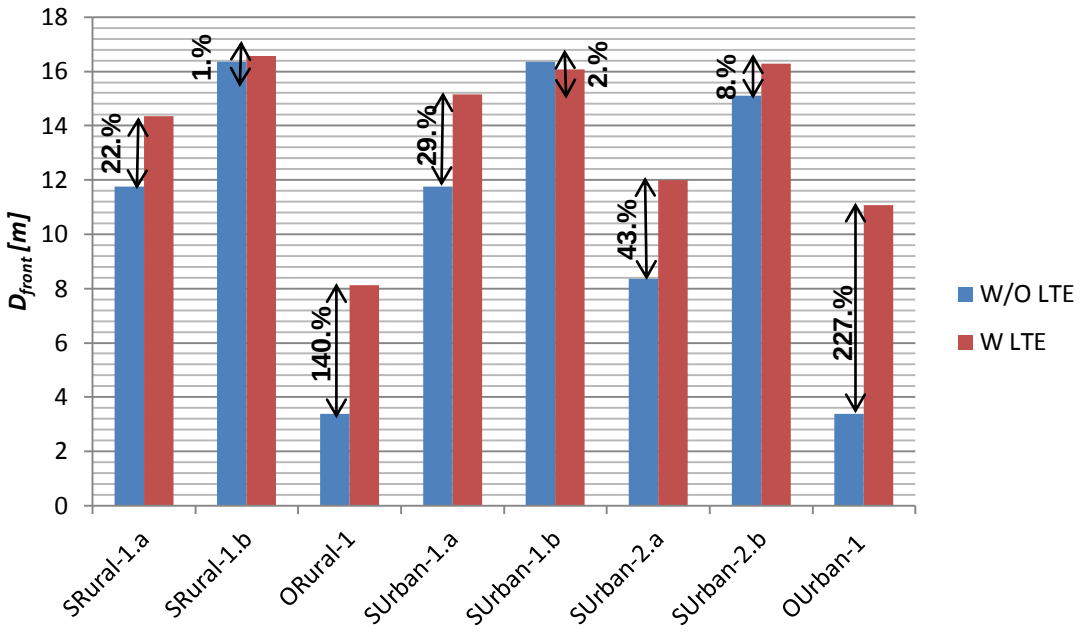

Figure 4.3 - Exclusion region results with the carrier configuration of 4/2 (or 4/4/2).

After the installation of LTE, D_{front} tends to be significantly higher than in the case of W/O LTE, with values 22% to 581% higher, mainly due to the use of 2x MIMO technology. SRural-1.b, SUrban-1.b and SUrban-2.b scenarios with carrier configuration of 4/4/2 ($N_{c,GSM900}/N_{c,GSM1800}/N_{c,UMTS}$) do not show such significant variations: +1%, -2% and +8% respectively. In these three scenarios, GSM1800 with 4 carriers is replaced by LTE1800 where there is a decrease of the exposure levels in the 1800 MHz

band. Scenarios OUrban-1 and ORural-1 present the highest variations of D_{front} between W/O and W LTE, where GSM and UMTS provide omnidirectional coverage. Note that the gain of the omnidirectional antennas is smaller than the gain of the sectorial ones, and the radiation levels are lower than in the sectorial case, when BSs are fed by the same input power. Thus, the introduction of LTE sectorial antennas causes a significant increase between 140% to 581% in D_{front} distance.

Taking into account that GSM is not typically installed with just one carrier, and rejecting the extreme cases previously studied, in sectorial outdoor environments D_{front} increases from 22% to 73% after the introduction of LTE. With the increasing number of carriers in GSM and UMTS, the difference of D_{front} between W/O LTE and W LTE decreases. When a practical analysis is required, these percentage differences between W/O and W LTE can be applied to the exclusion region W/O LTE if this value is known and whether the analysed BS are similar to those discussed scenarios.

In respect to the obtained values of the exclusion region, D_{front} has values between 4.9 and 6.7 m for the sectorial outdoor scenarios with carrier configuration of 2/1 and W/O LTE, and 8.5 to 11.5 m W LTE, Figure 4.2. With the 4/2 carrier configuration, initially D_{front} has values between 8.4 and 11.8 m, and 12.0 to 15.1 m in the W LTE case, Figure 4.3. For 2/2/1 configuration, D_{front} is equal to 7.9 to 10.2 and 13.2 to 13.6 m, for W/O LTE and W LTE respectively. In the case of 4/4/2, D_{front} W/O LTE has values between 15.1 to 16.4 m and 16.1 to 16.8 m for W LTE scenario. For Omni outdoor scenarios D_{front} W LTE and W/O LTE is equal to 2.10 to 3.39 and 7.59 to 11.07 m, respectively. The obtained values are large taking into account the results obtained by other studies.

In Table D.9 to Table D.11 (Section D.1), one shows the values of D_{front} for the suggested indoor scenarios, while in Figure D.12 to Figure D.27 (Section D.2) one presents the power ratios of the mobile systems. The typical values of EIRP used to obtain these results are shown in Table 4.3, assuming that the power in GSM is the same for all operators. The BSs that are not shared with other operators usually have values 6 dB higher than the ones shown in the Table 4.3 [KATH12b], [Opti12]. For the worst case scenario, the value that provides highest levels of power was used.

In indoor scenarios, GSM900 and GSM1800 contribute significantly to the levels of exposure to EMF due to the typical value of the powers involved in GSM, Figure D.12 to Figure D.27. Also in this case, LTE loses the influence on D_{front} with the increase of GSM and UMTS carriers. For the two scenarios with sectorial BSs, IPainel-1 and IPainel-2, D_{front} is less than λ_{GSM900} (32 cm) for both W/O and W LTE, regardless of the configuration of the carriers. In ICeiling-1 and ICeiling-2, D_{front} is less than 32 cm or decreases 8% to 18% due to the introduction of LTE. This decrease is due to the replacement of GSM1800 by LTE 1800 MHz with EIRP considerably lower, Table 4.3. The gain of the omnidirectional BSs is less than the sectorial BSs gain, which explains the higher values of D_{front} in the ICeiling-1 and ICeiling-2 scenarios.

Regarding the exclusion region in different directions of the maximum radiation, in Annex E (Section E.1) one presents CFs that allow to obtain the values of the D_{back}, D_{bottom}, D_{top} and D_{side} while in Section E.2 the results for each scenario are shown. In outdoor environments the values of D_{bottom}

and D_{top} are less than $2\lambda_{GSM900}$ (or $2\lambda_{LTE\,800MHz}$ if the BS is rural W LTE, where the greatest difference in the exclusion region between W/O and W LTE is equal to $2\lambda_{LTE\,800MHz} - 2\lambda_{GSM900} = 6$ cm).

Table 4.3 - Typical EIRP for indoor BS antennas shared by several operators.

System	$EIRP$ [dBm]
GSM	[24.8, 29.8]
UMTS	[18, 22]
LTE	

In the scenarios with sectorial BSs, the D_{back} also has values lower than $2\lambda_{GSM900}$ (or $2\lambda_{LTE\,800MHz}$) whereas in ORural-1 and OUrban-1 (W LTE) D_{back} has higher values due to the contribution of omnidirectional antennas. Note that for ORural-1 and OUrban-1 W/O LTE (such as ICeiling-1 and ICeiling-2 indoor scenarios), the definition of D_{back} and D_{side} is not relevant because the BS is completely omnidirectional. According to the analysed outdoor scenarios, D_{side} has values between 0.86 and 5.72 m. As explained in Annex E, the IPanel-1 and IPanel-2 scenarios have all the dimensions of the exclusion region below λ_{GSM900}, 32 cm.

After the quantitative analysis, it is intended to analyze the typical BS antennas installations and verify the impact of the results obtained in the definition of physical barriers. The installations analysed are described in Table 2.6 and the scenarios with one carrier for GSM are not analysed because these scenarios correspond to unlikely situations. Note that the model results correspond to the worst case, where the BS has the maximum load with the most of the GSM, UMTS and LTE resources being used by MTs.

Considering outdoor scenarios, the dimensions of the exclusion region for D_{bottom} and D_{top} do not present any need to define the limitation barriers regardless of the BS installation infrastructure due to its reduced values: lower than 0.70 m (see Section E.2). With the use of downtilts, the value of D'_{bottom} and D'_{top} is further reduced in accordance to (3.31) and (3.32), for any tilt angle.

D_{back} has highest values between 1.47 and 3.39 m for the scenarios with omnidirectional antennas, ORural-1 and Ourban-1. In rural environments, these values do not justify the definition of barriers, but in the Uroof or Upole typology it may need this requirement. If the BS is installed on a roof-top that can be accessible or if the pole is close to a building (or an area with higher ground level to the BS), it should be taken into account whether these accessible zones comprise the D_{back} exclusion region. However, in these two scenarios, the introduction of LTE (W LTE) provides a reduction in the exclusion region, not being necessary to change the barriers defined for W/O LTE. Note that the scenarios studied are formed by two or more antennas for each sector, being typically impracticable in

Upole installations due to the required robustness for the infrastructure installation that supports the antennas. Furthermore, the input powers of this analysis are very high for heights as small as those of the Upole (3 to 5 m). For other scenarios, Ufaçade causes no danger of exposure due to the attenuation caused by the concrete (between 10 and 20 dB) [Corr12a].

For D_{side} the concern may be the approximation of the site to buildings (Upole case) and particularly the balconies and windows in the Ufaçade typology. In Uroof it depends on the type of access that the public has in the lateral zones of BS: If these zones are accessible (terrace for example), the increase of D_{side} with the introduction of LTE should be taken into account. Also in the rural case, D_{side} is not considered a problem due to the typical heights of BSs. The highest value of the D_{side} (5.72 m) is verified to SUrban-1.b W/O LTE (4/4/2 carrier configuration), but this distance is reduced to 5.14 m after the installation of LTE. The SUrban-1.a scenario (4/2 carrier configuration) presents the highest value after the LTE implementation: $D_{side} = 5.31\ \mathrm{m}$. If an access zone is the high level of the BS but at distances greater than about 5 m from the BS side, the public will always be protected regardless of the scenario.

The direction of maximum radiation is typically without obstacles near the BS antennas, in “free space”, to provide efficient coverage. For small tilts, the definition of barriers at ground level may not be relevant, due to the height at which outdoor antennas are installed (from 3 m). But with the use of high downtiltsm, the inclination that the main lobe suffers should be taken into account, Figure 4.4. The inclination of D_{front} can be described according to the D'_{front} distance and h_a height:

$$D'_{front} = D_{front} \times \sin\ 90^o - \theta_{dt} \tag{4.1}$$

$$h_a = D_{front} \times \cos(90^o - \theta_{dt}) \tag{4.2}$$

Considering the typical height of a person as 1.8 m, [Corr12b], the following can be concluded: for the scenarios under study, one does need to place physical barriers at ground level if the antennas are at a height equal or higher than $1.8 + h_a = h_{\min}$ m, where $h_{\min}$ is the decision height that defines the necessity of installation of physical barriers at the front of the BS. Thus, when $h_{ant} < h_{min}$ the exclusion zone in the direction of maximum radiation,D'_{front}, corresponds to the distance necessary to define the physical barriers. Table D.18 to Table D.25, Annex D, Section D.3, show the results of D'_{front}, h_a e h_{min} for each outdoor scenario with a downtilt of 12º, considering this value as the typical maximum downtilt. The follow approximation is used: all antennas of the BS has the same tilt and are significantly close to each other.

According to the results in Table D.18 to Table D.25 and regardless of scenario, BSs installed at heights greater than about 5 m do not have the need to install physical barriers at the ground level. The typical height of a BS in a rural environment takes values between 20 and 50 m, being always ensured that the rural scenarios with the characteristics presented in this work do not require physical barriers at the ground level, since the exclusion region is confined to heights significantly higher.

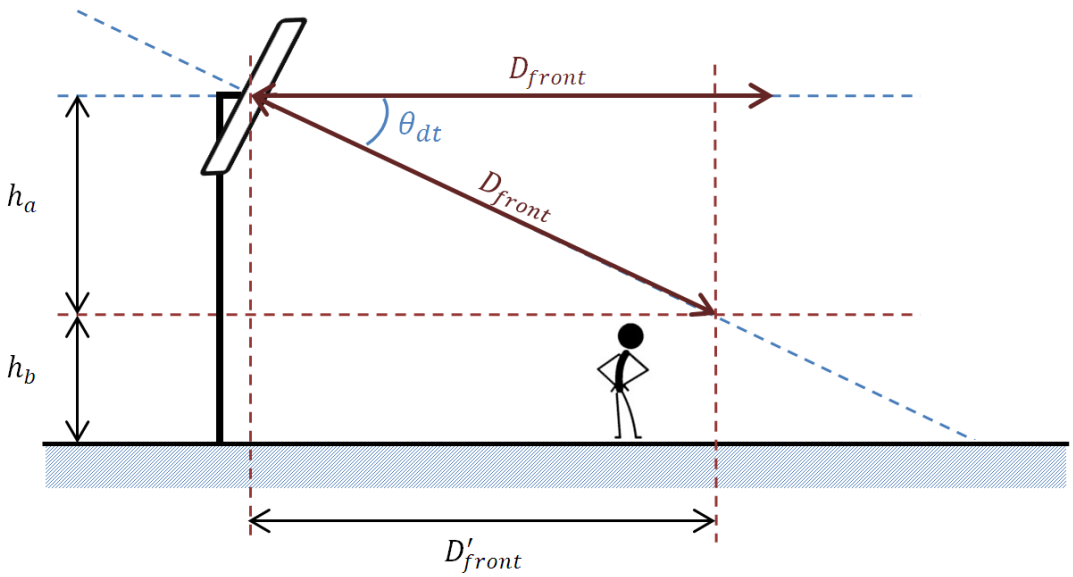

Figure 4.4 - Downtilt influence in the definition of the D_{front} exclusion region.

In same way, there is no need to define physical barriers if an urban BS height exceeds 5 m in areas accessible to the public (such as the street level) for both W/O LTE and W LTE sites. A careful analysis should be performed for BSs at heights lower than 5 m, verifying the common characteristics of the BS with the analysed scenarios. The two installation typologies that might lead to EM exposure problems at the street level are Ufaçade and Upole due to the typical minimum height of 3m. It is emphasised again that for the BSs at reduced heights, the power needed to cover the cell should be smaller in comparison with those used in this study (then with smaller exclusion zones) and the tilts will be practically null to increase the coverage area.

The results for ORural-1 and Ourban-1 scenarios present overestimated values of h_{min} for W LTE and have no practical meaning for W/O LTE, because the omnidirectional antennas usually are not installed with tilt to increase coverage. Neglecting these two scenarios, the maximum difference of h_{min} W/O LTE and W LTE is about 1 m. This means that the exclusion region may be 1 m closer to the ground level after LTE implementation.

The same approach is valid for the Uroof typology, being necessary to verify the impact than D_{front} has in the front building of a given BS, and to verify also the exposure that people will be subject at ground level.

First, the height that the antenna has at the street level is analysed. It assumes a building with 3 floors (approximate average number of floors in dwellings built in Lisbon in 2009 and 2010 according to [STAT09] and [STAT10]), with a height of 3 m each floor, [Corr12b], and a BS installation infrastructure with minimum height of 2 m (Table 2.6), then the BS will be $3 \times 3 + 2 = 11$ m above ground. Even assuming a high downtilt, the exclusion zone is not typically a problem at street level.

In the front building of a BS installed according to the Uroof typology, the top floor is exposed to more EM radiation from the BS, by assuming that the two constructions are identical, Figure 4.5. With a

downtilt of 12º, and a BS infrastructure 2 m height, the exclusion zone is not exceeded in the top floor of frontal building, regardless of the distance to the BS, such as discussed above. The attenuation that the signal suffers to cross the glass (1 to 2 dB) and concrete (10 to 20 dB) also provides additional reasons for that to happen.

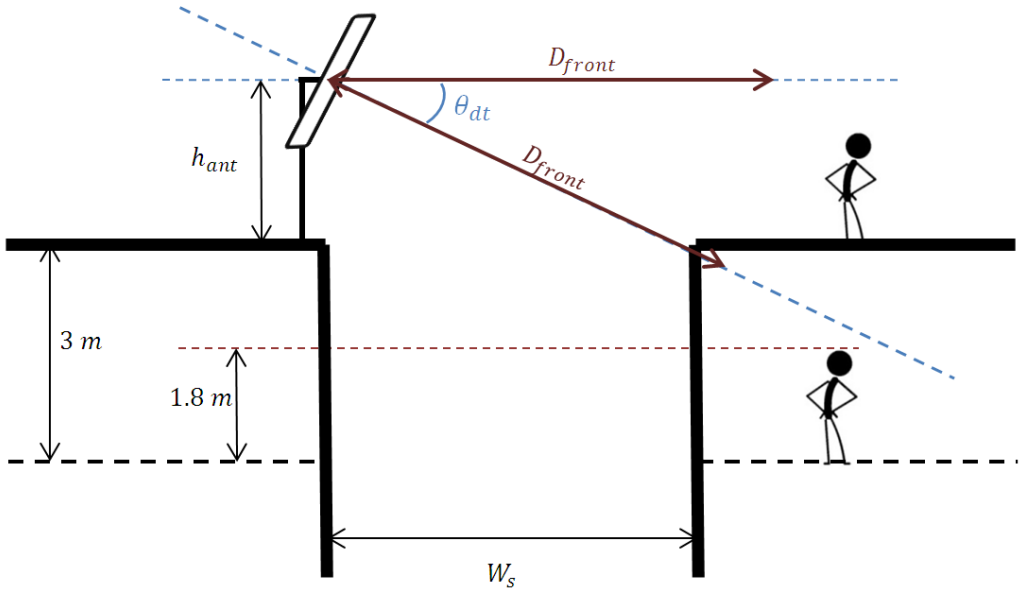

Figure 4.5 - Analysis of the D_{front} impact in Uroof installations.

At the roof level of the frontal building, the width of the street should be taken into account. For this case, BSs with small tilts provide more EM exposure, and thus a greater D_{front} exclusion zone. If the area of roof level is within easy reach, and if this area is at distances less than D'_{front} from the BS, the implementation of physical barriers can be required. Note that this hypothetical case where the antenna is 2 m above the roof, with a frontal building near the BS, is not advantageous in terms of coverage. Typically the BS is at a height and/or a distance significantly higher from a building or other frontal obstacle.

In the IPanel-1 and IPanel-2 scenarios, the exclusion region results have relatively small values, with no major changes with the introduction of LTE. For indoor sector antennas with similar characteristics to the studied scenarios, there is no need to define barriers around the antenna. The same conclusions can be obtained for the indoor omnidirectional antennas, where in the ICeiling-1 and ICeiling-2 scenarios the exclusion region decreases with the implementation of LTE.

The results of exclusion region appear to be extremely high values, especially when the definition of physical barriers is analysed in urban environments. In addition to the EMF estimation model achieves results for the worst-case scenario, the distance evaluation model estimates the exclusion region of all antennas simultaneously and with the direction of maximum radiation as to coincide at the same point, which affords that to happen. When a zone accessible to the public is inside an exclusion region

estimated by the model, the exclusion regions of the isolated antennas can be analysed separately if they are significantly far apart.

It is also worth mentioning, the model results of the isolated antennas/systems follow the same conclusions drawn from the BS scenarios. The exclusion region increases with the increase in the number of active carriers, with MIMO elements number, and with the decrease of the system frequency. D_{front} for outdoor antennas with a single mobile system has values between 2.47 m (UMTS antenna with one carrier, Table B.7) and 8.77 m (GSM900 antenna with four carriers, Table B.3). For the multi-band outdoor antennas, D_{front} is equal to 4.89 to 11.98 m, as seen in Sector B.4 to B.10 and Sector B.13. Omni outdoor antennas have D_{front} values between 1.21 and 2.24 m, Table B.32 and Table B.34, while for indoor environments, the highest value of D_{front} is obtained for GSM900 system with 4 active carriers: 0.63 m, Table B.40.

4.3 Input Power Variation

The study of the power impacts in the exclusion region, calculations were performed by iterations of the input power value of the antennas on four work scenarios: SRural-1.a, SUrban-1.a, IPanel-1 (W MIMO) and ICeiling-1 (W MIMO). It was taken into account that the input power range cannot have values significantly higher than the maximum transmitter output power, Table 2.1 to Table 2.3. The input power in outdoor environments varies between 37 and 47 dBm, while the two indoor scenarios have range variation from 34 to 38 dBm. As simplification, all mobile systems have the same value of input power.

The obtained results for SRural-1.a are presented in Figure D.1 (or Table D.12), and in Figure 4.6 (or Table D.13) the results for the SUrban-1.a scenario are shown. In both cases the evolution of D_{front} as a function of input power follows the same behavior. With 37 dBm of input power, D_{front} has lower values than 3.75 m. With the increase of input power, the difference in D_{front} between W/O LTE and W LTE progressively increases until 42 or 44.5 dBm of input power, where it begins to decrease, Table D.12 and Table D.13 (Section D.1). At an input power of 47 dBm the exclusion region has values between 8.5 and 21.62 m.

The transmitted power that each system radiates at a distance of D_{front} according to EM exposure is different for the two outdoor scenarios. In the SRural-1.a scenario, the input power variation does not change significantly as observed in the previous section for 2/1 and 4/2 carrier configuration, Figure D.29 and Figure D.30 respectively (Section D.2). However, for the 1/1 configuration, there is a change in the contribution of GSM and UMTS in D_{front} definition: UMTS in case W/O LTE contributes more than GSM 900 when the input power is less than 39.5 dBm, Figure D.28. Between 39.5 and 47 dBm, GSM is the main responsible for the exposure levels, but following the trend observed in Figure D.28, GSM and UMTS power ratio may intersect powers greater than 47 dBm. With the implementation of LTE800, GSM and UMTS have power ratios that tend towards the same value with the power

increase, expecting that this value is reached for an input power above 47 dBm.

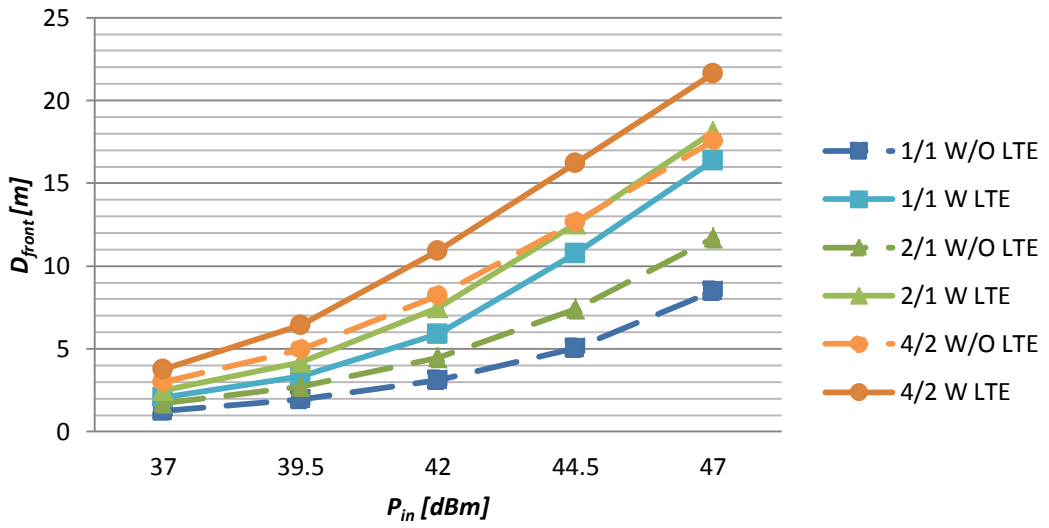

Figure 4.6 - Power impact in the D_{front} value for SUrban-1.a scenario.

For the SUrban-1.a scenario, the power ratio evolution in the 1/1 carrier configuration is analogous to the SRural-1.a case, Figure D.31. With the 2/1 configuration and W LTE, GSM900 and LTE2600 have nearly identical power ratio values up to 39.5 dBm, and from this value LTE influence increases and GSM decreases, whereas the UMTS power ratio does not suffer abrupt changes, Figure 4.7. As it can be seen in Figure 4.8, for the 4/2 configuration the opposite occurs: with the increase of input power, the GSM power ratio, which is initially higher than the LTE, one decreases while that the LTE contribution on exposure levels increases.

Also the behavior of D_{front} in indoor scenarios is similar, where the exclusion region evolution is close to linear with the growth of the input power, Figure 4.9. D_{front} results as a function of input power for the IPanel-1 scenario can be seen in Table D.14 or Figure D.2 (Section D.1), and the ICeiling-1 results in Table D.15 or Figure 4.9.

With the 4/4/2 carrier configuration, D_{front} has significantly higher values than in the other two configurations, although the introduction of LTE reduces the exclusion zone at 6 to 8% for the analysed input power range. The exclusion region increases 11 to 13% with the implementation of LTE for the 1/1/1 configuration, whereas D_{front} is not changed from W/O LTE to W LTE in the 2/2/1 configuration case, because in the 1800 MHz band the GSM1800 system with 2 carriers is removed and LTE1800 with two MIMO elements is introduced. From the radiation viewpoint, the LTE BS Transmits the same EM exposure levels than GSM1800 (with two carriers).

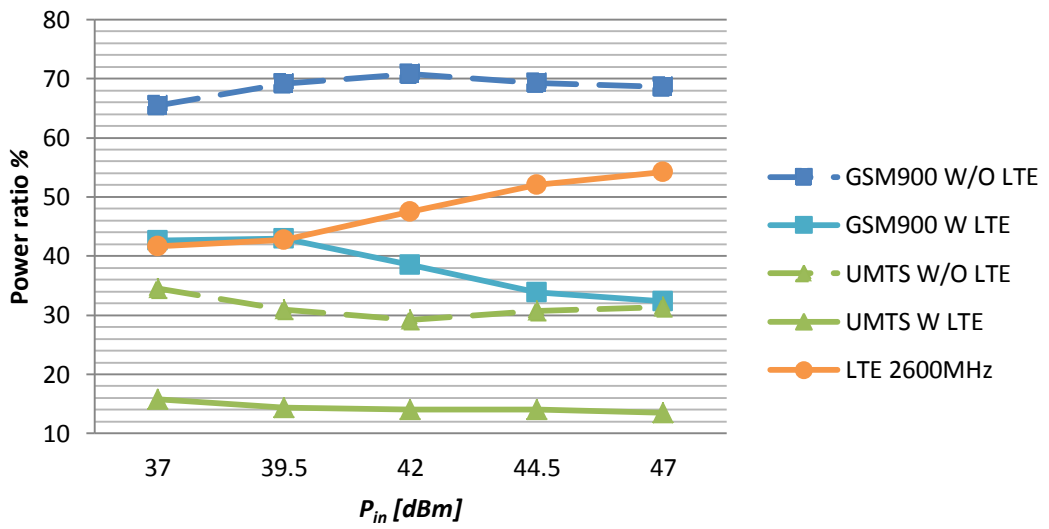

Figure 4.7 - Power ratio results with the variation of input power for SUrban-1.a (2/1).

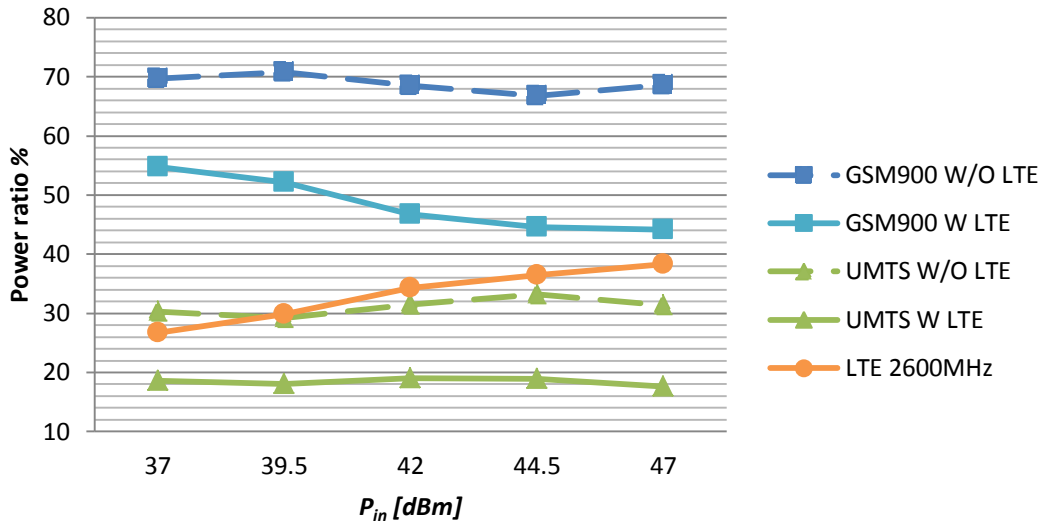

Figure 4.8 - Power ratio results with the variation of input power for SUrban-1.a (4/2).

The use of input power greater than 34 dBm in all systems leads to significantly high values of D_{front}, exceeding always λ_{GSM900}, in the ICeiling-1 scenario, Figure 4.9. As discussed in the previous section, UMTS and LTE typical input powers are significantly less than those considered in this section, this approach being relevant to study the evolution of D_{front} with the power variation.

The power ratio of GSM, UMTS and LTE do not change with the modification of power input, nor IPanel-1 and ICeiling-1 scenarios, Figure D.32, Section D.2. GSM900 is the main responsible for the EM exposure for a distance equal to D_{front} with levels of radiated power exceeding 50.4% in comparison with the other systems, excluding the 1/1/1 case W LTE where LTE1800 has exposure

levels 1.3% higher than GSM900.

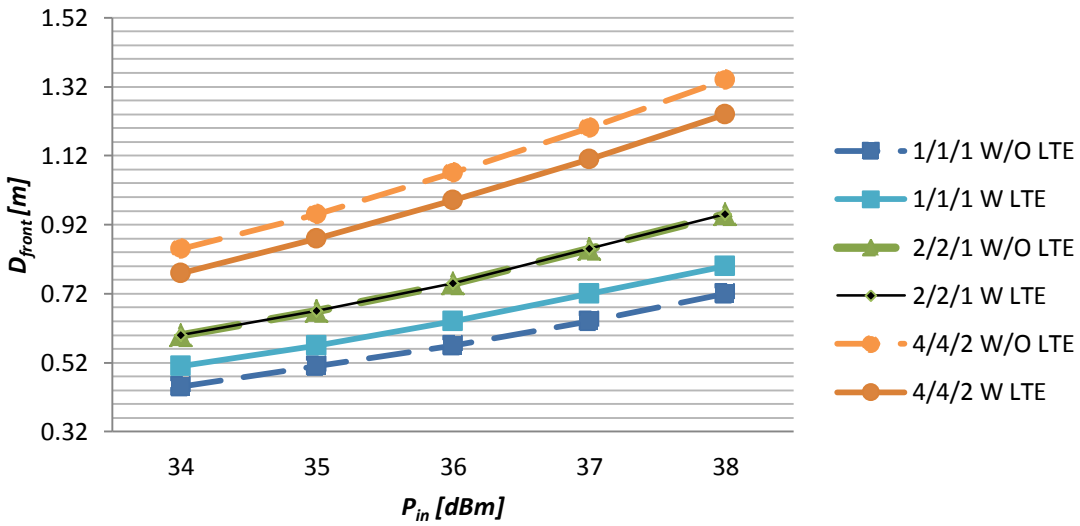

Figure 4.9 - Power impact in the D_{front} value for ICeiling-1 scenario.

For the antennas that are used in SRural-1.a, SUrban-1.a, IPanel-1 (W MIMO) and ICeiling-1 (W MIMO) scenarios, the results of these antennas with the power variation are shown in Annex B. The exclusion region of a single antenna/system tends to increase with the increase of the input power, as expected after analysing the scenario results.

4.4 Influence of the Antenna Element Number

The intrinsic characteristics of the antennas influence directly the level of radiated EM fields, therefore being relevant to study the impact that the change of these features causes in the estimation of exclusion region. One of these features is the number of array antenna elements, N_{el}. Calculations were performed varying 4, 6, 8 or 10 elements for a rural and urban scenario (SRural-1.a and SUrban-1.a respectively) where all the antennas of the BS have the same number of elements. In real situation the array gain of dipoles tends always to increase with increment of N_{el} as can be seen in Figure C.1 [Corre12a]. Since manner and to simplify the analysis, it is assumed that the gain is equal to the directivity of Figure C.1 when the d_a is equal to λ, neglecting the height of the BS antenna.

As it can be seen in Figure 4.10 (SUrban-1.a scenario) and Figure D.3 in Section D.1 (SRural-1.a), results in the two scenarios show the same tendency: the exclusion zone decreases with the increase of the N_{el} and the same is verified for the simulation of isolated antennas, see Annex B. The exclusion zone increases for N_{el} equal to 8.

Performing an analysis of decrease of the N_{el}, the antennas that have less elements, are fed by a higher element EIRP. Using a higher power and gain for an element provides the increased levels of EM field in the area next to the BS, because the field additive contribution of the element travels a d_i shorter distance than one element of an array with more elements that is farthest from the mass center of the antenna. However, the antenna gain significantly influences the results when the number of elements is equal to 8 or 10, breaking the decreasing tendency.

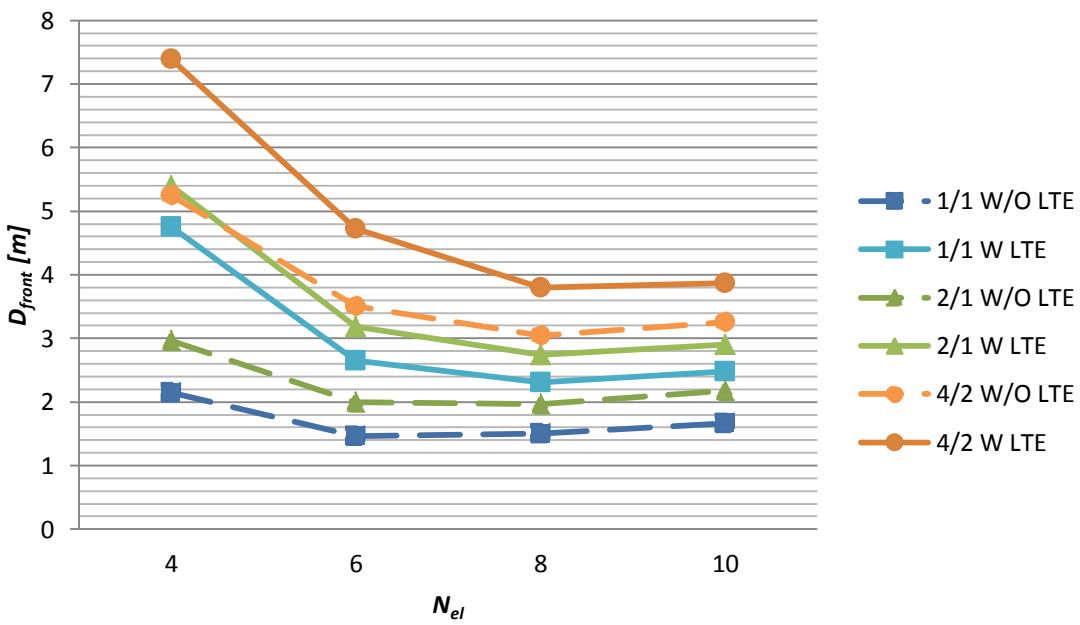

Figure 4.10 - D_{front} values with the N_{el} variation for SUrban-1.a.

One does not see a clear trend of the evolution of D_{front} difference between W/O LTE and W LTE varying the number of elements. In urban scenario the smallest difference between these two distances occurs for N_{el} equal to 10, with a D_{front} increase of 19 to 121% when LTE is introduced in the BS (see Table D.17), while in the SRural-1.a scenario the minimum difference is obtained for 4 elements with values of 18 to 73% (Table D.16).

For the two scenarios W/O LTE, the GSM900 contribution on EM exposure at a distance D_{front} increases with increasing N_{el} whereas the opposite occurs in UMTS, Figure 4.11. In SRural-1.a scenario W LTE, the power ratio of LTE800 has an increase pattern as a function of the N_{el} and the UMTS ratio has a tendency to decrease. With GSM, the power ratio seems to have a behaviour almost stable with the variation of the N_{el}, Figure D.33 to Figure D.35, Section D.2.

In SUrban-1.a, the GSM power ratio is increased monotonously as a function of the N_{el}, while LTE2600 has a decreasing behavior, occurring a maximum (and minimum of GSM) for N_{el} equal to 8. The influence of UMTS on the definition of the exclusion region is approximately constant with a small negative slope and approximate values at 20%, Figure D.36, Figure 4.11 and Figure D.37.

The near-field model assumes that each far-field of an element contributes additively to the total EM field. As the field strength is decreasing as a function of frequency for the far-field model, in systems with lower frequencies (GSM900 or LTE800), the contribution to the EM exposure tends to be more significant with the increase in N_{el}, while the power ratio of UMTS or LTE2600 (higher frequencies) decreases with the increase of N_{el}.

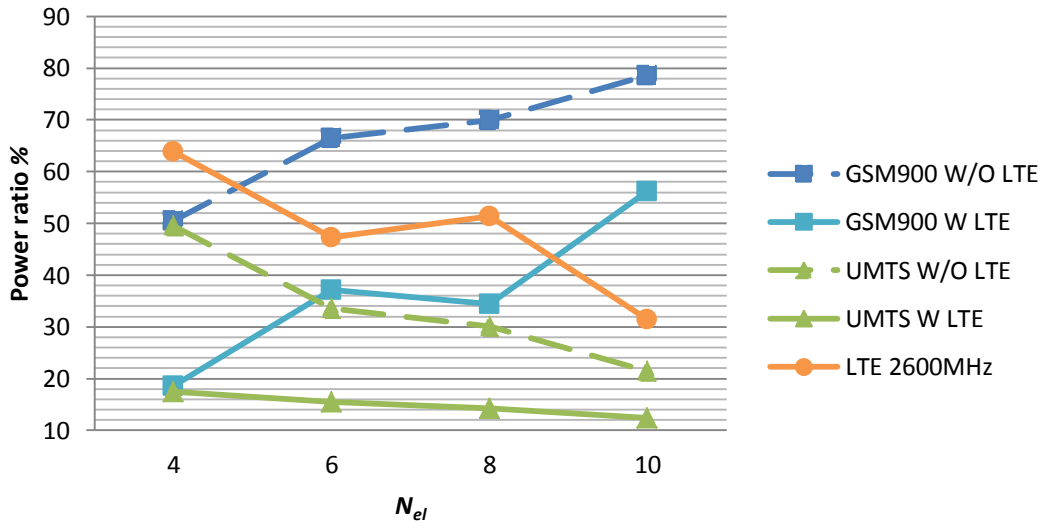

Figure 4.11 - Power ratio results with the variation of N_{el} for SUrban-1.a (2/1).

4.5 Comparison of Results

Measurements allow analysing the behaviour of the real electric field and its impact on EM exposure, and also comparing the measured data with the results of the theoretical model of this work. The conducted measurements were focused on public access areas in zones close to the BSs. A spectrum analyser with an omnidirectional antenna was used as measuring equipment, since the analyser allows discriminating clearly the contribution of each carrier [Nard07]. This equipment records digitally the collected data, and later the data can be processed automatically through the help of Excel or Matlab software. The model is also compared with results of [OFRC05].

The procedure to take each measurement campaign starts with the calibration of the measuring equipment, and then the BS should be characterised by the factors influencing its radiation as well as the environment surrounding it. The measurement points coincide with imaginary radials around the BS/antennas separated by about 45º. The number of points on each radial should be sufficient to describe the field behaviour as a function of distance, where the measured average values are recorded for 1 minute for each mobile communication system, in order to obtain a good resolution in each band. Note that the recommendations discussed in Section 2.5 advise the value of 6 minutes for

the duration of each measure, for the comparison with exposure limits. Nevertheless the decrease in time to 1 minute is sufficient to obtain values with an error less than 10%, which is considered acceptable [OSLA08].

The BSs where measurements were performed are shown in Table 4.4 together with the corresponding scenarios. All measurements were performed at BSs after installing LTE. The data obtained from measurements, as the average value of the signal and the standard deviation for each measurement point and each band (σ_{GSM}, σ_{UMTS} and σ_{LTE}), and as the layout of the measurement site are presented in Annex F. Note that it is considered that all carriers are active, being recorded only the value of the carrier with the greater intensity in GSM900 (the analysed antennas had only one carrier in UMTS and four in GSM900). In the outdoor case, the output power of the PA is equal to 40 W for GSM and UMS, and 2 x 30 W (BS1 and BS2 sites) or 2 x 40 W for LTE (BS3). For the BS4 scenario, the EIRP of GSM is equal to 23.1 dBm, while UMTS and LTE EIRPs are equal to 9.9 dBm. In the BS5 installation, the EIRP is equal to 29.6 and 15.7 dBm for GSM and UMTS/LTE, respectively.

Table 4.4 - General characteristics of the BS's that were targeted measures.

BS's	Environment	Scenario	Installed Systems	Measurement sites
BS1	Outdoor	SUrban-1.a	GSM900, UMTS and LTE2600	Back side of the BS on the building terrace
BS2				
BS3		SRural-1.a*	GSM900, UMTS and LTE800	Front side of the BS on the building terrace
BS4	Indoor	ICeiling-1 (W MIMO)	GSM900, UMTS and LTE1800	Front side of the BS
BS5		IPanel-1 (WO MIMO)		

*BS antenna described in Table A.17

In Figure 4.12, the progress of $R(d)$ obtained from measurements and estimated by the theoretical model is presented for the BS1 installation. As the measurements were performed practically at the antenna level, Section F.1, the calculation take the radiation pattern in the H plane into account, by applying the normalised gains (Section E.1) in the total gain of the antenna. The results presented are related to four GSM carriers. The measured exposure levels are significantly lower than the theoretical values: the minimum difference of $R(d)$ between measured data and model data is equal to -16.34 dB. The behaviour of $R(d)$ tends to decrease with the increase of the distance to the BS, as it can be seen in the model results. As the sectorial antenna gain is higher in the direction of 135° and 225° than 180° in the horizontal plane, the measured EMF levels at 1st or 3rd set data would be higher than the 2nd set; this does not always occur, and may be due to reflections or other factors that influence the measurement process.

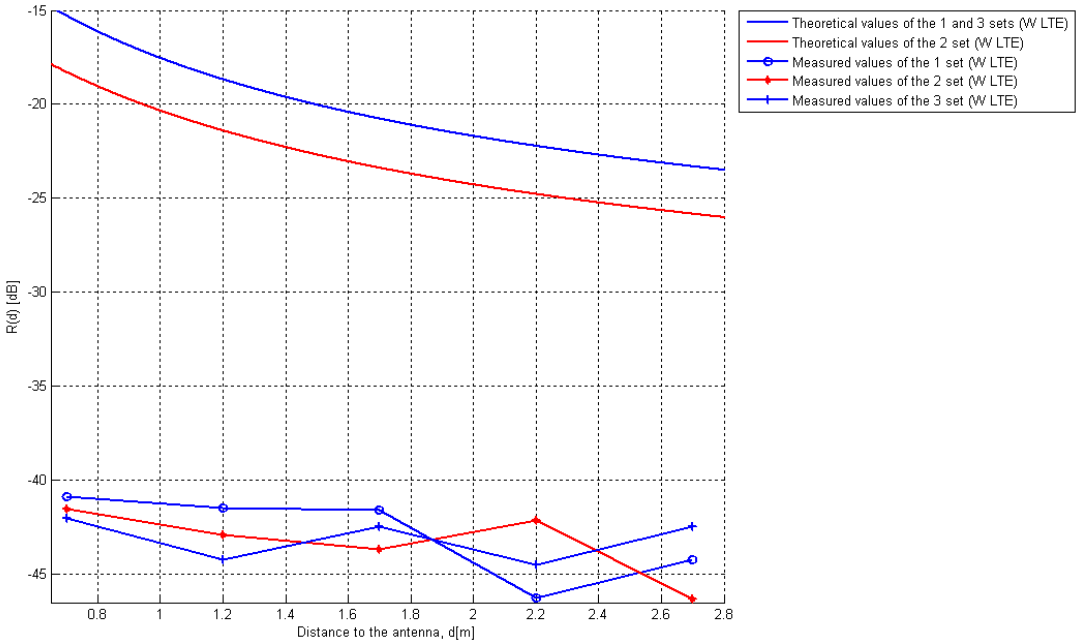

Figure 4.12 - Measured and theoretical results of R as function of d, for BS1 W LTE.

To study the impact of LTE installation, the simulation of this scenario without the contribution of the LTE system was performed, assuming a BS with co-location of GSM900 and UMTS. Note that the measurements were performed in environments W LTE, and for all other scenarios the procedure is the same. The BS results are presented in Figures 4.13 and 4.14. The difference between $R(d)$ W/O and W LTE in the obtained measurement data has values between 0.4% and 12.1%. With the theoretical values for the same distances, the difference is much greater: about 95% for the 1st and 3rd set, while for the 2nd set it ranges between 53% and 70%. This significant difference between the theoretical and measurement results suggests that the model is overestimating the influence of LTE on EM exposure. Anyway, measurements were not performed at the front of the BS antennas, where it is expected that the model is more accurate.

BS2 antennas are about 2 m height, and the measurements were performed at the back of the BS, see Section F.2. In this case, the three dimensional radiation pattern should have been analysed for the theoretical estimation of $R(d)$. As antenna manufacturers do not provide this information, it was only considered the H plane, because this plane provides higher exposure levels than the V one.

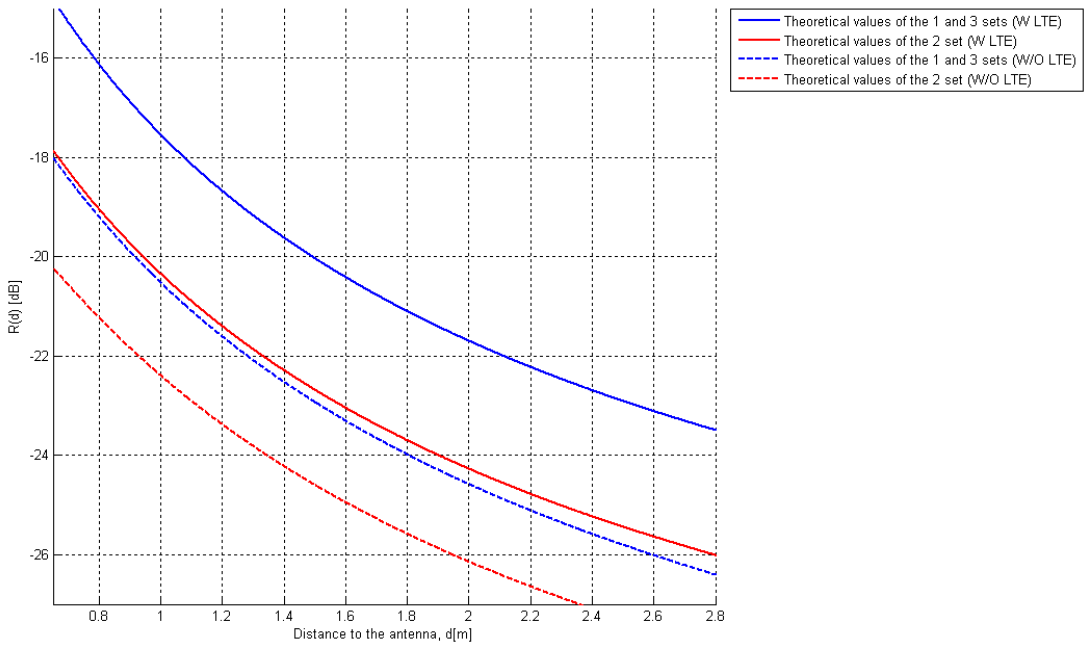

Figure 4.13 - Theoretical results of R as function of d, for BS1 and BS2 W and W/O LTE.

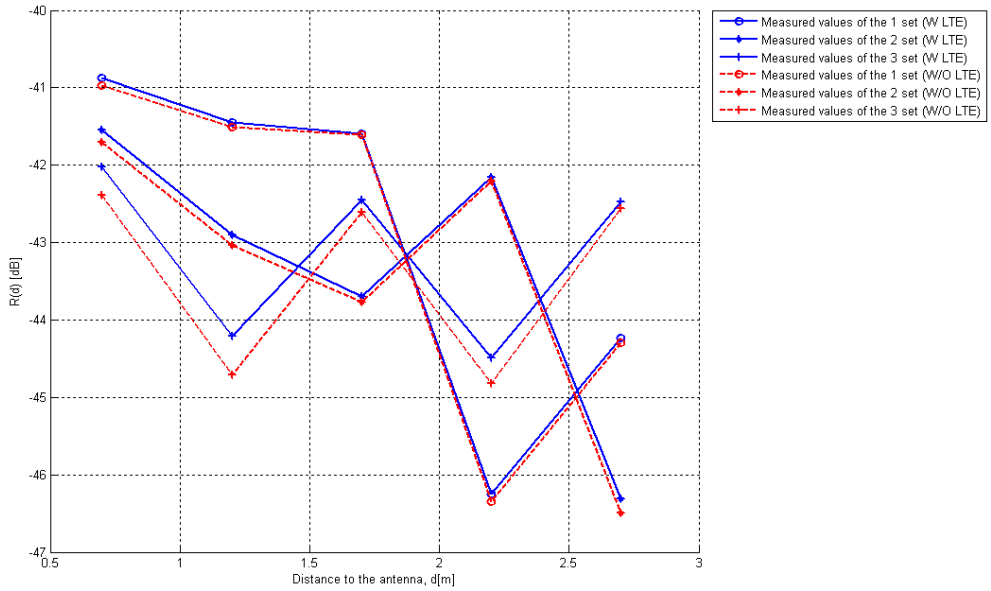

Figure 4.14 - Measured results of R as function of d, for BS1 W and W/O LTE.

The $R(d)$ values obtained from measurements and the model can be seen in Figures 4.13, 4.15 and 4.16. The minimum difference between the theoretical and measured results is equal to -9.85 dB, and the measured levels are below 30.07 dB the exposure limits. The measured values for the 1st set data are significantly larger than the 2nd or 3rd sets. This can happen because the azimuth of the two antennas is not exactly the same, or due to reflections that are being detected in the radial of the 1st set. This fact also increases the error in the approach made by the theoretical model.

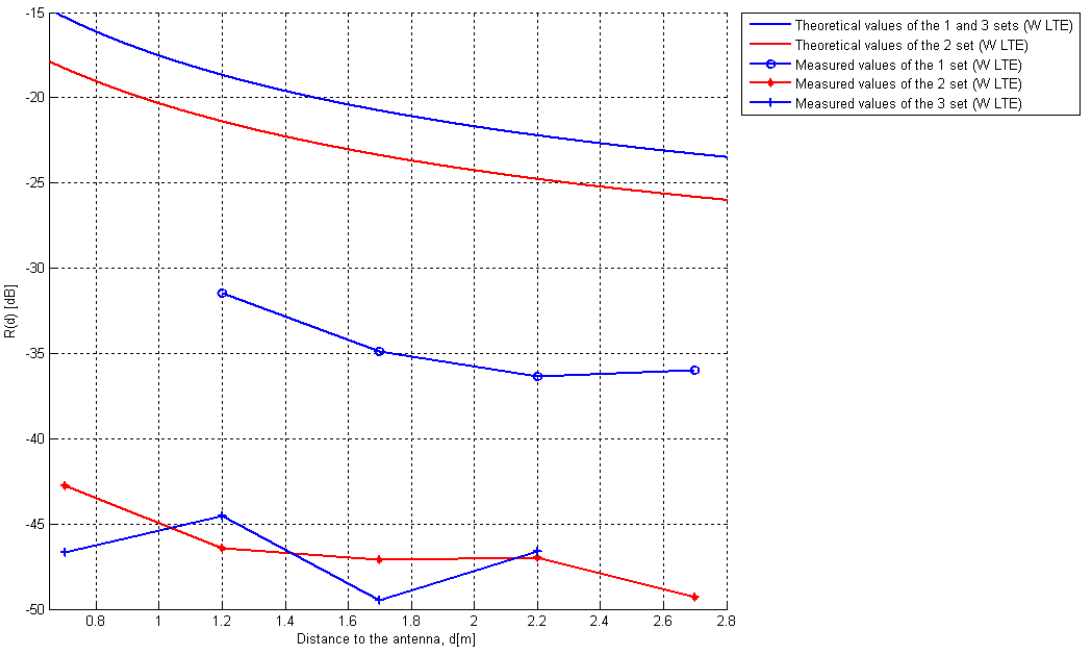

Figure 4.15 - Measured and theoretical results of R as function of d, for BS2 W LTE.

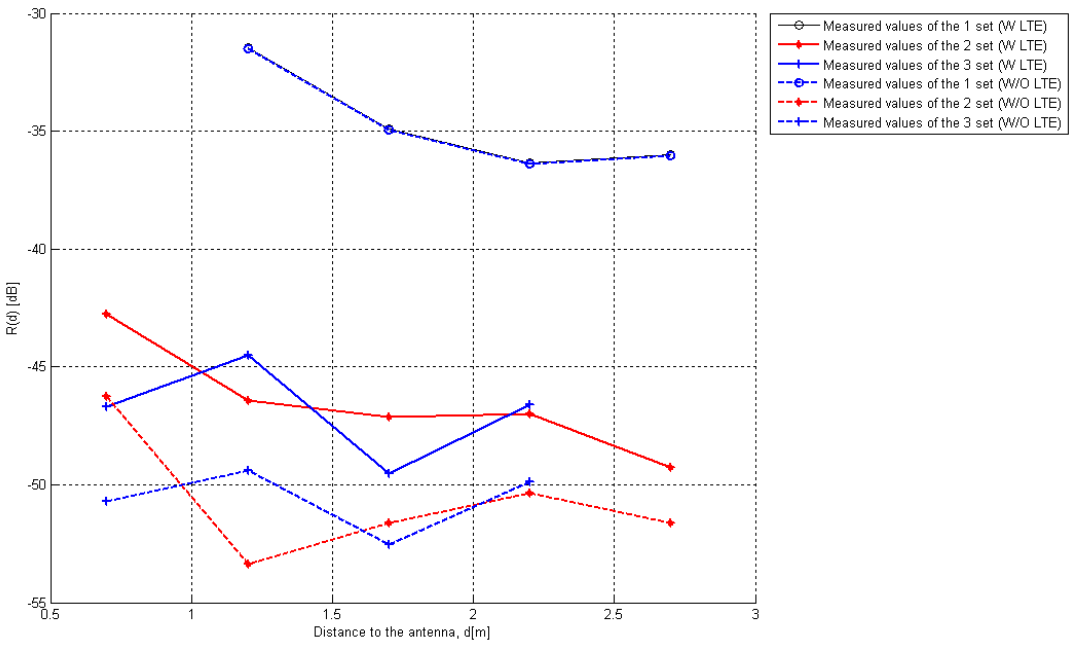

Figure 4.16 - Measured results of R as function of d, for BS2 W and W/O LTE.

A comparison between the theoretical results from W and W/O have already been analysed, as the BS1 and BS3 share the same characteristics. For the 2nd and 3rd set of data, the $R(s)$ W LTE is 71% to 395% greater than the $R(s)$ W/O LTE, while for the 1st set a significant difference is not observed, as seen in Figure 4.16.

For BS3, measurements were taken in the direction of maximum radiation, at a height of about 4 m from the BS, Section F.3. The V plane of the antenna radiation pattern and the antenna downtilt (3º) are relevant in order to estimate exposure levels: the normalised gain of the antenna decreases with the increase of distance, which implies a decrease of EM exposure. After reaching the point of maximum radiation, EMF levels decrease following the evolution of the radiation pattern. As the gain is different for each distance point (Table F.4), different calculations were performed for each point. The results are presented in Figure 4.17. The measured EMF levels remain below the levels estimated by the model, with a minimum difference of -24.73 dB. The $R(d)$ obtained by the measured values is below 39.37 dB compared to the recommended limits, $R(d) = 1$. The difference in $R\ (d)$ between W / O and W LTE takes values between 17% and 283% for data obtained by the measurements whereas for the theoretical model this difference is equal to about 40%.

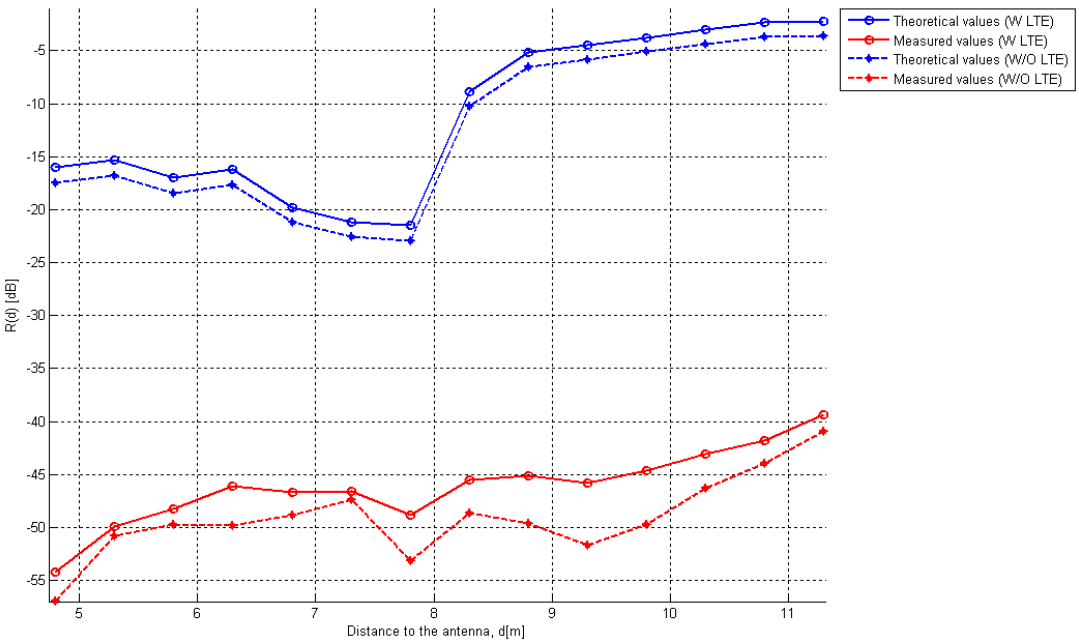

Figure 4.17 - Measured and theoretical results of R as function of d, for BS3.

The values of $R(d)$ obtained from the measured data in BS4 were compared with the model results from a worst-case perspective, resulting in a minimum difference of -39.5 dB regarding the simulation with 4 active GSM carriers. The worst-case scenario corresponds to the simulation of antenna at a certain height level and not at ground one, since the radiation pattern of the antenna was not provided, and the exact antenna height is unknown. EM exposure levels have a decreasing trend with the increase of distance, as it is verified in Figure 4.18. In this scenario, LTE does not have a relevant impact on the definition of distances for both the theoretical and measured data, due to the magnitude of the involved input powers in LTE.

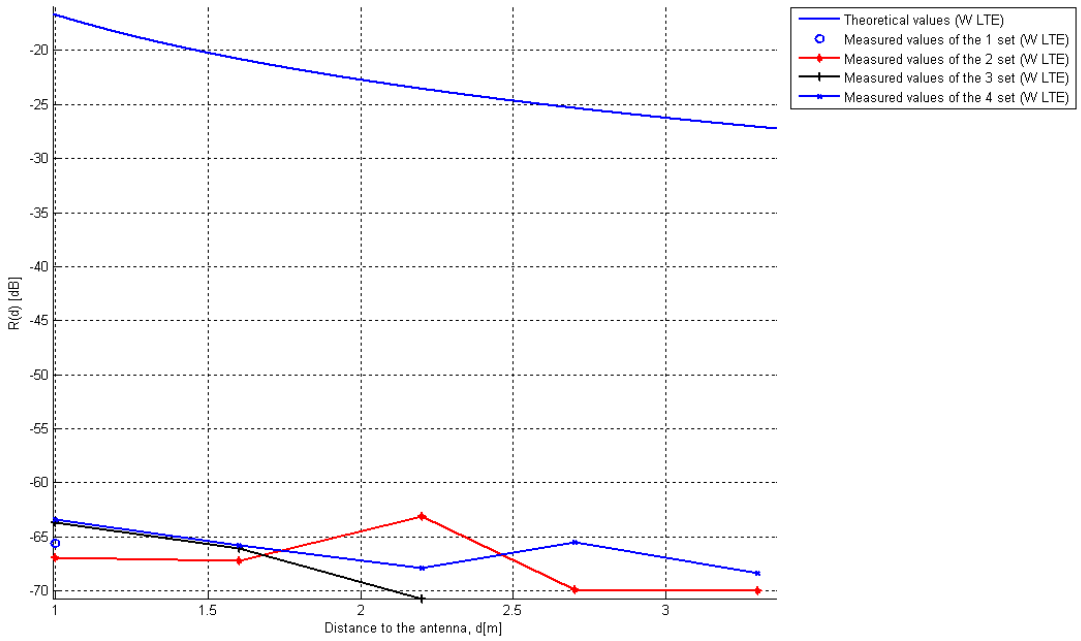

Figure 4.18 - Measured and theoretical results of R as function of d, for BS4.

Also the measured data of BS5 were compared with the worst-case scenario, Figure 4.20. The measured data of the 2nd set has higher values than the 1st and 3rd sets, since the radial of 2nd set is in the direction of maximum radiation. The values of $R(d)$ obtained through measurements are 19.52 dB below the model ones with 4 carriers in GSM. In this case, theoretical results for W/O LTE have a difference of 0.61% in comparison with W LTE, whereas the results obtained from the measures have a difference up to 13.3%. Note that the model and manufacturer of the BS5 antenna is unknown, and therefore the calculations were performed for the antenna of the IPainel-1 scenario.

Since most of the measured data is 20 dB lower than the model estimation, it is concluded that the model overestimates the real values by a factor of 100. Using the results model, It was determined that the difference in distance corresponding to this value is about 25 to 30 dB. Thus, the estimated distances are 17 to 30 times higher than the reality according to the performed measurements. As the main objective of the work is the estimation of the exclusion regions in co-located BS antennas for worst-case scenario, the public health is safeguarded with this overestimation and the developed model achieves the initial expectations. All analysed BSs have the radiation levels below the safety recommendations in the public access areas, as estimated by the model.

Concerning the model evaluation, by comparing with measured data, the analysis of peak values would also be an interesting approach to consider. The data from measurements were influenced by some factors difficult to control, such as the existence of reflecting surfaces, or the oscillations of the measuring equipment. Furthermore, the values of $R(d)$ obtained from measurement are also affected by the difficulty in determining the distance of some measuring points with accuracy. The lack of access to detailed radiation patterns in electronic format also affects the comparison of the model with measurements. Note also that the measurements were not performed in front of the antenna and at

the same level, in which the assumptions of the electric field estimation model developed in this work are more accurate.

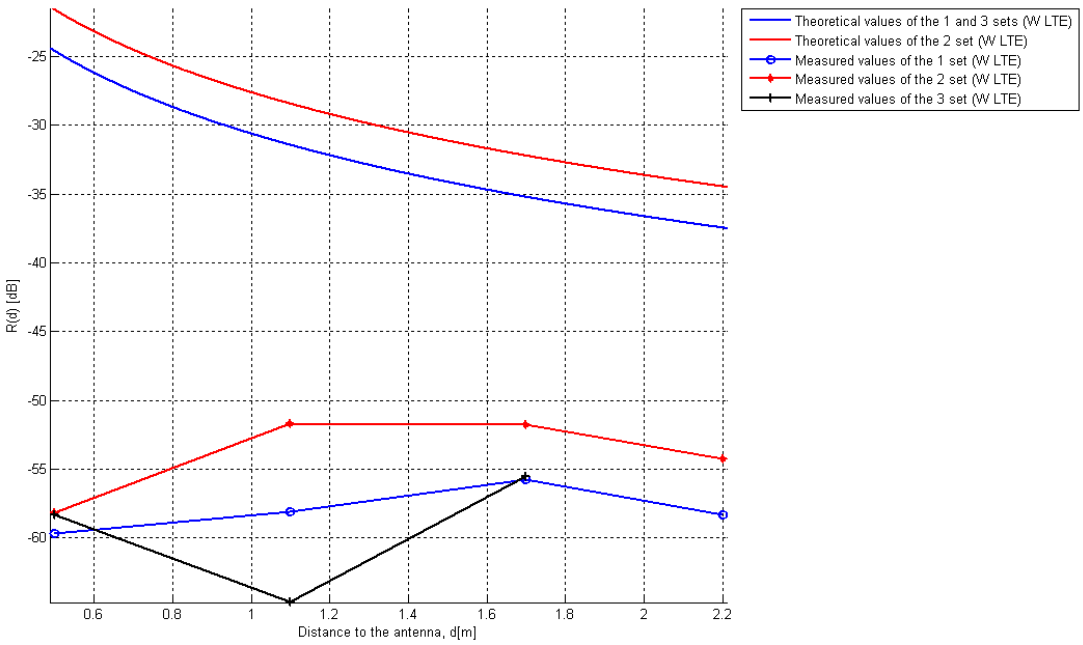

Figure 4.19 - Measured and theoretical results of R as function of d, for BS5.

Another interesting comparison is to analyse the results obtained in [OFRC05], Table 2.8. The model results for D_{front} are shown in Table 4.5, with the same characteristics of the antennas and systems used in [OFRC05]. For two outdoor scenarios (Rtower/Utower and Uroof) with one carrier per system, all of the developed model results of the exclusion region are lower than those obtained by the model used in [OFRC05], far-field approximation model. For this case, and in accordance with the far-field approximation model, the exclusion region is below the minimum valid distance of the model, so this limit value is regarded as the exclusion region, as a preventive method. This reflects the agreement between the two models. However, with four carriers per system, the results of the developed model are higher than to those obtained via the far-field approximation model, even when the exclusion zone estimated by this model is greater than the minimum valid distance. Note that the far-field approximation model does not take the contributions of all array elements into account, since it considers the antenna as an isolated point. This factor is relevant when estimating the EMF in areas near the BS antenna. In the indoor environment (Iceil), data show a trend opposite to the previous one: the model data for four carriers per system are lower than to those obtained in [OFRC05].

For two outdoor scenarios (Rtower/Utower and Uroof) with one carrier per system, all the model results for the exclusion region are lower than those obtained by the model used in [OFRC05], the far-field approximation model. For this case, the exclusion region is below the minimum valid distance of the model, so this limit value is regarded as the exclusion region, as a preventive method. However, with four carriers per system, the results of the developed model are higher than those obtained with

far-field approximation model, even when the exclusion zone estimated by this model is greater than the minimum valid distance. Note again that the far-field approximation model does not take the contributions of all array elements into account, since it considers the antenna as an isolated point. This factor is relevant when estimating the EMF in areas near the BS antenna. In indoor environment (Iceil), data show a trend opposite to the previous one: data for four carriers per system are lower than to those obtained in [OFRC05].

Table 4.5 - Model Results for developed scenarios of [OFRC05].

D_{front} [m]	Rtower/Utower		Uroof		Iceil	
	1 carrier	4 carriers	1 carrier	4 carriers	1 carrier	4 carriers
GSM 900	2.00	6.85	2.03	6.95	$< \lambda$	0.57
GSM 1800	1.17	3.11	1.17	3.11	0.21	0.41
UMTS	1.28	3.30	1.28	3.30	0.20	0.39
GSM 900/GSM 1800	2.75	9.42	2.79	9.51	0.35	0.70
GSM 900/UMTS	2.82	9.31	2.85	9.39	0.35	0.69
GSM900/GSM 1800/UMTS	3.48	11.94	3.51	12.01	0.40	0.81

The proposed model is a practical tool to estimate exclusion regions and determine the need to change the physical barriers after introducing LTE. An interesting approach is to use the model to see if any public access is inside the exclusion region. If this occurs, measurements can be performed to verify that the limit levels are exceeded, and if there is need to define/redefine physical barriers in this zone.

Chapter 5

Conclusions

This chapter finalizes the thesis, summarising the main conclusions as well as some suggestions for future work.

The objective of this work was to estimate the exclusion regions of a BS with several mobile communication systems co-located, in particular LTE and its influence on the change of the exclusion regions already defined for GSM and UMTS BS antennas. It was intended also to establish design rules that simplify the estimation process. Exclusion regions are zones around antennas where the reference levels are exceeded, becoming crucial to define physical barriers when these regions comprise public access zones. As the exclusion regions are usually defined in the near-field region, it is necessary to develop a model of the EMF behavior valid in areas very close to the BS antennas.

To achieve the proposed objectives, the radio interface of GSM, UMTS and LTE systems were studied, being identified some parameters that can influence the estimation of exclusion regions. Relevant features that influence the BS antenna performance were also analysed, such as radiation regions or the infrastructure typologies support the BS antennas. Another study area was the EM exposure, by examining the reference levels and guidelines for EMF assessment, and measurement established by several international entities. Finally, the estimation models of the EMF levels around antennas were studied, by analysing also the methodologies of exclusion region estimation adopted by other entities.

In the development process of the estimation model of the EMF, three typical antennas were identified:

- The arrays of vertically stacked elements (usually half wavelength dipoles) used in outdoor scenarios;
- The omnidirectional indoor antennas, placed on the ceiling of rooms and corridors, which can be regarded as a monopole;
- The directional indoor antennas, typically a microstrip antenna.

For the indoor environment, the general expressions well known from the literature are used: the EMF of a microstrip antenna is obtained from the Cavity model while the EMF of a monopole is given by the far-field model. As the use of these expressions in the radiating near-field region has practically a residual error, and as the input power has typically reduced values that lead to exclusion regions in the near-field region, it is considered that these two expressions are valid from one wavelength onward, in a perspective of worst-case scenario.

In this thesis, the EMF of an outdoor antenna is described by two theoretical models: the far-field model with validity in far-field region, and the gain-based model that is valid for distances greater than two wavelengths. The continuity of the EMF as a function of the distance is ensured by an interpolation process, where an appropriate polynomial function intersects the two models.

The distance evaluation model was developed and implemented in Matlab, by allowing to estimate the exclusion region in the direction of maximum radiation, D_{front}. For the other directions, the approach adopted is the cylindrical exclusion zone model, in which the normalised gains taken from the antenna radiation patterns are applied as correction factors on the exclusion region obtained in the direction of maximum radiation. It is considered that all systems are at maximum load, in which the model

presents the worst case in terms of EM exposure.

The BS scenarios were defined according to the typical antennas installed before the implementation of LTE, co-located with GSM and UMTS, before and after the installation of LTE. After the analysis of these scenarios, results were related to typical BS installation typologies and to the situations that lead to the need for define/redefine physical barriers. The analysed carrier configurations were 1/1 ($N_{c,GSM}$/ $N_{c,UMTS}$), 2/1 and 4/2, although GSM is usually never supported by a single carrier. Note that it is possible to "turn off" carriers when its resources are not being used, in which case the results with one GSM carrier can be interesting. However, exclusion regions must be defined for the worst-case scenario, so the obtained results with one GSM carrier are not analysed in the following considerations.

For the first set of analysis, the PA output power of 40 W (and 2x40 W for MIMO case) was maintained in the outdoor scenarios. With the increase of carriers in a given BS, the exclusion region tends to be larger, while the difference of obtained values W/O and W LTE tend to be lower:

- For the sectorial outdoor scenarios with co-location of GSM900/UMTS and carrier configuration of 2/1, D_{front} has values between 4.9 and 6.7 m. In the W LTE case, the D_{front} increases to values between 8.5 and 11.5 m, representing a maximum increase of 73% for urban scenarios and 53% for rural scenarios.
- With the 4/2 carrier configuration, initially the D_{front} has values between 8.4 and 11.8 m, and 12.0 to 15.1 m in the W LTE case. In urban scenarios, the D_{front} maximum difference between W/O and W LTE is equal to 43% while for rural scenarios, the D_{front} increases by 22%.
- Regarding the co-location of GSM900/GSM1800/UMTS, D_{front} takes numerical values in between 7.9 and 10.2 m for the sectorial outdoor scenarios with the 2/2/1 carrier configuration. D_{front} W LTE is equal to about 13.2 to 13.6 m, representing a maximum increase of 30% in the urban case, and 33% in rural scenarios.
- For the carrier configuration of 4/4/2, D_{front} W/O LTE has values between 15.1 and 16.4 m. The influence of the MIMO elements introduced with LTE is not significant, implying a D_{front} maximum increase of 8% and 1% for the urban and rural case respectively. D_{front} W LTE has values between 16.1 and 16.8 m.

In the scenarios with GSM and UMTS omnidirectional BS antennas, D_{front} suffers a maximum increase of about 395% after insertion of LTE sectorial BS antennas. Note that the technological trend is to replace the omnidirectional by sectorial antennas in order to provide an increase in cell capacity.

The D_{front} results are relatively high, so if an accessible area to the public is the same height of the BS and at a distance less than the D_{front}, as a balcony on a building frontal to the BS, additional measurements should be performed to verify the need to define physical barriers. However, the direction of maximum radiation is typically without obstacles near the BS to provide an efficient coverage.

With the BS antennas at a minimum typical height of 3 m of a zone accessible to the public, people are protected for small downtilts. Note also that for the BSs at reduced heights, the tilts are practically null and the power needed to cover should be smaller in comparison with those used in this study, thus with a smaller exclusion region.

The use of high downtilts was analysed: there is no need to define physical barriers at the front of a BS, regardless of the distance to the BS, if the BS is more than 5 m high of a public access area. To this end, the value of 12º was considered as the used maximum tilt. A careful analysis should be performed when a BS antenna is at a height less than 5 m. The rural scenarios with the characteristics presented in this work do not require physical barriers at the ground level. In the urban case, the Ufaçade and Upole installations might lead to EM exposure problems at the street level. For Uroof installations, the top floor of frontal building is exposed to more EM radiation, but a BS typical infrastructure of 2 m of height ensures that the exclusion zone is not exceeded.

The back, bottom, top and side border of the exclusion region are not typically problematic in the rural environment due to the environment characteristics and the infrastructures that support the antennas: very high masts or towers with few obstacles near the BS antenna. In the urban environment, these dimensions should be taken into account, whenever a public access area is next to the back, bottom, top or side of the BS antennas, e.g., terraces where the BS is installed (Uroof typology) or balconies/windows very close to the Upole/Ufaçade installation. The D_{back}, D_{bottom} and D_{top} have values below $2\lambda_{GSM900}$, 0.64 m, therefore not alarming in terms of EM exposure. The exception is the BS with omnidirectional antennas, wherein the D_{back} have values less than 2.2 m. With the installation of LTE, the maximum value of D_{side} is equal to about 4.4 and 5.3 m, for the carrier configuration of 2/1 and 4/2 respectively.

The access to inaccurate radiation patterns could affect the results. The obtained values for D_{back}, D_{bottom}, D_{top} and D_{side} are considered sufficient to estimate the total exclusion region of a BS, but a more detailed study of the radiation pattern is suggested for accurate results.

In indoor scenarios, the exclusion region results have relatively small values when using the maximum typical value of EIRP, without major changes with the introduction of LTE. The maximum result of D_{front} W LTE, 0.66 m, was obtained for an omnidirectional antenna with MIMO, not shared with other operators and with the 4/2 carrier configuration. There is no need to define physical barriers due to the magnitude order of the indoor results.

As discussed in Chapter 4, the increase of input power is accompanied by increase of the exclusion regions and also by the increase of the difference between the D_{front} W/O LTE and W LTE. Another interesting conclusion is the decrease of the exclusion region with increasing number of elements in an outdoor antenna.

In the scenarios that were measured, the smallest difference between the measured and the theoretical values is equal to about -20 dB for the majority of cases, whereas in indoor Omni BS scenario is equal to about -40 dB. The estimated distances are 17 to 30 times higher than the real values according to the performed measurements. Thus for most scenarios, a factor of 17 to 30

should be taken into account when using the developed model. Although confidence in the results is proportional to the increase of measurements number, it can be concluded that the developed model overestimates the real value of the EMF and consequently the exclusion region, in the worst case perspective. For the conditions assumed in this work, the public access areas that are outside of any exclusion region estimated by this model are not exposed to radiation levels exceeding the reference limits. When the public access areas are within an exclusion region, a more careful analysis should be performed. Note that in this case, the analysis of exclusion regions of the isolated antennas may be important, particularly if the installation structure supports several antennas spaced apart significantly.

For future research, one suggestes the study of the influence of the surrounding environment on the total exclusion region, taking into account some simulation results as [Oliv06], which presents results twice the ones obtained under free space conditions and in worst-case perspective. Note that the developed model assumes also the worst-case perspective, being a practical method for the estimation of exclusion regions. The simulation of other antenna types as the outdoor arrays of patch antennas, arrays in the indoor case, or variation of other antenna parameters, could also be interesting. In future studies, the analysis of other carrier configurations, the co-location of mobile systems/Wi-Fi in indoor environments and the exposure penetration in buildings will be relevant.

Annex A

Typical Base Station Antennas

The present annex shows the technical characteristics of BS antennas used in the systems considered in this study.

Some examples of antennas used by Portuguese Operators for GSM, UMTS and LTE communication systems are presented in this annex, where the technical information about this antennas were used to generate the data in this work. The examples presented are summarised in the Table A.1. The outdoor antennas that support LTE technology have MIMO elements. In the Table A.18, the normalised gains of these antennas are presented, according to the criterion described in Chapter 3.

Table A.1 - Summary of BS antennas used in this work.

	Antenna	Technical description
Outdoor	Sector GSM900	Table A.2
	Sector GSM1800	Table A.3
	Sector UMTS	Table A.3
	Sector GSM900/UMTS	Table A.4
	Sector GSM900/LTE800	Table A.5
	Sector UMTS/LTE2600	Table A.6
	Sector GSM900/UMTS/LTE2600	Table A.7
	Sector UMTS/LTE1800	Table A.8
	Sector GSM900/LTE1800	Table A.9
	Sector LTE1800/LTE2600	Table A.6
	Omni GSM900/UMTS	Table A.10
	Omni GSM1800	Table A.11
	Sector LTE800/LTE1800	Table A.12
	Sector LTE800/GSM900/UMTS	Table A.17
Indoor	Sector GSM900/GSM1800/UMTS	Table A.13
	Sector GSM900/LTE1800/UMTS/LTE2600 (W/O MIMO)	Table A.13
	Sector GSM900/LTE1800/UMTS (W/O MIMO)	Table A.13
	Sector GSM900/LTE1800/UMTS/LTE2600 (W MIMO)	Table A.14
	Sector GSM900/LTE1800/UMTS (W MIMO)	Table A.14
	Omni GSM900/GSM1800/UMTS	Table A.15
	Omni GSM900/LTE1800/UMTS/LTE2600 (W/O MIMO)	Table A.15

Table A.1 (cont.) - Summary of BS antennas used in this work.

Indoor	Omni GSM900/LTE1800/UMTS (W/O MIMO)	Table A.15
	Omni GSM900/LTE1800/UMTS/LTE2600MHz (W MIMO)	Table A.16
	Omni GSM900/LTE1800/UMTS (W MIMO)	Table A.16

Table A.2 - Technical specifications of the Sector GSM900 BS antenna [RFSy12].

Model	RFS AP906516
Frequency range [MHz]	824-960
Gain [dBi]	17.5
Horizontal Beamwidth [deg]	65
Vertical Beamwidth [deg]	8.5
Polarisation	Vertical
Dimensions [mm] (height/width/depth)	1977/262/140

Table A.3 - Specifications of Sector BS antenna for UMTS or GSM1800 system [Allg12].

Model	Allgon 7721.00	
Frequency range [MHz]	1710-1880	1850-2170
Gain [dBi]	17.6	18.3
Horizontal Beamwidth [deg]	67	66
Vertical Beamwidth [deg]	7.0	6.6
Polarisation	Dual linear ±45º	
Dimensions [mm] (height/width/depth)	1309/167/89.5	

Table A.4 - Technical specifications of Sector GSM900/UMTS BS antenna [Allg12].

Model	Allgon 7755.00	
Frequency range [MHz]	824-896	1710-2170
Gain [dBi]	17.3	17.8

Table A.4 (cont.) - Technical specifications of Sector GSM900/UMTS BS antenna [Allg12].

Horizontal Beamwidth [deg]	71	65
Vertical Beamwidth [deg]	7.4	6.9
Polarisation	Dual linear ±45º	
Dimensions [mm] (height/width/depth)	2658/280/125	

Table A.5 - Specifications of Sector GSM900/LTE800 BS antenna [KATH12a].

Model	Kathrein 80010647v01
Frequency range [MHz]	760-960
Gain [dBi]	17.5
Horizontal Beamwidth [deg]	65
Vertical Beamwidth [deg]	9.0
Polarisation	Dual linear ±45º
Number of MIMO antennas	2
Dimensions [mm] (height/width/depth)	2254/576/99

Table A.6 - Sector LTE2600/(UMTS or LTE1800) BS specifications [KATH12a].

Model	Kathrein 80010622	
Frequency range [MHz]	1710-2200	2200-2690
Gain [dBi]	17.4	18
Horizontal Beamwidth [deg]	65	61
Vertical Beamwidth [deg]	7.1	5.7
Polarisation	Dual linear ±45º	
Number of MIMO antennas	2	
Dimensions [mm] (height/width/depth)	1415/323/71	

Table A.7 - Specifications of Sector GSM900/UMTS/LTE2600 BS antenna [KATH12a].

Model	Kathrein 80010692		
Frequency range [MHz]	790-960	1710-2170	2490-2690
Gain [dBi]	17.2	16.9	17
Horizontal Beamwidth [deg]	68	65	67
Vertical Beamwidth [deg]	7.0	7.7	5.9
Polarisation	Dual linear ±45º		
Number of MIMO antennas	2		
Dimensions [mm] (height/width/depth)	2622/300/152		

Table A.8 - Technical specifications of Sector UMTS/LTE1800 BS antenna [RFSy12].

Model	RFS APXVLL13N-C	
Frequency range [MHz]	1710-1990	1920-2700
Gain [dBi]	17.6	17.7
Horizontal Beamwidth [deg]	65	
Vertical Beamwidth [deg]	7.5	7
Polarisation	Dual linear ±45º	
Number of MIMO antennas	2	
Dimensions [mm] (height/width/depth)	1375/ 288/118	

Table A.9 - Specifications of Sector GSM900/LTE1800 BS antenna [Allg12].

Model	Allgon 5782.00	
Frequency range [MHz]	824-960	1710-2170
Gain [dBi]	16.2	16.5
Horizontal Beamwidth [deg]	67	65
Vertical Beamwidth [deg]	8.6	9.4
Polarisation	Dual linear ±45º	
Number of MIMO antennas	2	

Table A.9 (cont.) - Specifications of Sector GSM900/LTE1800 BS antenna [Allg12].

Dimensions [mm] (height/width/depth)	2033/280/125

Table A.10 - Technical specifications of Omni GSM900/UMTS BS antenna [KATH12a].

Model	Kathrein 736347	
Frequency range [MHz]	870-960	1920-2170
Gain [dBi]	9	10
Horizontal Beamwidth [deg]	365	
Vertical Beamwidth [deg]	11	9
Polarisation	Vertical	
Dimensions [mm] (height)	3033	

Table A.11 - Technical specifications of Omni GSM1800 BS antenna [KATH12a].

Model	Kathrein 738187
Frequency range [MHz]	1710-1880
Gain [dBi]	11
Horizontal Beamwidth [deg]	365
Vertical Beamwidth [deg]	7
Polarisation	Vertical
Number of MIMO antennas	1
Dimensions [mm] (height)	1568

Table A.12 - Specifications of Sector LTE800/LTE1800 BS antenna [Allg12].

Model	Allgon P65-17-XXCH-N	
Frequency range [MHz]	824-960	1710-2170
Gain [dBi]	16.7	17.1
Horizontal Beamwidth [deg]	67	63

Table A.12 (cont.) - Specifications of Sector LTE800/LTE1800 BS antenna [Allg12].

Vertical Beamwidth [deg]	8.9	6.6
Polarisation	Dual linear ±45º	
Number of MIMO antennas	2	
Dimensions [mm] (height/width/depth)	2045/565/142	

Table A.13 - Technical specifications of Indoor Sector (W/O MIMO) BS antenna [KATH12a].

Model	Kathrein 80010465	
Frequency range [MHz]	790-960	1710-2700
Gain [dBi]	~7	
Horizontal Beamwidth [deg]	~90	
Polarisation	Vertical	
Number of MIMO antennas	1	
Impedance [Ω]	50	
Dimensions [mm] (height/width/depth)	231/140/ 50	

Table A.14 - Technical specifications of Indoor Sector (W MIMO) BS antenna [KATH12a].

Model	Kathrein 80010677	
Frequency range [MHz]	790-960	1710-2700
Gain [dBi]	~7	
Horizontal Beamwidth [deg]	~90	
Polarisation	Vertical	Dual linear ±45º
Number of MIMO antennas	2	
Impedance [Ω]	50	
Dimensions [mm] (height/width/depth)	232/140/ 50	

Table A.15 - Technical specifications of Indoor Omni (W/O MIMO) BS antenna [KATH12a].

Model	Kathrein 80010749	
Frequency range [MHz]	876-960	1710-2700
Gain [dBi]	2	
Horizontal Beamwidth [deg]	360	
Polarisation	Vertical	
Number of MIMO antennas	1	
Impedance [Ω]	50	
Dimensions [mm] (diameter/height)	215/85	

Table A.16 - Technical specifications of Indoor Omni (W MIMO) BS antenna [KATH12a].

Model	Kathrein 80010709		
Frequency range [MHz]	790-960	1710-2500	2500-2700
Gain [dBi]	2		
Horizontal Beamwidth [deg]	360		
Polarisation	Vertical		Horizontal
Number of MIMO antennas	2		
Impedance [Ω]	50		
Dimensions [mm] (diameter/height)	258/94		

The BS antenna specified in Table A.17 does not belong to the set of considered scenarios, being used solely to generate results for comparison with the measured rural scenario.

Table A.17 - Specifications of Sector LTE800/GSM900/UMTS BS antenna [KATH12a].

Model	Kathrein 80010709		
Frequency range [MHz]	790-960	880-960	1710-2180
Gain [dBi]	15.1	15.6	18.5

Table A.17 (cont.) - Specifications of Sector LTE800/GSM900/UMTS BS antenna [KATH12a].

Horizontal Beamwidth [deg]	65		
Vertical Beamwidth [deg]	11.5	10.1	4.6
Polarisation	Dual linear ±45º		
Number of MIMO antennas	2		
Dimensions [mm] (height/width/depth)	1932/269/154		

The normalised gains of the antennas described in the Table A.2 to Table A.16 are presented in Table A.18. This information is useful for estimating the EMF or the exclusion region of a BS antenna in directions different from the one of maximum radiation.

Table A.18 - Normalised gains of the antennas analysed in this work.

Normalised gains [dB]									
Antennas	**Plane**	**-135º**	**-90º**	**-45º**	**0º**	**45º**	**90º**	**135º**	**180º**
Sector GSM900	**H**	-	-	-	0	-4.5	-20	<-35	<-35
	V	<-30	-25	-15	0	-10	<-35	<-30	<-30
Sector GSM1800	**H**	-	-	-	0	-5.1	-16.6	-26.1	-30.7
	V	<-30	<-30	-27	0	-22.5	<-30	<-30	<-30
Sector UMTS	**H**	-30.4	-18.7	-5.8	0	-6	-18.6	-30	-41.8
	V	<-30	<-30	-27	0	-27.8	<-30	<-30	<-30
Sector GSM900/ UMTS	**H**	-27.8	-22.5	-6.4	0	-	-	-	-37
	V	<-30	<-30	-18	0	-	-	-	<-30
Sector GSM900/ LTE800	**H**	<-20	<-20	-7.5	0	-	-	-	<-20
	V	<-20	<-20	<-20	0	<-20	<-20	<-20	<-20
Sector UMTS/ LTE2600	**H**	-	-	-	0	-5	-18.5	-28	-32
	V	<-30	<-30	-25	0	-15	<-30	<-30	<-30
Sector GSM900/UMTS/ LTE2600	**H**	-27	-17	-4	0	-5	-17	-28	-30
	V	<-30	<-30	-13	0	-17	28	<-30	-27

Table A.18 (cont.) - Normalised gains of the antennas analysed in this work.

Normalised gains [dB]									
Antennas	**Plane**	**-135°**	**-90°**	**-45°**	**0°**	**45°**	**90°**	**135°**	**180°**
Sector UMTS/ LTE1800	**H**	-	-	-	0	-5	-18.5	-28	-32
	V	<-30	<-30	-25	0	-15	<-30	<-30	<-30
Sector GSM900/ LTE1800	**H**	-25.6	-18.7	-5.1	0	-	-	-	-34.9
	V	<-30	<-30	-17.5	0	-	-	-	<-30
Sector LTE1800/ LTE2600	**H**	-	-	-	0	-5	-18.5	-28	-32
	V	<-30	<-30	-25	0	-15	<-30	<-30	<-30
Omni GSM900/UMTS	**H**	-	-	-	0	-	-	-	-
	V	<-20	<-20	<-20	0	<-20	<-20	<-20	<-20
Omni GSM1800	**H**	-	-	-	0	-	-	-	-
	V	<-15	<-15	<-15	0	<-15	<-15	<-15	<-15
Sector LTE800/ LTE1800	**H**	-29.3	-18	-5.7	0	-	-	-	-31.2
	V	<-30	<-30	-21.8	0	-19.5	<-30	<-30	-27
Indoor Sector (W/O MIMO)	**H**	<-20	-10	-3	0	-	-	-	<-20
	V	*	*	*	0	*	*	*	*
Indoor Sector (W MIMO)	**H**	<-20	-10	-3	0	-	-	-	<-20
	V	*	*	*	0	*	*	*	*
Indoor Omni (W/O MIMO)	**H**	-	-	-	0	-	-	-	-
	V	-	-	-	0	-	-	-	-
Indoor Omni (W MIMO)	**H**	-	-	-	0	-	-	-	-
	V	-	-	-	0	-	-	-	-

*Without access to the data.

Annex B

Global Model Simulation

This annex presents radiated electric field results obtained from the global model, for the antennas used in this work. The parameters that lead to these results are also presented.

B.1 Introduction

The estimation of the radiated electric field by an antenna according to the model developed in this thesis was performed, being necessary to take into account the characteristics of the BS antennas and proposed scenarios. The parameters that are used in all the simulations, excluding the case where this is indicated, are the following:

- $N_{sp} = 60000$;
- System values:

Table B.1 - System parameters of the simulation program.

System	Frequency $[\mathrm{MHz}]$	$\lambda\ [\mathrm{m}]$	$2\lambda\ [\mathrm{m}]$	$S_{ref}\ [\mathrm{W/m^2}]$
LTE800	860	0.35	0.70	4.30
GSM900	935	0.32	0.64	4.67
GSM1800	1805	0.17	0.34	9.03
LTE1800				
UMTS	2110	0.14	0.28	10.00
LTE2600	2620	0.11	0.22	

For outdoor environment parameters:

- d_{min} for Near-field model $d_{min} = 2\lambda$;
- d_{max} for Global model: $d_{max} = 1.6 \times 2D^2 \ / \ \lambda$;
- d_{max} for Near-field model: $d_{max[m]} = 6$;
- Phase shift ψ_i= 0;
- Estimation of Δ_{da}: Yes;
- Acceptable value tolerance of Δ_{da}: 0;
- $N_{el} = 8$;
- Dipole length: $\lambda \ \ 2$;
- Elevation angle $\theta = \pi \ \ 2$;
- Maximum permissible RMSE $RMSE_{max} = 3$;
- Maximum number of iterations to perform when $RMSE \geq RMSE_{max}$: 15;
- Maximum number of iterations performed by each invocation of the interpolation function: 2000;
- Maximum number of evaluations of the model interpolation: 50000;
- Acceptable value of Δ_{max} after the performing of upper bound method: 0;
- Auxiliary variable which indicates from which value of d would be to find a point of intersection d_{Pa}: 4 m.

For indoor case:

- $d_{min} = \lambda$;
- $d_{max[m]} = 6$;
- Length of the patch $L = \lambda\ \ 2$;
- Dielectric constant $\varepsilon_r = 4.4$;
- Substrate thickness $h = 1.6\ mm$;
- Azimuth angle $\phi = 0$;
- Elevation angle $\theta = \pi\ \ 2$;
- Monopole length $l = \lambda\ \ 4$.
- Microstrip parameters:

Table B.2 - Parameters of the microstrip antennas.

System	L [mm]	ε_{ref}	L_{ef} [mm]	W [mm]
GSM900	160.	4.25	162.	98.
GSM1800	83.	4.15	85.	51.
LTE 1800MHz				
UMTS	71.	4.11	73.	43.
LTE 2600MHz	57.	4.06	59.	35.

The following sections present the Global Model simulation results for each BS antenna described in Annex A, as well as the exclusion zone for each isolated antenna/system.

B.2 Sector GSM900 Antenna

As this antenna is vertical polarised and not dual, the height of the array element is equal to $h_{el} = \lambda\ \ 2$, by changing the value of the auxiliary variable pol from 1 to 2.

Table B.3 - Global Model simulation of the Sector GSM900 antenna.

P_{in} [W]	25.24
Δ_{sp} [m]	6.3944×10^{-4}
Δ_{da}	0.81
Δ_{max} [V/m]	0.0120

Table B.3 (cont.) - Global Model simulation of the Sector GSM900 antenna.

d_{Pa} [m]	2.44
$\frac{2D^2}{\lambda}$ [m]	24.38
$A_{[\mathrm{Vm}]}/B_{[\mathrm{V}]}/C_{[\mathrm{Vm}^{-1}]}$	-18.03/72.04/17.07
$A'_{[\mathrm{W}]}/B'_{[\mathrm{Wm}^{-1}]}/C'_{[\mathrm{Wm}^{-2}]}$	0.22/13.37/-0.36
D_{front} [m] $N_c = 1\ \ 2/4$	2.67/4.97/8.77

Table B.4 - Simulation of the power variation of the Sector GSM900 antenna.

P_{in} [W]	5.01	8.91	15.85	28.18	50.12
$A_{[\mathrm{Vm}]}/B_{[\mathrm{V}]}/C_{[\mathrm{Vm}^{-1}]}$	-8.03/ 32.10/7.61	-10.71/ 42.81/10.15	-14.29/ 57.09/13.53	-19.05/ 76.13/18.04	-25.41/ 101.52/24.06
$A'_{[\mathrm{W}]}/B'_{[Wm^{-1}]}$ $/C'_{[\mathrm{Wm}^{-2}]}$	0.04/ 2.65/-0.07	0.08/ 4.72/ -0.13	0.14/ 8.39/-0.23	0.24/ 14.93/-0.40	0.43/ 26.55/-0.71
D_{front} [m] $N_c = 1\ \ 2/4$	$(< \lambda)$/ 1.16/2.16	1.04/ 1.94/ 3.66	1.75/ 3.29/6.04	2.96/ 5.47/9.53	4.94/ 8.72/14.13

Table B.5 - Simulation of the N_{el} variation of the Sector GSM900 antenna.

N_{el}	4	6	8	10
G [dBi]	8.5	10	11.4	12.8
Δ_{max} [V/m]	0.0276	0.0172	0.0757	0.1564
d_{Pa} [m]	1.63	3.95	6.24	6.00
$A_{[\mathrm{Vm}]}/B_{[\mathrm{V}]}/C_{[\mathrm{Vm}^{-1}]}$	5.01/ 32.47/11.98	4.50/ 30.42/7.97	-5.52/ 44.46/2.19	-11.62/ 52.72/0.18
$A'_{[\mathrm{W}]}/B'_{[Wm^{-1}]}$ $/C'_{[\mathrm{Wm}^{-2}]}$	3.07/ 3.53/-0.13	-1.28/ 3.51/-0.11	5.28/ 0.71/0.01	11.12/ -0.71/0.07
D_{front} [m] $N_c = 1\ \ 2/4$	1.26/ 2.04/3.42	1.04/ 1.57/2.54	1.07/ 1.62/2.44	1.19/ 1.82/2.69

B.3 Sector GSM1800 Antenna

Table B.6 - Global Model simulation of the Directional GSM1800 antenna.

$\boldsymbol{P_{in}}$ $[\mathbf{W}]$	25.24
Δ_{sp} $[\mathbf{m}]$	5. 4468x10^{-4}
$\boldsymbol{\Delta_{da}}$	1
$\boldsymbol{\Delta_{max}}$ $[\mathbf{V/m}]$	0.0917
$\boldsymbol{d_{Pa}}$ $[\mathbf{m}]$	11.89
$\frac{\mathbf{2}\boldsymbol{D}^{\mathbf{2}}}{\boldsymbol{\lambda}}$ $[\mathbf{m}]$	20.63
$\boldsymbol{A}_{[\mathrm{Vm}]}/\boldsymbol{B}_{[\mathrm{V}]}/\boldsymbol{C}_{[\mathrm{Vm}^{-1}]}$	-3.70/82.24/15.50
$\boldsymbol{A'}_{[\mathrm{W}]}/\boldsymbol{B'}_{[\mathrm{Wm}^{-1}]}/\boldsymbol{C'}_{[\mathrm{Wm}^{-2}]}$	-710.84/131.08/-4.41
$\boldsymbol{D_{front}}$ $[\mathbf{m}]$ $\boldsymbol{N_c} = \mathbf{1}\ \ \mathbf{2/4}$	2.12/3.64/7.28

B.4 Sector UMTS Antenna

Table B.7 - Global Model simulation of the Sector UMTS antenna

$\boldsymbol{P_{in}}$ $[\mathbf{W}]$	25.24
Δ_{sp} $[\mathbf{m}]$	6.3845x10^{-4}
$\boldsymbol{\Delta_{da}}$	1
$\boldsymbol{\Delta_{max}}$ $[\mathbf{V/m}]$	0.1727
$\boldsymbol{d_{Pa}}$ $[\mathbf{m}]$	8.02
$\frac{\mathbf{2}\boldsymbol{D}^{\mathbf{2}}}{\boldsymbol{\lambda}}$ $[\mathbf{m}]$	24.12
$\boldsymbol{A}_{[\mathrm{Vm}]}/\boldsymbol{B}_{[\mathrm{V}]}/\boldsymbol{C}_{[\mathrm{Vm}^{-1}]}$	-4.70/94.86/14.75
$\boldsymbol{A'}_{[\mathrm{W}]}/\boldsymbol{B'}_{[\mathrm{Wm}^{-1}]}/\boldsymbol{C'}_{[\mathrm{Wm}^{-2}]}$	-118.74/47.72/-1.54
$\boldsymbol{D_{front}}$ $[\mathbf{m}]$ $\boldsymbol{N_c} = \mathbf{1}\ \ \mathbf{2/4}$	2.47/4.21

Table B.8 - Simulation of the power variation of the Sector UMTS antenna.

P_{in} $[W]$	5.01	8.91	15.85	28.18	50.12
$A_{[\mathrm{Vm}]}/B_{[\mathrm{V}]}/C_{[\mathrm{Vm}^{-1}]}$	-2.10/ 42.27/6.57	-2.80/ 56.37/8.77	-3.73/ 75.17/11.69	-4.97/ 100.24/15.59	-6.63/ 133.68/20.79
$A'_{[\mathrm{W}]}/B'_{[\mathrm{Wm}^{-1}]}$ $/C'_{[\mathrm{Wm}^{-2}]}$	-23.58/ 9.48/-0.31	-41.92/ 16.85/-0.54	-74.55/ 29.96/-0.97	-132.58/ 53.28/-1.72	-235.63/ 94.73/-3.06
D_{front} $[\mathrm{m}]$ $N_c = 1\ \ 2/4$	0.87/1.34	1.24/1.94	1.80/2.92	2.68/4.63	4.18/8.18

Table B.9 - Simulation of the $\mathrm{N_{el}}$ variation of the Sector UMTS antenna.

N_{el}	4	6	8	10
G $[\mathrm{dBi}]$	8.5	10	11.4	12.8
Δ_{max} $[\mathrm{V/m}]$	0.1699	0.0469	0.1727	0.2489
d_{Pa} $[\mathrm{m}]$	2.87	1.76	8.02	5.14
$A_{[\mathrm{Vm}]}/B_{[\mathrm{V}]}/C_{[\mathrm{Vm}^{-1}]}$	0.15/ 42.11/18.63	1.46/ 32.92/15.71	-2.13/ 42.86/6.67	-4.10/ 48.04/4.45
$A'_{[\mathrm{W}]}/B'_{[\mathrm{Wm}^{-1}]}$ $/C'_{[\mathrm{Wm}^{-2}]}$	-9.19/ 16.63/-0.65	0.69/ 6.23/-0.22	-24.25/ 9.74/-0.31	4.19/ 3.61/-0.09
D_{front} $[\mathrm{m}]$ $N_c = 1\ \ 2$	1.25/2.28	0.81/1.32	0.88/1.36	0.98/1.49

For $\mathrm{N_{el}}$ equal to 10, d_{min} has the value of 0.37 m in the near-field model instead of 2λ, since the interpolation function becomes more efficient.

B.5 Sector GSM900/UMTS Antenna

Table B.10 - Global Model simulation of the Sector GSM900/UMTS antenna.

System	GSM900	UMTS
$\boldsymbol{P_{in}}$ $[\mathbf{W}]$	25.24	25.24
Δ_{sp} $[\mathbf{m}]$	1.1645×10^{-3}	2.6472×10^{-3}
$\boldsymbol{\Delta_{da}}$	1	1
$\boldsymbol{\Delta_{max}}$ $[\mathbf{V/m}]$	0.0757	0.1722
$\boldsymbol{d_{Pa}}$ $[\mathbf{m}]$	6.24	8.04
$\frac{\mathbf{2}\boldsymbol{D^2}}{\boldsymbol{\lambda}}$ $[\mathbf{m}]$	44.07	99.45
$\boldsymbol{A}_{[\mathrm{Vm}]}/\boldsymbol{B}_{[\mathrm{V}]}/\boldsymbol{C}_{[\mathrm{Vm}^{-1}]}$	-10.88/87.69/4.33	-4.40/89.37/14.00
$\boldsymbol{A'}_{[\mathrm{W}]}/\boldsymbol{B'}_{[\mathrm{Wm}^{-1}]}/\boldsymbol{C'}_{[\mathrm{Wm}^{-2}]}$	17.80/3.65/-0.04	-33.01/24.33/-0.23
$\boldsymbol{D_{front}}$ $[\mathbf{m}]$ $\boldsymbol{N_c = 1\ \ 2/4}$	2.40/3.64/5.65	2.28/3.83/-

Table B.11 - Exclusion zone for Sector GSM900/UMTS antenna.

$\boldsymbol{N_{c,GSM}}$	$\boldsymbol{D_{front}}$ $[\mathbf{m}]$
1	3.72
2	4.89
4	8.37

B.6 Sector GSM900/LTE800 Antenna

Concerning GSM900, d_{min} has the value of 0.85 m in the near-field model instead of 2λ, because the interpolation becomes more efficient.

Table B.12 - Global Model simulation of the Sector GSM900/LTE800 antenna.

System	GSM900	LTE800
P_{in} [W]	25.24	2x25.24
Δ_{sp} [m]	8.3438x10^{-4}	7.6567x10^{-4}
Δ_{da}	0.95	0.87
Δ_{max} [V/m]	0.0193	0.0093
d_{Pa} [m]	6.28	5.89
$\frac{2D^2}{\lambda}$ [m]	31.69	29.15
$A_{[\mathrm{Vm}]}/B_{[\mathrm{V}]}/C_{[\mathrm{Vm}^{-1}]}$	-5.22/67.98/12.04	-19.24/72.75/13.22
$A'_{[\mathrm{W}]}/B'_{[\mathrm{Wm}^{-1}]}/C'_{[\mathrm{Wm}^{-2}]}$	-15.38/13.21/-0.29	-18.90/15.36/-0.37
D_{front} [m] $N_c = 1\ \ 2/4$	2.25/3.90/7.69	4.57/-/-

Table B.13 - Exclusion zone for Sector GSM900/LTE800 antenna.

$N_{c,GSM}$	D_{front} [m]
1	6.59
2	8.47
4	11.66

Table B.14 - Power variation of the Sector GSM900/LTE800 antenna for the GSM900.

P_{in} [W]	5.01	8.91	15.85	28.18	50.12
$A_{[\mathrm{Vm}]}/B_{[\mathrm{V}]}/C_{[\mathrm{Vm}^{-1}]}$	-2.33/ 30.30/5.37	-3.10/ 40.40/7.16	-4.14/ 53.87/9.54	-5.52/ 71.84/12.72	-7.36/ 95.80/16.97
$A'_{[\mathrm{W}]}/B'_{[W\mathrm{m}^{-1}]}$ $/C'_{[\mathrm{Wm}^{-2}]}$	-3.05/ 2.62/-0.06	-5.42/ 4.66/-0.10	-9.65/ 8.29/-0.18	-17.17/ 14.75/-0.32	-30.51/ 26.23/-0.57
D_{front} [m] $N_c = 1\ \ 2/4$	0.76/ 1.19/1.91	1.10/ 1.76/2.93	1.62/ 2.67/4.80	2.44/ 4.30/8.54	3.88/ 7.64/13.78

Table B.15 - Power variation of the Sector GSM900/LTE800 antenna for the LTE.

P_{in} $[W]$	5.01	8.91	15.85	28.18	50.12
$A_{[\mathrm{Vm}]}/B_{[\mathrm{V}]}/C_{[\mathrm{Vm}^{-1}]}$	-8.57/ 32.42/5.89	-11.43/ 43.23/7.86	-15.25/ 57.65/10.48	-20.33/ 76.87/13.98	-27.12/ 102.51/18.64
$A'_{[\mathrm{W}]}/B'_{[W\mathrm{m}^{-1}]}$ $/C'_{[\mathrm{Wm}^{-2}]}$	-3.76/ 3.05/-0.07	-6.67/ 5.43/-0.13	-11.87/ 9.65/-0.23	-21.12/ 17.16/-0.42	-37.52/ 30.51/-0.74
D_{front} $[\mathrm{m}]$	1.10	1.81	2.96	5.12	9.14

Table B.16 - N_{el} variation of the Sector GSM900/LTE800 antenna for GSM900.

N_{el}	4	6	8	10
G $[\mathrm{dBi}]$	8.5	10	11.4	12.8
Δ_{max} $[\mathrm{V/m}]$	0.0275	0.0171	0.0757	0.1562
d_{Pa} $[\mathrm{m}]$	1.64	3.95	6.24	6.00
$A_{[\mathrm{Vm}]}/B_{[\mathrm{V}]}/C_{[\mathrm{Vm}^{-1}]}$	5.00/ 32.48/11.97	4.50/ 30.41/7.97	-5.50/ 44.42/2.20	-11.61/ 52.71/0.18
$A'_{[\mathrm{W}]}/B'_{[\mathrm{Wm}^{-1}]}$ $/C'_{[\mathrm{Wm}^{-2}]}$	3.15/ 3.44/-0.10	-0.90/ 3.32/-0.08	4.73/ 0.89/-0.01	9.74/ -0.25/0.04
D_{front} $[\mathrm{m}]$ $N_c = 1\ \ 2/4$	1.26/ 2.04/3.44	1.04/ 1.57/2.54	1.07/ 1.62/2.44	1.19/ 1.82/2.69

Table B.17 - N_{el} variation of the Sector GSM900/LTE800 antenna for LTE system.

N_{el}	4	6	8	10
G $[\mathrm{dBi}]$	8.5	10	11.4	12.8
Δ_{max} $[\mathrm{V/m}]$	0.0272	0.0172	0.1455	0.1416
d_{Pa} $[\mathrm{m}]$	1.78	4.30	6.60	4.62
$A_{[\mathrm{Vm}]}/B_{[\mathrm{V}]}/C_{[\mathrm{Vm}^{-1}]}$	5.33/ 32.69/10.94	4.88/ 30.43/7.33	-7.97/ 48.26/0.51	-14.91/ 57.01/-1.47

Table B.17 (cont.) - N_{el} variation of the Sector GSM900/LTE800 antenna for LTE system.

$A'_{[W]}/B'_{[Wm^{-1}]}/C'_{[Wm^{-2}]}$	3.13/3.20/-0.10	-1.13/3.16/-0.08	8.37/-0.10/0.03	10.08/-0.81/0.06
D_{front} [m]	2.09	1.62	1.80	1.85

For LTE with the N_{el} equal to 10, t d_{min} has the numerical value of 0.96 m in the near-field model instead of 2λ, since the interpolation function becomes more efficient.

B.7 Sector UMTS/LTE2600MHz Antenna

Table B.18 - Global Model simulation of the Sector UMTS/LTE2600 antenna.

System	UMTS	LTE 2600
P_{in} [W]	25.24	2x25.24
Δ_{sp} [m]	7.4683x10^{-4}	9.2942x10^{-4}
Δ_{da}	1	1
Δ_{max} [V/m]	0.1724	0.1030
d_{Pa} [m]	8.03	7.54
$\frac{2D^2}{\lambda}$ [m]	28.18	35.00
$A_{[Vm]}/B_{[V]}/C_{[Vm^{-1}]}$	-4.20/85.38/13.35	-2.81/86.92/22.69
$A'_{[W]}/B'_{[Wm^{-1}]}/C'_{[Wm^{-2}]}$	-80.53/34.75/-0.99	-155.90/60.34/-1.49
D_{front} [m] $N_c = 1\ \ 2$	2.14/3.56	5.18/-

Table B.19 - Exclusion zone for Sector UMTS/LTE2600 antenna.

$N_{c,UMTS}$	D_{front} [m]
1	7.27
2	9.31

Table B.20 - Power variation of the Sector UMTS/LTE2600 antenna for the UMTS system.

P_{in} [W]	5.01	8.91	15.85	28.18	50.12
$A_{[\mathrm{Vm}]}/B_{[\mathrm{V}]}/C_{[\mathrm{Vm}^{-1}]}$	-1.87/ 38.05/5.95	-2.50/ 50.74/7.93	-3.33/ 67.66/10.58	-4.44/ 90.22/14.11	-5.93/ 120.31/18.82
$A'_{[\mathrm{W}]}/B'_{[W\mathrm{m}^{-1}]}$ $/C'_{[\mathrm{Wm}^{-2}]}$	-15.99/ 6.90/-0.20	-28.44/ 12.27/-0.35	-50.55/ 21.82/-0.62	-89.92/ 38.80/-1.11	-159.95 /69.01/-1.97
D_{front} [m] $N_c = 1\ \ 2$	0.77/1.17	1.09/1.69	1.57/2.51	2.31/3.89	3.54/6.55

Table B.21 - Power variation of the Sector UMTS/LTE2600 antenna for the LTE system.

P_{in} [W]	5.01	8.91	15.85	28.18	50.12
$A_{[\mathrm{Vm}]}/B_{[\mathrm{V}]}/C_{[\mathrm{Vm}^{-1}]}$	-1.25/ 38.73/10.11	-1.67/ 51.65/13.48	-2.23/ 68.88/17.98	-2.97/ 91.85/23.97	-3.96/ 122.49/31.97
$A'_{[\mathrm{W}]}/B'_{[\mathrm{Wm}^{-1}]}$ $/C'_{[\mathrm{Wm}^{-2}]}$	-30.95/ 11.98/-0.30	-55.07/ 21.31/-0.53	-97.92/ 37.89/-0.94	-174.11/ 67.38/-1.67	-309.62/ 119.83/-2.97
D_{front} [m]	1.29	1.96	3.19	5.94	11.73

Table B.22 - N_{el} variation of the Sector UMTS/LTE2600 antenna for UMTS system.

N_{el}	4	6	8	10
G [dBi]	8.5	10	11.4	12.8
Δ_{max} [V/m]	0.1700	0.0472	0.1724	0.2485
d_{Pa} [m]	2.86	1.76	8.03	5.14
$A_{[\mathrm{Vm}]}/B_{[\mathrm{V}]}/C_{[\mathrm{Vm}^{-1}]}$	0.16/ 42.05/18.64	1.47/ 32.88/15.72	-2.11/ 42.79/6.69	-4.10/ 48.02/4.46
$A'_{[\mathrm{W}]}/B'_{[\mathrm{Wm}^{-1}]}$ $/C'_{[\mathrm{Wm}^{-2}]}$	-8.31/ 16.01/-0.54	- 0.79/ 6.12/-0.19	-20.23/ 8.73/-0.25	4.42/ 3.52/-0.08
D_{front} [m] $N_c = 1\ \ 2$	1.26/2.28	0.81/1.32	0.88/1.36	0.98/1.49

Table B.23 - N_{el} variation of the Sector UMTS/LTE2600 antenna for LTE system.

N_{el}	4	6	8	10
$\mathbf{G}\ [\mathbf{dBi}]$	8.5	10	11.4	12.8
$\boldsymbol{\Delta_{max}}\ [\mathbf{V/m}]$	0.2233	0.0470	0.1030	0.2481
$\boldsymbol{d_{Pa}}\ [\mathbf{m}]$	2.39	1.42	7.54	4.14
$\boldsymbol{A}_{[\mathrm{Vm}]}/\boldsymbol{B}_{[\mathrm{V}]}/\boldsymbol{C}_{[\mathrm{Vm}^{-1}]}$	-0.40/ 45.02/20.19	1.17/ 32.92/19.50	-1.32/ 40.66/10.61	-3.30/ 48.00/5.54
$\boldsymbol{A'}_{[\mathrm{W}]}/\boldsymbol{B'}_{[\mathrm{Wm}^{-1}]}$ $/\boldsymbol{C'}_{[\mathrm{Wm}^{-2}]}$	-4.07/ 17.24/-0.48	1.00/ 7.30/-0.19	-34.11/ 13.20/-0.33	5.05/ 4.06/-0.09
$\boldsymbol{D_{front}}\ [\mathbf{m}]$	2.89	1.53	1.38	1.57

B.8 Sector GSM900/UMTS/LTE2600 Antenna

Table B.24 - Global Model simulation of the Sector GSM900/UMTS/LTE2600 antenna.

System	GSM900	UMTS	LTE 2600MHz
$\boldsymbol{P_{in}}\ [\mathbf{W}]$	25.24	25.24	2x25.24
$\Delta_{sp}\ [\mathbf{m}]$	1.1329×10^{-3}	2.5759×10^{-3}	3.2005×10^{-3}
$\boldsymbol{\Delta_{da}}$	1	1	1
$\boldsymbol{\Delta_{max}}\ [\mathbf{V/m}]$	0.0757	0.1726	0.1026
$\boldsymbol{d_{Pa}}\ [\mathbf{m}]$	6.24	8.02	7.59
$\frac{\mathbf{2}\boldsymbol{D}^{\mathbf{2}}}{\boldsymbol{\lambda}}\ [\mathbf{m}]$	42.88	96.77	120.16
$\boldsymbol{A}_{[\mathrm{Vm}]}/\boldsymbol{B}_{[\mathrm{V}]}/\boldsymbol{C}_{[\mathrm{Vm}^{-1}]}$	-10.78/86.73/4.27	-3.99/80.70/12.57	-2.47/77.31/20.29
$\boldsymbol{A'}_{[\mathrm{W}]}/\boldsymbol{B'}_{[\mathrm{Wm}^{-1}]}/\boldsymbol{C'}_{[\mathrm{Wm}^{-2}]}$	17.45/3.55/-0.04	-26.60/19.75/-0.19	-73.67/34.46/-0.27
$\boldsymbol{D_{front}}\ [\mathbf{m}]$ $\boldsymbol{N_c} = \mathbf{1}\ \ \mathbf{2/4}$	2.36/3.59/5.56	1.98/3.25/-	4.02/-/-

Table B.25 - Exclusion zone for Sector GSM900/UMTS/LTE2600 antenna.

$N_{c,GSM}/N_{c,UMTS}$	D_{front} [m]
1/1	7.15
2/1	8.46
4/2	11.98

B.9 Sector UMTS/LTE1800 Antenna

Table B.26 - Global Model simulation of the Sector UMTS/LTE1800 antenna.

System	UMTS	LTE 1800MHz
P_{in} [W]	25.24	2x25.24
Δ_{sp} [m]	7.0494 x10^{-4}	6.0156x10^{-4}
Δ_{da}	1	1
Δ_{max} [V/m]	0.1725	0.0919
d_{Pa} [m]	8.03	11.77
$\frac{2D^2}{\lambda}$ [m]	26.61	22.77
$A_{[Vm]}/B_{[V]}/C_{[Vm^{-1}]}$	-4.37/88.45/13.80	-3.72/82.32/15.47
$A'_{[W]}/B'_{[Wm^{-1}]}/C'_{[Wm^{-2}]}$	-91.82/38.64/-1.16	-530.97/101.79/-3.22
D_{front} [m] $N_c = 1\ \ 2$	2.24/3.76	3.64/-

Table B.27 - Exclusion zone for Sector UMTS/LTE1800 antenna.

$N_{c,UMTS}$	D_{front} [m]
1	5.32
2	7.18

B.10 Sector GSM900/LTE1800 Antenna

Concerning to GSM900, d_{min} has the value of 1 m in the near-field model instead of 2λ, because the interpolation becomes more efficient.

Table B.28 - Global Model simulation of the Sector GSM900/LTE1800 antenna.

System	GSM900	LTE 1800
$\boldsymbol{P_{in}}$ $[\mathbf{W}]$	25.24	2x25.24
Δ_{sp} $[\mathbf{m}]$	6.7679x10^{-4}	1.3216x10^{-4}
$\boldsymbol{\Delta_{da}}$	0.86	1
$\boldsymbol{\Delta_{max}}$ $[\mathbf{V/m}]$	0.0103	0.0919
$\boldsymbol{d_{Pa}}$ $[\mathbf{m}]$	2.77	11.79
$\frac{\mathbf{2}\boldsymbol{D}^{\mathbf{2}}}{\boldsymbol{\lambda}}$ $[\mathbf{m}]$	25.78	49.77
$\boldsymbol{A}_{[\mathrm{Vm}]}/\boldsymbol{B}_{[\mathrm{V}]}/\boldsymbol{C}_{[\mathrm{Vm}^{-1}]}$	-15.09/62.15/13.05	-3.28/72.52/13.63
$\boldsymbol{A'}_{[\mathrm{W}]}/\boldsymbol{B'}_{[\mathrm{Wm}^{-1}]}/\boldsymbol{C'}_{[\mathrm{Wm}^{-2}]}$	0.77/8.74/-0.21	-147.15/33.95/-0.59
$\boldsymbol{D_{front}}$ $[\mathbf{m}]$ $\boldsymbol{N_c} = \mathbf{1}\ \ \mathbf{2/4}$	1.90/3.51/6.40	2.96/-/-

Table B.29 - Exclusion zone for Sector GSM900/LTE1800 antenna.

$\boldsymbol{N_{c,GSM}}$	$\boldsymbol{D_{front}}$ $[\mathbf{m}]$
1	4.46
2	6.00
4	8.87

B.11 Sector LTE1800/LTE2600 Antenna

Table B.30 - Global Model simulation of the Sector LTE1800/LTE2600 antenna.

System	LTE 1800	LTE 2600
P_{in} [W]	2x25.24	2x25.24
Δ_{sp} [m]	6.3739x10^{-4}	9.2942x10^{-4}
Δ_{da}	1	1
Δ_{max} [V/m]	0.0912	0.1030
d_{Pa} [m]	12.04	7.54
$\frac{2D^2}{\lambda}$ [m]	24.11	35.00
$A_{[Vm]}/B_{[V]}/C_{[Vm^{-1}]}$	-3.60/80.33/15.17	-2.81/86.92/22.69
$A'_{[W]}/B'_{[Wm^{-1}]}/C'_{[Wm^{-2}]}$	-495.82/93.34/-2.83	-155.92/60.34/-1.49
D_{front} [m]	3.50	5.18

Table B.31 - Exclusion zone for Sector LTE1800/LTE2600 antenna.

D_{front} [m]
9.67

B.12 Omni GSM900/UMTS Antenna

Table B.32 - Global Model simulation of the Omni GSM900/UMTS antenna.

System	GSM900	UMTS
P_{in} [W]	25.24	25.24
Δ_{sp} [m]	1.5195x10^{-3}	3.4483 x10^{-3}
Δ_{da}	1	1
Δ_{max} [V/m]	0.0758	0.1718

Table B.32 (cont.) - Global Model simulation of the Omni GSM900/UMTS antenna.

d_{Pa} [m]	6.24	8.03
$\frac{2D^2}{\lambda}$ [m]	57.38	129.49
$A_{[Vm]}/B_{[V]}/C_{[Vm^{-1}]}$	-4.19/33.73/1.66	-1.80/36.44/5.70
$A'_{[W]}/B'_{[Wm^{-1}]}/C'_{[Wm^{-2}]}$	2.64/0.54/-0.01	-4.83/3.88/-0.03
D_{front} [m] $N_c = 1\ \ 2/4$	0.75/1.16/1.76	0.73/1.11/-

Table B.33 - Exclusion zone for Omni GSM900/UMTS antenna.

$N_{c,GSM}/N_{c,UMTS}$	D_{front} [m]
1/1	1.13
2/1	1.47
4/2	2.24

B.13 Omni GSM1800 Antenna

Table B.34 - Global Model simulation of the Omni GSM1800 antenna.

P_{in} [W]	25.24
Δ_{sp} [m]	7.8395×10^{-4}
Δ_{da}	1
Δ_{max} [V/m]	0.0921
d_{Pa} [m]	11.76
$\frac{2D^2}{\lambda}$ [m]	29.61
$A_{[Vm]}/B_{[V]}/C_{[Vm^{-1}]}$	-1.74/38.50/7.23
$A'_{[W]}/B'_{[Wm^{-1}]}/C'_{[Wm^{-2}]}$	-72.15/14.81/-0.39

Table B.34 (cont.) - Global Model simulation of the Omni GSM1800 antenna.

D_{front} [m] $N_c = 1\ \ 2\ /4$	0.79/1.21/1.93

B.14 Sector LTE800/LTE1800 Antenna

Table B.35 - Global Model simulation of the Sector LTE800/LTE1800 antenna.

System	LTE 800	LTE 1800
P_{in} [W]	2x25.24	2x25.24
Δ_{sp} [m]	6.2820×10^{-4}	1.3373×10^{-4}
Δ_{da}	0.79	1
Δ_{max} [V/m]	0.0134	0.0909
d_{Pa} [m]	2.49	3.76
$\frac{2D^2}{\lambda}$ [m]	23.99	50.36
$A_{[Vm]}/B_{[V]}/C_{[Vm^{-1}]}$	-17.02/64.84/15.34	-3.45/77.50/14.69
$A'_{[W]}/B'_{[Wm^{-1}]}/C'_{[Wm^{-2}]}$	-0.21/10.94/-0.29	4.63/14.28/-0.24
D_{front} [m]	4.46	3.31

Table B.36 - Exclusion zone for Sector LTE800/LTE1800 antenna.

D_{front} [m]
7.04

B.15 Indoor sector Antennas

Table B.37 - Simulation of the Indoor sector antennas, when the BS is not shared.

System	GSM900	GSM1800	LTE1800		UMTS	LTE 2600	
			W/O MIMO	W MIMO		W/O MIMO	W MIMO
P_{in} [mW]	759.		126.	2x126.	126.	126.	2x126.
V_0 [V]	6.16		2.51				
Δ_{sp} [m]	9.4658x10^{-5}	9.7233 x10^{-5}	9.7233 x10^{-5}		9.7634 x10^{-5}	9.8095 x10^{-5}	
D_{front} [m] $N_c = 1\ \ 2/4$	$< \lambda$						

Table B.38 - Simulation of the Indoor sector antennas, when the BS is shared.

System	GSM900	GSM1800	LTE1800		UMTS	LTE2600	
			W/O MIMO	W MIMO		W/O MIMO	W MIMO
P_{in} [mW]	191.		32.	2x32.	32.	32.	2x32.
V_0 [V]	3.09		1.26				
Δ_{sp} [m]	9.4658x10^{-5}	9.7233 x10^{-5}	9.7233 x10^{-5}		9.7634 x10^{-5}	9.8095 x10^{-5}	
D_{front} [m] $N_c = 1\ \ 2/4$	$< \lambda$						

Table B.39 - Power variation of the Indoor sector antenna (W MIMO).

P_{in} [mW]		2.51	3.16	3.98	5.01	6.31
V_0 [V]		11.21	12.57	14.11	15.83	17.76
D_{front} [m] $N_c = 1\ \ 2/4$	**GSM900**	$< \lambda$/ $< \lambda$/0.32	$< \lambda$/ $< \lambda$/0.36	$< \lambda$/ $< \lambda$/0.41	$< \lambda$ /0.32/0.46	$< \lambda$ /0.36/ 0.51
	GSM1800	$< \lambda$/ $< \lambda$/0.23	$< \lambda$ /0.19/0.26	$< \lambda$ /0.21/0.29	$< \lambda$ /0.23/0.33	0.19/0.26/ 0.37
	UMTS	$< \lambda$/0.16/-	$< \lambda$/0.18/-	$< \lambda$/0.20/-	0.16/0.22/-	0.18/0.25/-
	LTE1800	$< \lambda$/-/-	0.19/-/-	0.21/-/-	0.23/-/-	0.26/-/-

B.16 Indoor Omnidirectional Antennas

Table B.40 - Simulation of the Indoor Omnidirectional antennas, when the BS is not shared.

System	GSM900	GSM1800	LTE1800		UMTS	LTE2600	
			W/O MIMO	W MIMO		W/O MIMO	W MIMO
P_{in} [W]	2.399		0.398	2x0.398	0.398	0.398	2x0.398
I_0 [A]	0.22		0.09				
Δ_{sp} [m]	9.4658x10^{-5}	9.7233 x10^{-5}	9.7233 x10^{-5}		9.7634 x10^{-5}	9.8095 x10^{-5}	
D_{front} [m] $N_c = 1\ \ 2\ /4$	$< \lambda$/0.44/0.63	0.23/0.32/0.45	$< \lambda$		$< \lambda$	$< \lambda$	0.12

Table B.41 - Simulation of the Indoor Omnidirectional antennas, when the BS is shared.

System	GSM900	GSM1800	LTE1800		UMTS	LTE 2600	
			W/O MIMO	W MIMO		W/O MIMO	W MIMO
P_{in} [W]	0.603		0.100	2x0.100	0.398	0.398	2x0.100
I_0 [A]	0.11		0.04				
Δ_{sp} [m]	9.4658x10^{-5}	9.7233 x10^{-5}	9.7233 x10^{-5}		9.7634 x10^{-5}	9.8095 x10^{-5}	
D_{front} [m] $N_c = 1\ \ 2\ /4$	$< \lambda$	$< \lambda$ /$< \lambda$/0.23	$< \lambda$		$< \lambda$	$< \lambda$	

Table B.42 - Power variation of the Indoor Omnidirectional antenna (W MIMO).

P_{in} [mW]		2.51	3.16	3.98	5.01	6.31
I_0 [A]		0.22	0.25	0.28	0.32	0.36
D_{front} [m] $N_c = 1\ \ 2\ /4$	**GSM900**	$< \lambda$/ 0.45/0.64	0.36/ 0.51/0.72	0.40/ 0.57/0.81	0.45/ 0.64/0.90	0.51/ 0.72/1.02
	GSM1800	0.23/ 0.33/0.46	0.26/ 0.37/0.52	0.29/ 0.41/0.58	0.33/ 0.46/0.65	0.37/ 0.52/0.73
	UMTS	0.22/0.31/-	0.25/0.35/-	0.28/0.39/-	0.31/0.44/-	0.35/0.49/-

Table B.42 (cont.) - Power variation of the Indoor Omnidirectional antenna (W MIMO).

	LTE 1800	0.33/-/-	0.37/-/-	0.41/-/-	0.46/-/-	0.52/-/-

Annex C

Additional Results

This annex provides supplementary information to support the performed work.

In order to study the validity minimum distances of this model, $2D^2 \ \lambda$, one should assume the value of higher frequency of each band, because it corresponds to higher values of this distance. Table C.1 shows these results, assuming the largest dimension of the antenna, D, minimum and maximum of 1.3 m and 2.6 m respectively [Andr12], [Allg12], [JAYB12], [KATH12a]. The bands corresponding LTE at 900 MHz, 1800 MHz and 2100 MHz are not analysed as they are very close to those used for GSM and UMTS.

Table C.1 - Distance of far-field region for typical outdoor and indoor scenarios.

System	Outdoor		Indoor	
	D [m]	$2D^2 \ \lambda$ [m]	D [m]	$2D^2 \ \lambda$ [m]
LTE 800 MHz (875 MHz)	1.300	9.86	0.175	0.18
	2.600	39.43	0.305	0.54
GSM 900 (960 MHz)	1.300	10.82	0.175	0.20
	2.600	43.26	0.305	0.60
GSM 1800 (1880 MHz)	1.300	21.18	0.175	0.38
	2.600	84.73	0.305	1.17
UMTS (2170 MHz)	1.300	24.45	0.175	0.44
	2.600	97.79	0.305	1.35
LTE 2600 MHz (2690 MHz)	1.300	30.30	0.175	0.55
	2.600	121.23	0.305	1.67

Figure C.1 shows the evolution of the directivity of a collinear transversal array as a function of normalised distance between elements and for different values of the elements number.

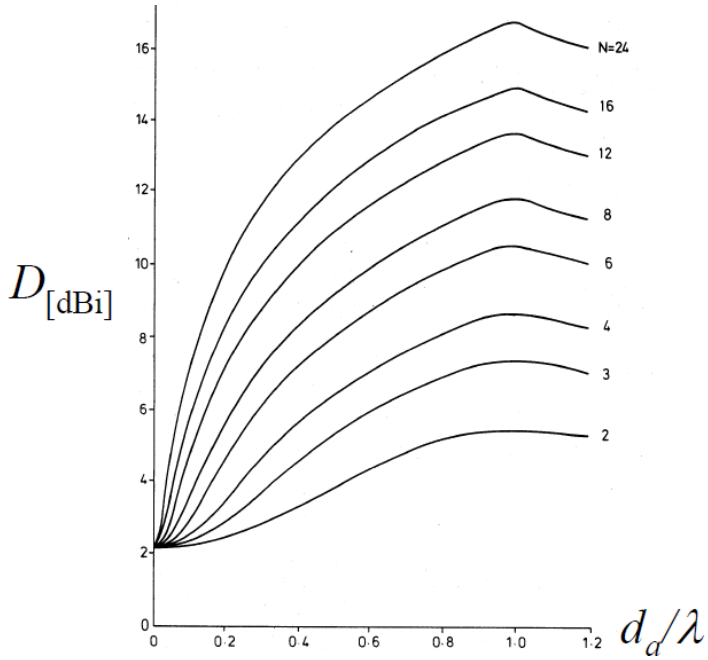

Figure C.1 - Directivity for a collinear transversal array of dipoles [Corre12a].

Annex D

Distance Evaluation Results

The values of the estimated exclusion region in the BS frontal zone for each scenario under study are presented in this annex. The associated power ratio with these distances and the auxiliary results of the qualitative analysis are also shown.

D.1 Exclusion zone results for the work scenarios

In the following, results of frontal side border of the exclusion region are presented for the work scenarios, W and W/O LTE system. The results are obtained from the electric field global model described in Section 3.5, with simulations of the BS antennas in Annex B. The percentage differences between the exclusion region W/O and W LTE are also presented.

Table D.1 - Obtained $\mathrm{D_{front}}$ for SRural-1.a scenario.

	$N_{c,GSM900}/N_{c,UMTS}$	D_{front} [m]		$\frac{D_{front}^{W}-D_{front}^{W/O}}{D_{front}^{W/O}}$ [%]
		W/O LTE	W LTE	
SRural-1.a	1/1	4.59	8.61	88.
	2/1	6.73	10.28	53.
	4/2	11.75	14.35	22.

Table D.2 - Obtained $\mathrm{D_{front}}$ for SRural-1.b scenario.

	$N_{c,GSM900}/N_{c,GSM1800}/N_{c,UMTS}$	D_{front} [m]		$\frac{D_{front}^{W}-D_{front}^{W/O}}{D_{front}^{W/O}}$ [%]
		W/O LTE	W LTE	
SRural-1.b	1/1/1	6.20	12.03	94.
	2/2/1	10.16	13.48	33.
	4/4/2	16.35	16.57	1.

Table D.3 - Obtained $\mathrm{D_{front}}$ for ORural-1 scenario.

	$N_{c,GSM900}/N_{c,GSM1800}/N_{c,UMTS}$	D_{front} [m]		$\frac{D_{front}^{W}-D_{front}^{W/O}}{D_{front}^{W/O}}$ [%]
		W/O LTE	W LTE	
ORural-1	1/1/1	1.50	7.44	396.
	2/2/1	2.10	7.59	261.
	4/4/2	3.39	8.13	140.

Table D.4 - Obtained D_{front} for SUrban-1.a scenario.

	$N_{c,GSM900}/N_{c,UMTS}$	D_{front} [m]		$\frac{D_{front}^{W}-D_{front}^{W/O}}{D_{front}^{W/O}}$ [%]
		W/O LTE	W LTE	
SUrban-1.a	1/1	4.59	9.75	112.
	2/1	6.73	11.51	71.
	4/2	11.75	15.16	29.

Table D.5 - Obtained D_{front} for SUrban-1.b scenario.

	$N_{c,GSM900}/N_{c,GSM1800}/N_{c,UMTS}$	D_{front} [m]		$\frac{D_{front}^{W}-D_{front}^{W/O}}{D_{front}^{W/O}}$ [%]
		W/O LTE	W LTE	
SUrban-1.b	1/1/1	6.20	12.07	95.
	2/2/1	10.16	13.21	30.
	4/4/2	16.35	16.07	-2

Table D.6 - Obtained D_{front} for SUrban-2.a scenario.

	$N_{c,GSM900}/N_{c,UMTS}$	D_{front} [m]		$\frac{D_{front}^{W}-D_{front}^{W/O}}{D_{front}^{W/O}}$ [%]
		W/O LTE	W LTE	
SUrban-2.a	1/1	3.72	7.15	92.
	2/1	4.89	8.46	73.
	4/2	8.37	11.98	43.

Table D.7 - Obtained D_{front} for SUrban-2.b scenario.

	$N_{c,GSM900}/N_{c,GSM1800}/N_{c,UMTS}$	D_{front} [m]		$\frac{D_{front}^{W}-D_{front}^{W/O}}{D_{front}^{W/O}}$ [%]
		W/O LTE	W LTE	
SUrban-2.b	1/1/1	5.09	12.75	150.

Table D.7 (cont.) - Obtained D_{front} for SUrban-2.b scenario.

	2/2/1	7.93	13.58	71.
	4/4/2	15.10	16.28	8.

Table D.8 - Obtained D_{front} for OUrban-1 scenario.

	$N_{c,GSM900}/N_{c,GSM1800}/N_{c,UMTS}$	D_{front} [m]		$\frac{D_{front}^{W} - D_{front}^{W/O}}{D_{front}^{W/O}}$ [%]
		W/O LTE	**W LTE**	
OUrban-1	**1/1/1**	1.50	10.21	581.
	2/2/1	2.10	10.39	395.
	4/4/2	3.39	11.07	227.

Table D.9 - Obtained D_{front} for IPainel1 and IPainel2 scenario.

$N_{c,GSM900}/N_{c,GSM1800}/N_{c,UMTS}$		D_{front} [m]				$\frac{D_{front}^{W} - D_{front}^{W/O}}{D_{front}^{W/O}}$ [%]	
		BS Shared		**BS No Shared**		**BS Shared**	**BS No Shared**
		W/O LTE	**W LTE**	**W/O LTE**	**W LTE**		
1/1/1	**W/O MIMO**	$< \lambda_{GSM900}$		$< \lambda_{GSM900}$		-	
	W MIMO						
2/2/1	**W/O MIMO**						
	W MIMO						
4/4/2	**W/O MIMO**						
	W MIMO						

Table D.10 - Obtained D_{front} for ICeiling-1 scenario.

$N_{c,GSM900}/N_{c,GSM1800}/N_{c,UMTS}$		D_{front} [m] BS Shared W/O LTE	D_{front} [m] BS Shared W LTE	D_{front} [m] BS No Shared W/O LTE	D_{front} [m] BS No Shared W LTE	$\frac{D_{front}^{W}-D_{front}^{W/O}}{D_{front}^{W/O}}$ [%] BS Shared	$\frac{D_{front}^{W}-D_{front}^{W/O}}{D_{front}^{W/O}}$ [%] BS No Shared
1/1/1	W/O MIMO	$< \lambda_{GSM900}$		0.40	0.34	-	-15.
	W MIMO				0.35		-13.
2/2/1	W/O MIMO			0.78	0.64		-16
	W MIMO				0.65		-15
4/4/2	W/O MIMO	0.39	0.32	0.78	0.64	-18.	-18.
	W MIMO		0.33		0.65	-15.	-17

Table D.11 - Obtained D_{front} for ICeiling-2 scenario.

$N_{c,GSM900}/N_{c,GSM1800}/N_{c,UMTS}$		D_{front} [m] BS Shared W/O LTE	D_{front} [m] BS Shared W LTE	D_{front} [m] BS No Shared W/O LTE	D_{front} [m] BS No Shared W LTE	$\frac{D_{front}^{W}-D_{front}^{W/O}}{D_{front}^{W/O}}$ [%] BS Shared	$\frac{D_{front}^{W}-D_{front}^{W/O}}{D_{front}^{W/O}}$ [%] BS No Shared
1/1/1	W/O MIMO	$< \lambda_{GSM900}$		0.40	0.35	-	-13.
	W MIMO				0.37		-8.
2/2/1	W/O MIMO			0.55	0.47		-15.
	W MIMO				0.49		-11.
4/4/2	W/O MIMO	0.39	0.33	0.78	0.65	-15.	-17.
	W MIMO				0.66		-15.

Table D.12 - Power impact in the D_{front} value for SRural-1.a scenario.

$N_{c,GSM900}/N_{c,UMTS}$		P_{in} [dBm]				
		37	**39.5**	**42**	**44.5**	**47**
1/1	D_{front} [m] **W/O LTE**	1.26	1.94	3.09	5.06	8.50
	D_{front} [m] **W LTE**	2.01	3.17	5.36	9.52	14.69
	$\frac{D_{front}^{W} - D_{front}^{W/O}}{D_{front}^{W/O}}$ [%]	60.	63.	73.	88.	73.
2/1	D_{front} [m] **W/O LTE**	1.70	2.72	4.48	7.41	11.69
	D_{front} [m] **W LTE**	2.35	3.77	6.62	11.25	16.70
	$\frac{D_{front}^{W} - D_{front}^{W/O}}{D_{front}^{W/O}}$ [%]	38.	39.	48.	52.	43.
4/2	D_{front} [m] **W/O LTE**	3.01	4.96	8.20	12.66	17.56
	D_{front} [m] **W LTE**	3.39	5.76	10.11	15.41	20.95
	$\frac{D_{front}^{W} - D_{front}^{W/O}}{D_{front}^{W/O}}$ [%]	13.	16.	23.	22.	19.

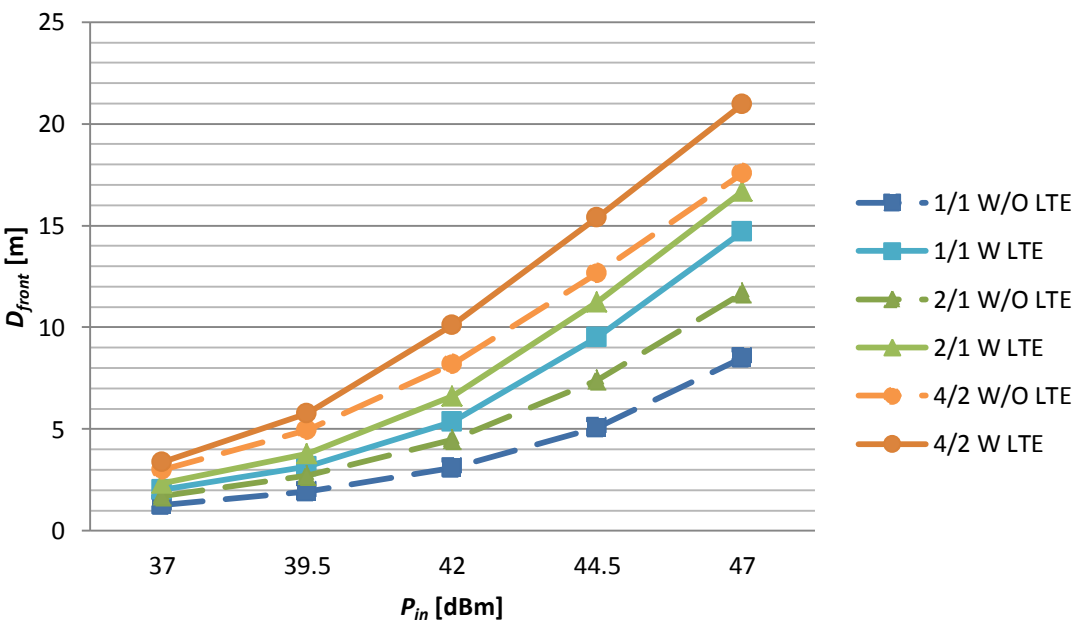

Figure D.1 - Power impact in the D_{front} value for SRural-1.a scenario

Table D.13 - Power impact in the D_{front} value for SUrban-1.a scenario.

$N_{c,GSM900}/N_{c,UMTS}$		P_{in} [dBm]				
		37	**39.5**	**42**	**44.5**	**47**
1/1	D_{front} [m] **W/O LTE**	1.26	1.94	3.09	5.06	8.50
	D_{front} [m] **W LTE**	2.06	3.35	5.89	10.78	16.36
	$\frac{D_{front}^{W}-D_{front}^{W/O}}{D_{front}^{W/O}}$ [%]	63.	73.	91.	113.	92.
2/1	D_{front} [m] **W/O LTE**	1.70	2.72	4.48	7.41	11.69
	D_{front} [m] **W LTE**	2.50	4.19	7.48	12.54	18.10
	$\frac{D_{front}^{W}-D_{front}^{W/O}}{D_{front}^{W/O}}$ [%]	47.	54.	67.	69.	55.
4/2	D_{front} [m] **W/O LTE**	3.01	4.96	8.20	12.66	17.56
	D_{front} [m] **W LTE**	3.75	6.43	10.90	16.21	21.62
	$\frac{D_{front}^{W}-D_{front}^{W/O}}{D_{front}^{W/O}}$ [%]	25.	30.	33.	28.	23.

Table D.14 - Power impact in the D_{front} value for IPanel-1 scenario (W MIMO).

$N_{c,GSM900}/N_{c,GSM1800}/N_{c,UMTS}$		P_{in} [dBm]				
		34	**35**	**36**	**37**	**38**
1/1/1	D_{front} [m] **W/O LTE**	$< \lambda_{GSM900}$		$< \lambda_{GSM900}$	0.32	0.36
	D_{front} [m] **W LTE**			0.32	0.36	0.41
	$\frac{D_{front}^{W}-D_{front}^{W/O}}{D_{front}^{W/O}}$ [%]	-		-	13.	14.
2/2/1	D_{front} [m] **W/O LTE**	$< \lambda_{GSM900}$	0.34	0.38	0.43	0.48
	D_{front} [m] **W LTE**					
	$\frac{D_{front}^{W}-D_{front}^{W/O}}{D_{front}^{W/O}}$ [%]	-	-	-	-	-

Table D.14 (cont.)- Power impact in the D_{front} value for IPanel-1 scenario (W MIMO).

4/4/2	D_{front} [m] W/O LTE	0.43	0.48	0.54	0.61	0.68
	D_{front} [m] W LTE	0.40	0.45	0.50	0.56	0.63
	$\frac{D_{front}^{W} - D_{front}^{W/O}}{D_{front}^{W/O}}$ [%]	-7.	-6.	-7.	-8.	-7.

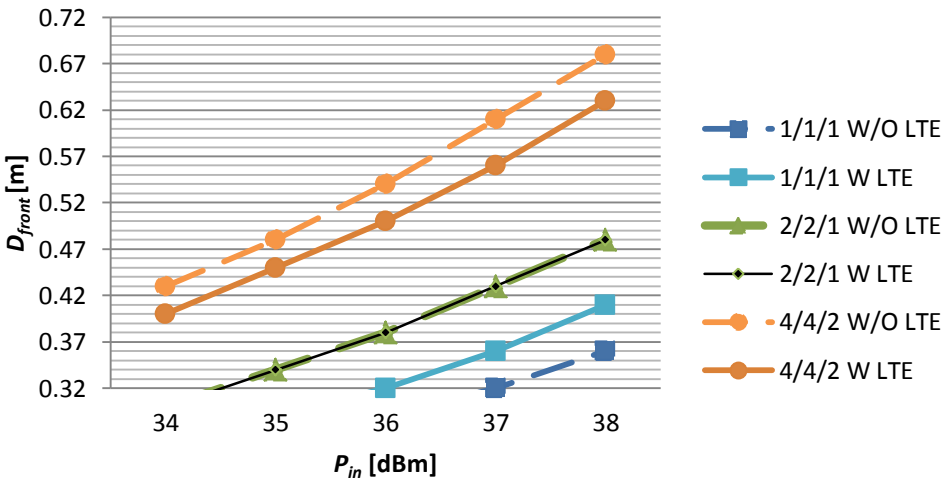

Figure D.2 - Power impact in the D_{front} value for IPanel-1 scenario (W MIMO).

Table D.15 - Power impact in the D_{front} value for ICeiling-1 scenario (W MIMO).

$N_{c,GSM900}/N_{c,GSM1800}/N_{c,UMTS}$		P_{in} [dBm] 34	35	36	37	38
1/1/1	D_{front} [m] W/O LTE	0.45	0.51	0.57	0.64	0.72
	D_{front} [m] W LTE	0.51	0.57	0.64	0.72	0.80
	$\frac{D_{front}^{W} - D_{front}^{W/O}}{D_{front}^{W/O}}$ [%]	13.	12.	12.	13.	11.
2/2/1	D_{front} [m] W/O LTE / W LTE	0.60	0.67	0.75	0.85	0.95
	$\frac{D_{front}^{W} - D_{front}^{W/O}}{D_{front}^{W/O}}$ [%]	-	-	-	-	-

Table D.15 (cont.) - Power impact in the D_{front} value for ICeiling-1 scenario (W MIMO).

4/4/2	D_{front} [m] W/O LTE	0.85	0.95	1.07	1.20	1.34
	D_{front} [m] W LTE	0.78	0.88	0.99	1.11	1.24
	$\frac{D_{front}^{W} - D_{front}^{W/O}}{D_{front}^{W/O}}$ [%]	-8.	-7.	-7.	-7.	-7.

Table D.16 - D_{front} values with the N_{el} variation for SRural-1.a.

	$N_{c,GSM900}/N_{c,UMTS}$		N_{el} 4	6	8	10
SRural-1.a	1/1	D_{front} [m] W/O LTE	2.15	1.46	1.50	1.66
		D_{front} [m] W LTE	3.72	2.53	2.50	2.61
		$\frac{D_{front}^{W} - D_{front}^{W/O}}{D_{front}^{W/O}}$ [%]	73.	73.	67.	57.
	2/1	D_{front} [m] W/O LTE	2.96	2.00	1.97	2.18
		D_{front} [m] W LTE	4.39	3.03	2.83	2.97
		$\frac{D_{front}^{W} - D_{front}^{W/O}}{D_{front}^{W/O}}$ [%]	48.	52.	44.	36.
	4/2	D_{front} [m] W/O LTE	5.25	3.51	3.04	3.26
		D_{front} [m] W LTE	6.45	4.59	3.73	3.84
		$\frac{D_{front}^{W} - D_{front}^{W/O}}{D_{front}^{W/O}}$ [%]	23.	31.	23.	18.

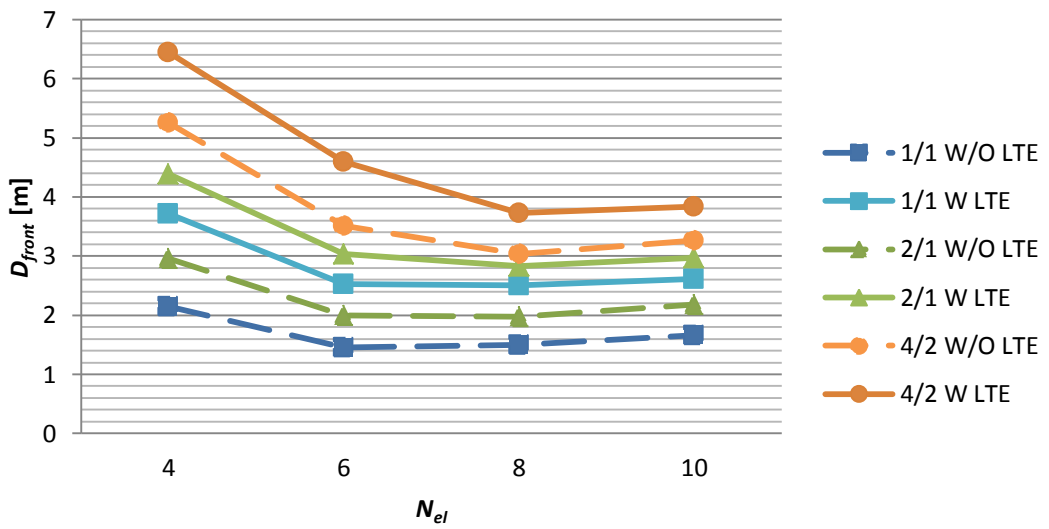

Figure D.3 - D_{front} values with the N_{el} variation for SRural-1.a.

Table D.17 - D_{front} values with the N_{el} variation for SUrban-1.a.

	$N_{c,GSM900}/N_{c,UMTS}$		N_{el}			
			4	**6**	**8**	**10**
SUrban-1.a	**1/1**	D_{front} [m] **W/O LTE**	2.15	1.46	1.50	1.66
		D_{front} [m] **W LTE**	4.76	2.65	2.31	2.48
		$\frac{D_{front}^{W}-D_{front}^{W/O}}{D_{front}^{W/O}}$ [%]	121.	82.	54.	49.
	2/1	D_{front} [m] **W/O LTE**	2.96	2.00	1.97	2.18
		D_{front} [m] **W LTE**	5.40	3.18	2.74	2.90
		$\frac{D_{front}^{W}-D_{front}^{W/O}}{D_{front}^{W/O}}$ [%]	82.	59.	39.	33.
	4/2	D_{front} [m] **W/O LTE**	5.25	3.51	3.04	3.26
		D_{front} [m] **W LTE**	7.39	4.73	3.80	3.87
		$\frac{D_{front}^{W}-D_{front}^{W/O}}{D_{front}^{W/O}}$ [%]	41.	35.	25.	19.

D.2 Power Ratio Results

The power contribution that the GSM, UMTS or LTE BS antenna has on the exclusion region of the total BS site is presented for the study scenarios, according to (3.30). The different carrier topologies are taken into account.

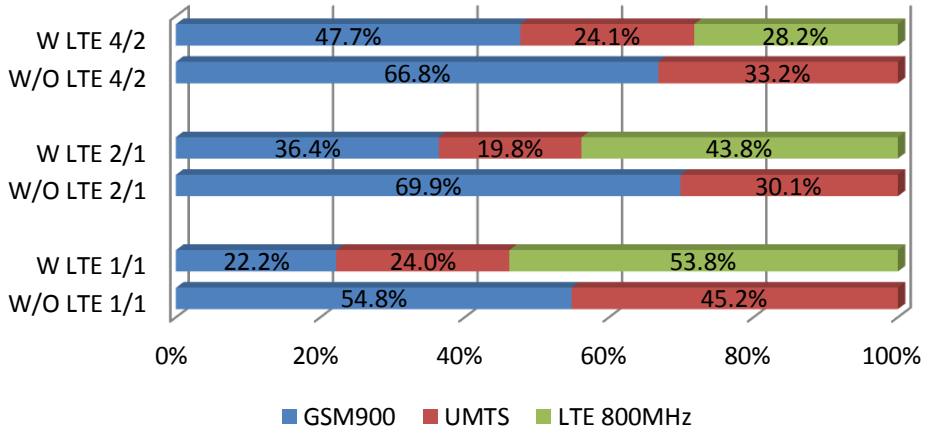

Figure D.4 - Power ratio involved in the simulation of SRural-1.a.

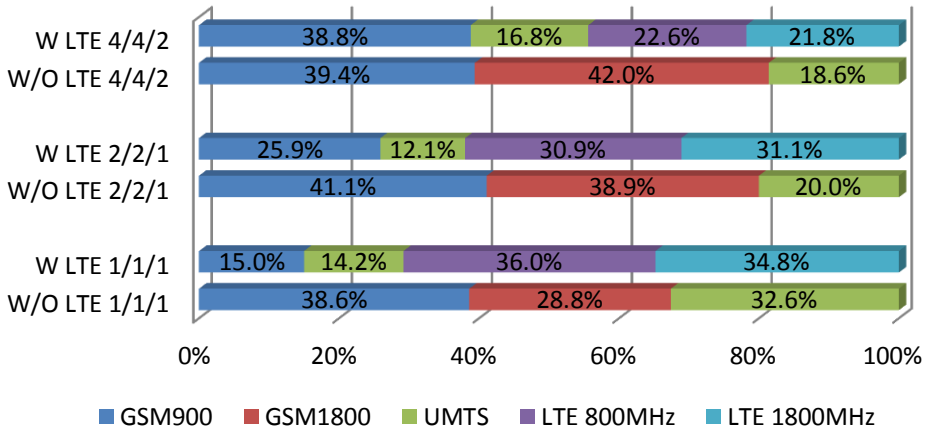

Figure D.5 - Power ratio involved in the simulation of SRural-1.b.

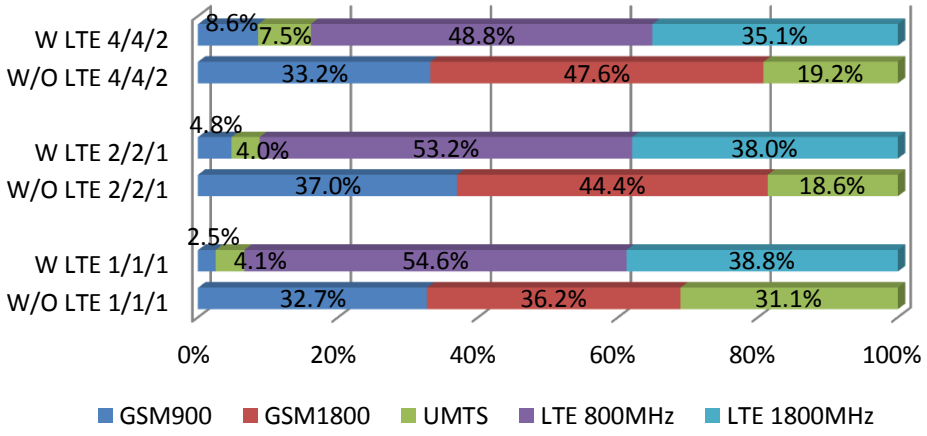

Figure D.6 - Power ratio involved in the simulation of ORural-1.

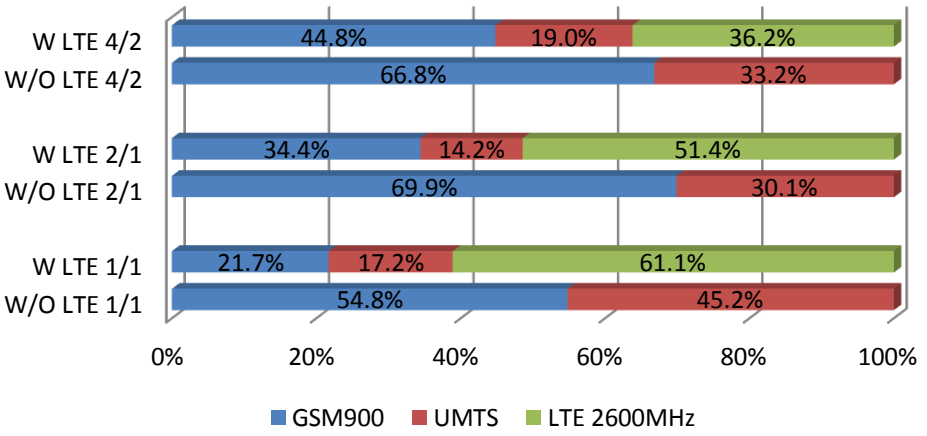

Figure D.7 - Power ratio involved in the simulation of SUrban-1.a.

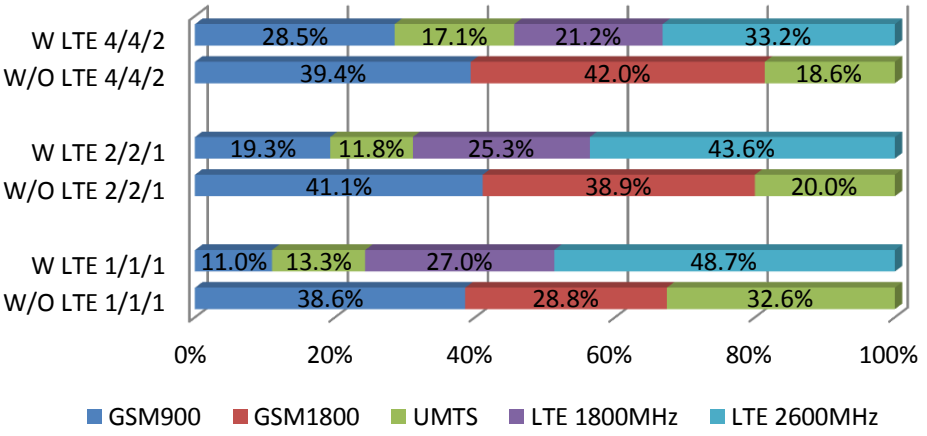

Figure D.8 - Power ratio involved in the simulation of SUrban-1.b.

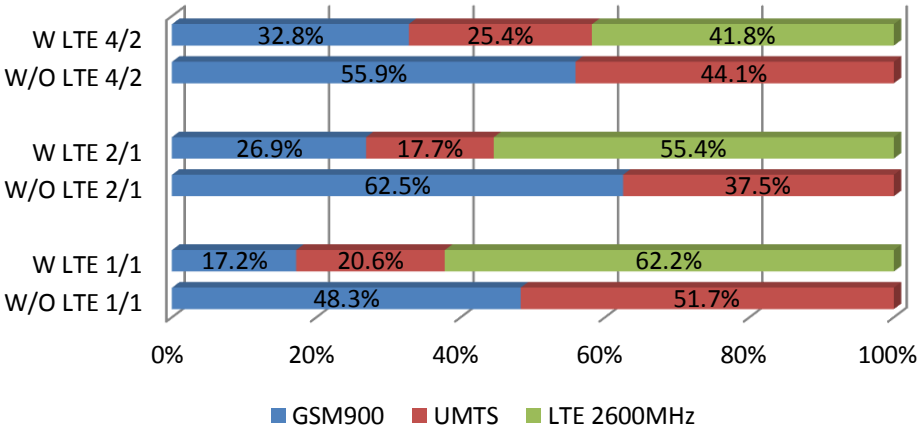

Figure D.9 - Power ratio involved in the simulation of SUrban-2.a.

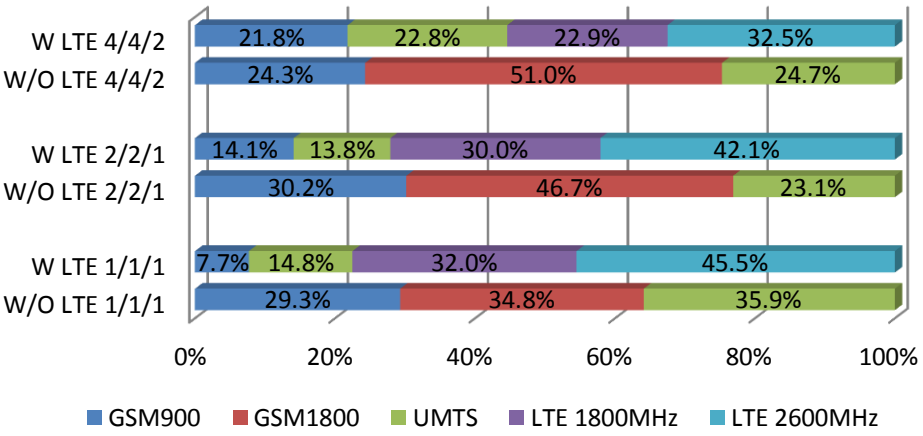

Figure D.10 - Power ratio involved in the simulation of SUrban-2.b.

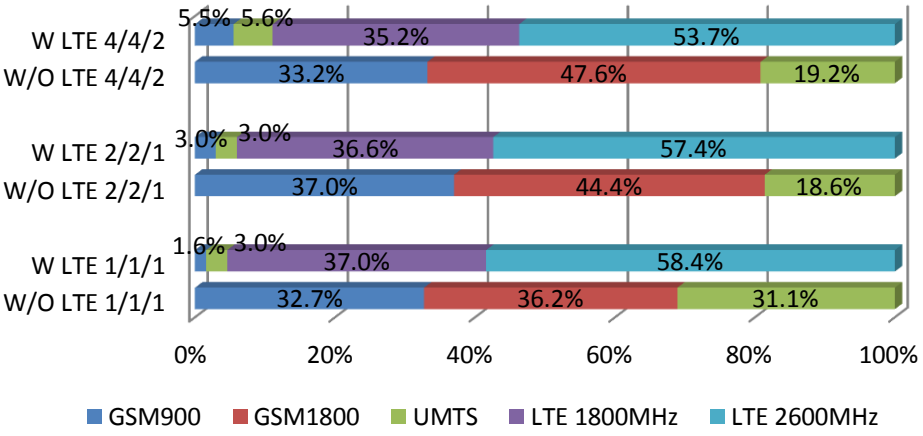

Figure D.11 - Power ratio involved in the simulation of OUrban-1.

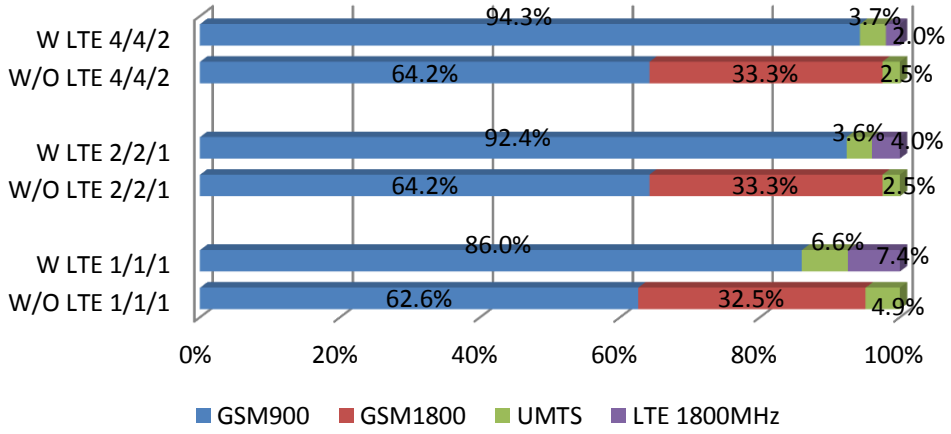

Figure D.12 - Power ratio involved in the simulation of IPanel-1 (BS Shared, WO MIMO).

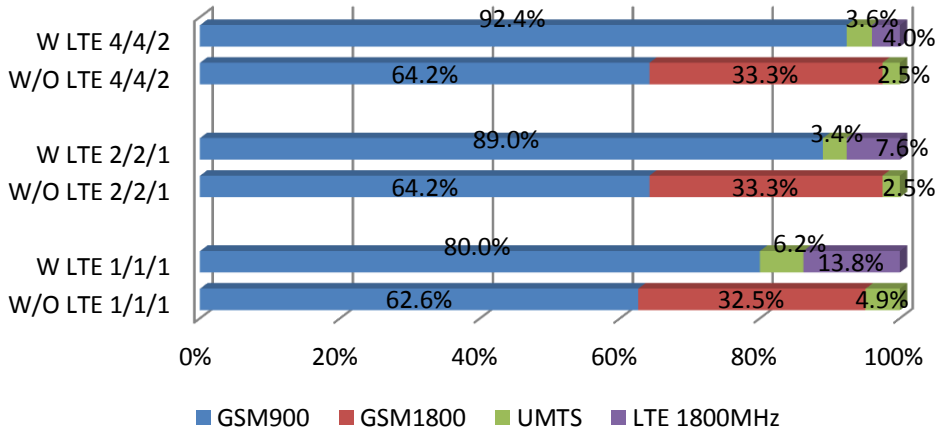

Figure D.13 - Power ratio involved in the simulation of IPanel-1 (BS Shared, W MIMO).

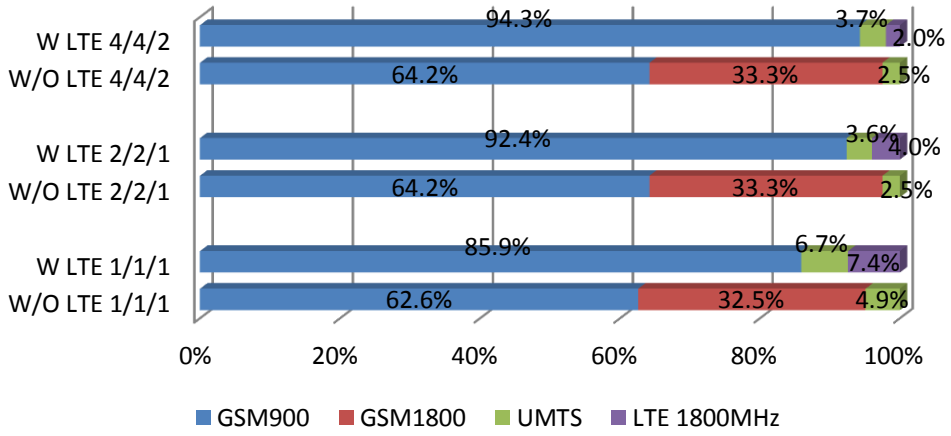

Figure D.14 - Power ratio involved in the simulation of IPanel-1 (BS No Shared, WO MIMO).

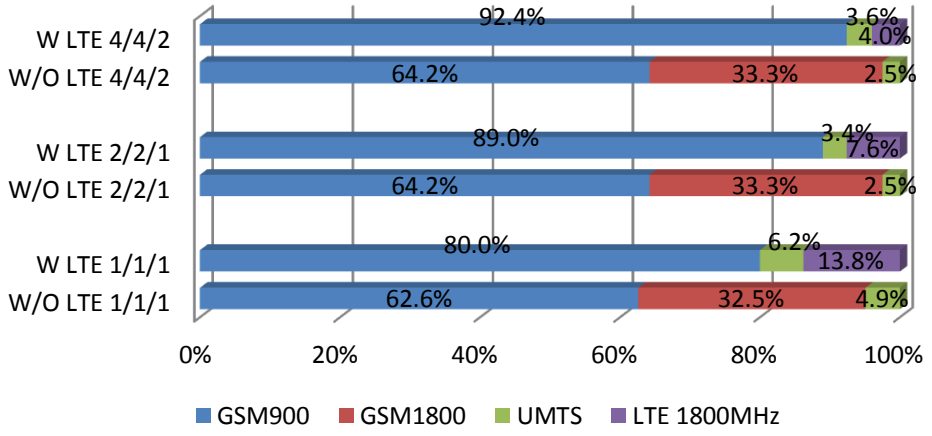

Figure D.15 - Power ratio involved in the simulation of IPanel-1 (BS No Shared, W MIMO).

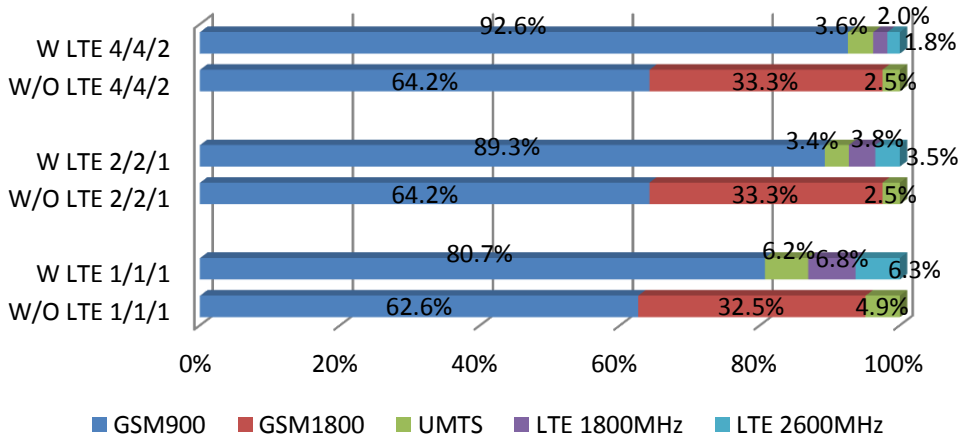

Figure D.16 - Power ratio involved in the simulation of IPanel-2 (BS Shared, WO MIMO).

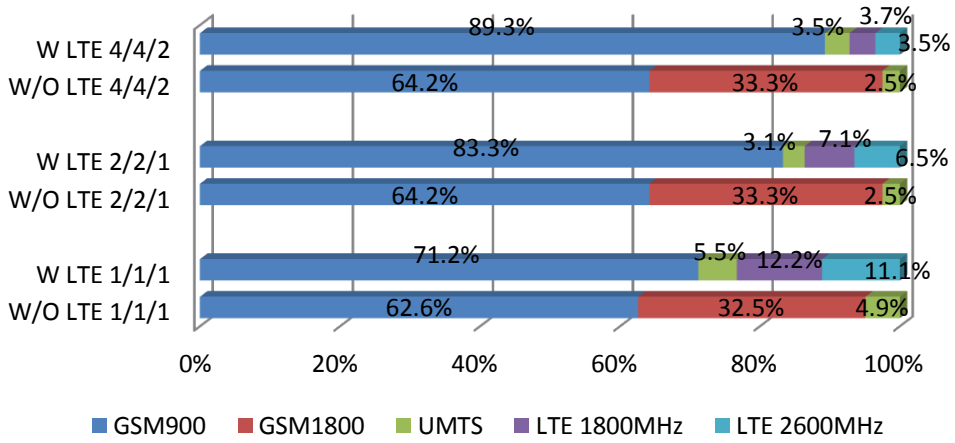

Figure D.17 - Power ratio involved in the simulation of IPanel-2 (BS Shared, W MIMO).

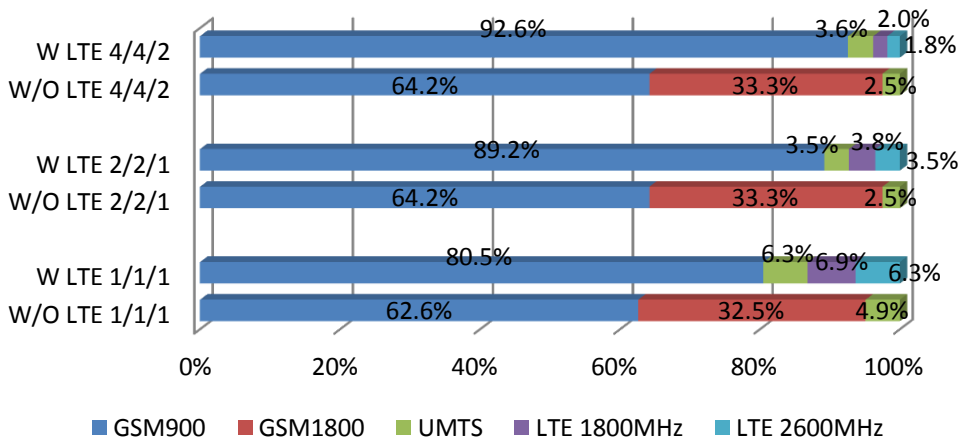

Figure D.18 - Power ratio involved in the simulation of IPanel-2 (BS No Shared, WO MIMO).

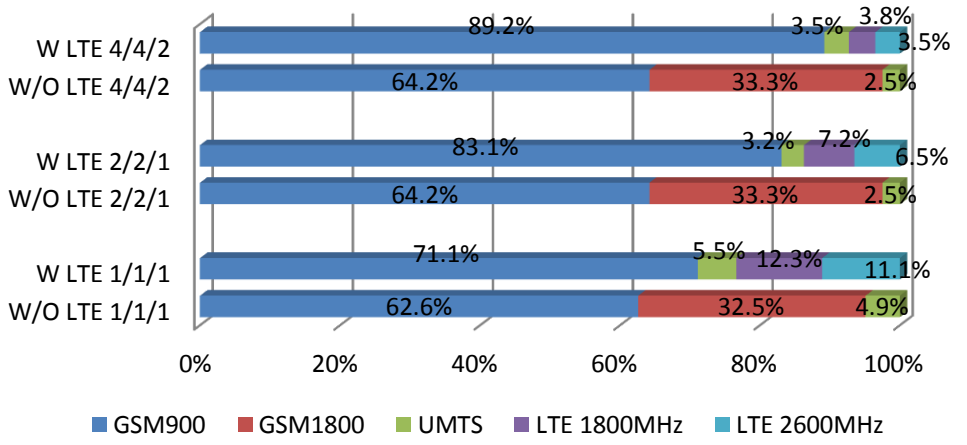

Figure D.19 - Power ratio involved in the simulation of IPanel-2 (BS No Shared, W MIMO).

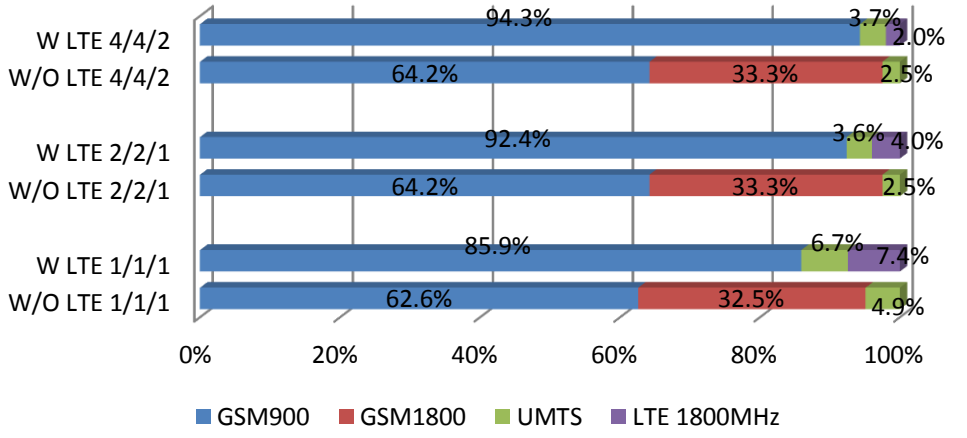

Figure D.20 - Power ratio involved in the simulation of ICeiling-1 (BS Shared, WO MIMO).

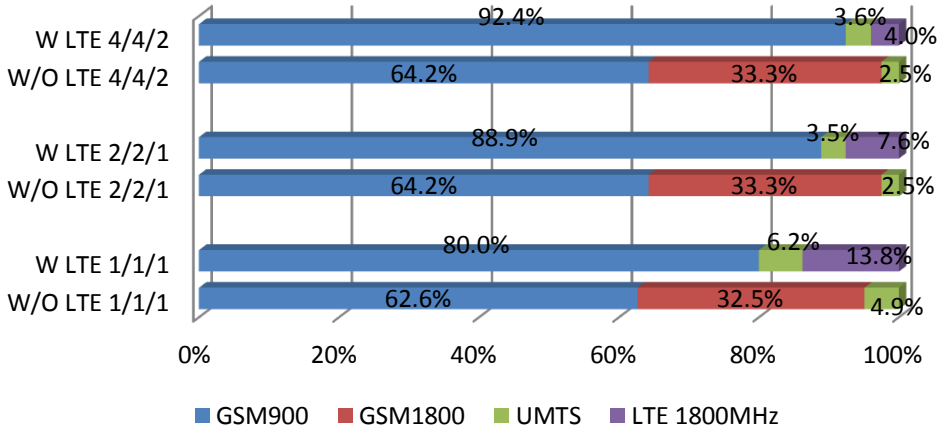

Figure D.21 - Power ratio involved in the simulation of ICeiling-1 (BS Shared, W MIMO).

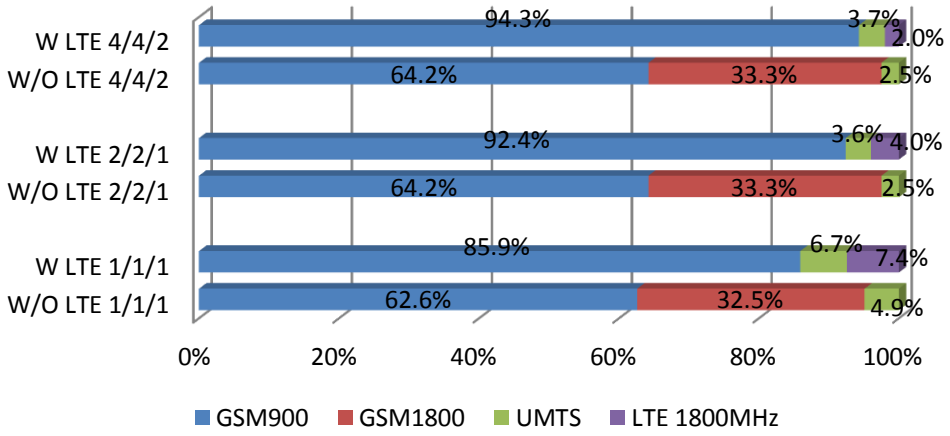

Figure D.22 - Power ratio involved in the simulation of ICeiling-1 (BS No Shared, WO MIMO).

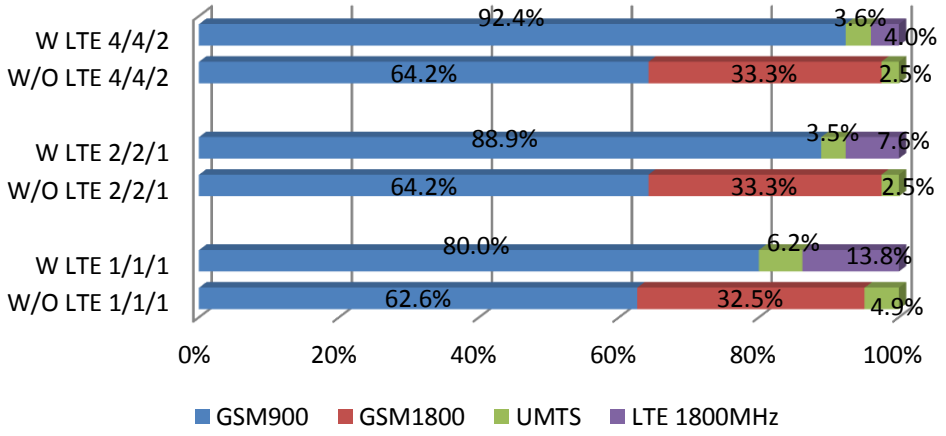

Figure D.23 - Power ratio involved in the simulation of ICeiling-1 (BS No Shared, W MIMO).

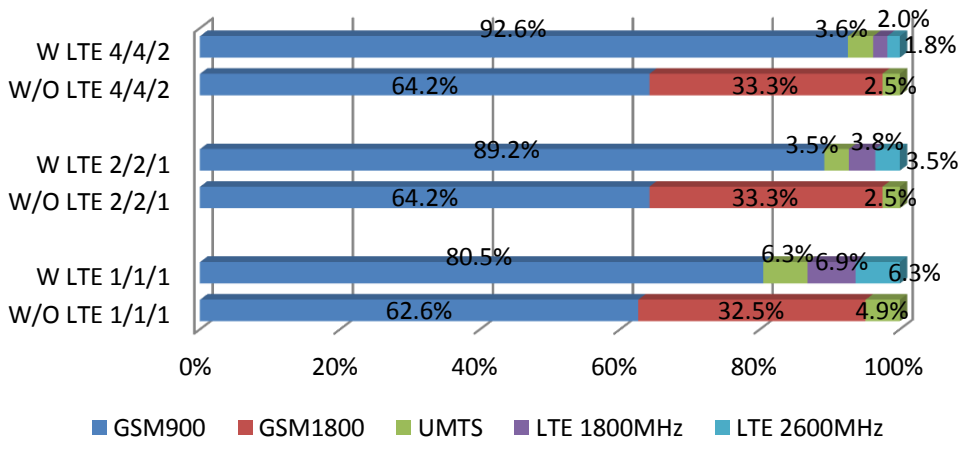

Figure D.24 - Power ratio involved in the simulation of ICeiling-2 (BS Shared, WO MIMO).

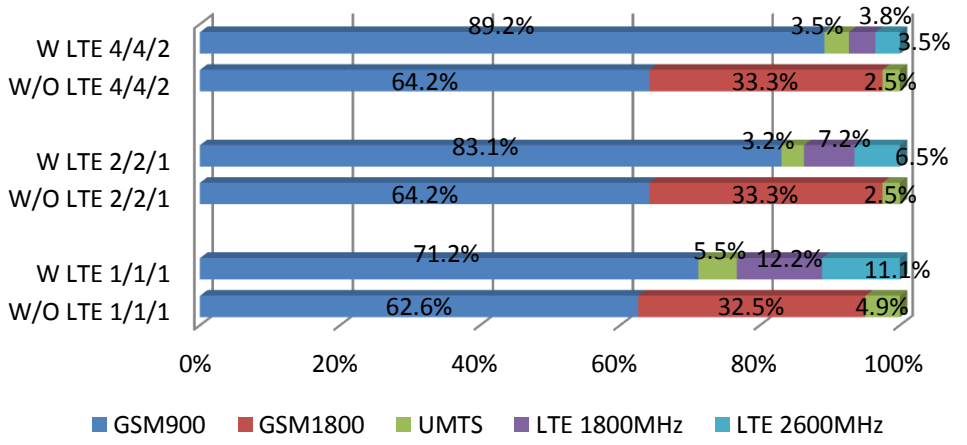

Figure D.25 - Power ratio involved in the simulation of ICeiling-2 (BS Shared, W MIMO).

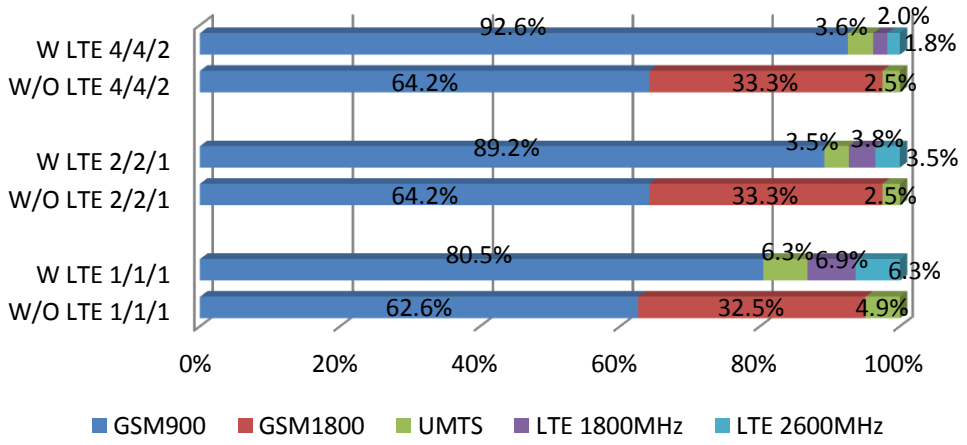

Figure D.26 - Power ratio involved in the simulation of ICeiling-2 (BS No Shared, WO MIMO).

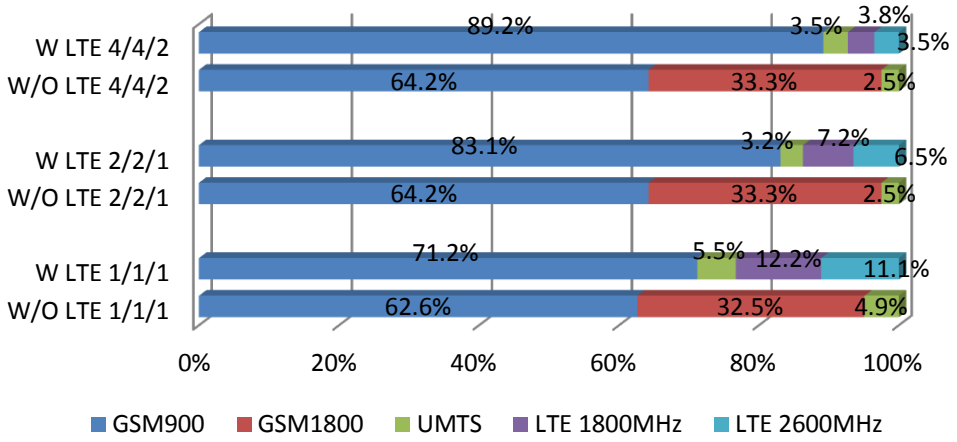

Figure D.27 - Power ratio involved in the simulation of ICeiling-2 (BS No Shared, W MIMO).

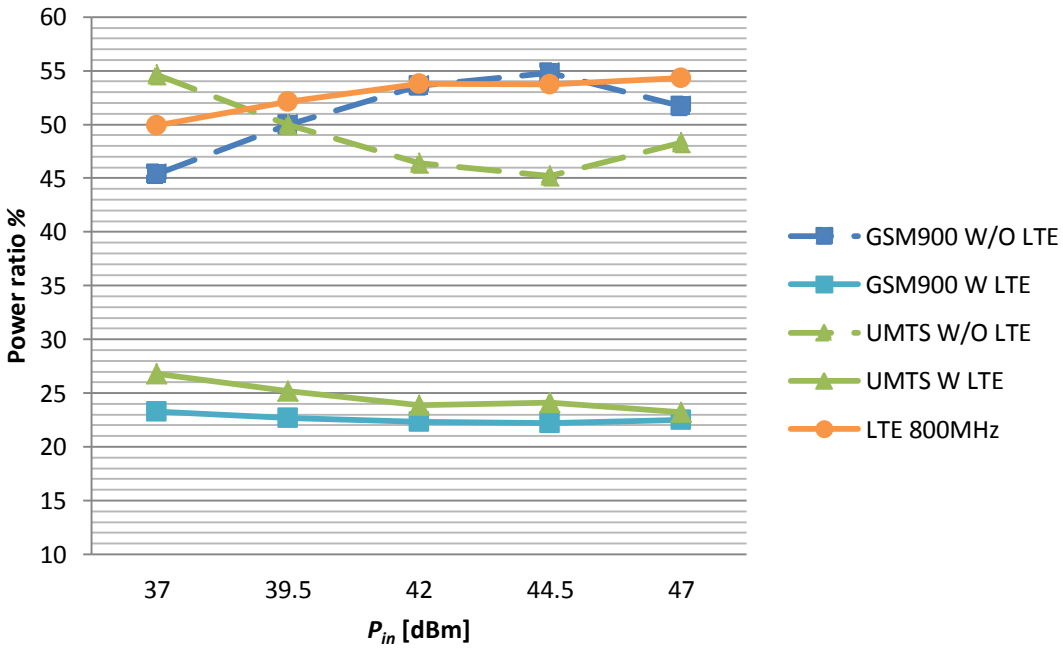

Figure D.28 - Power ratio results with the variation of input power for SRural-1.a (1/1).

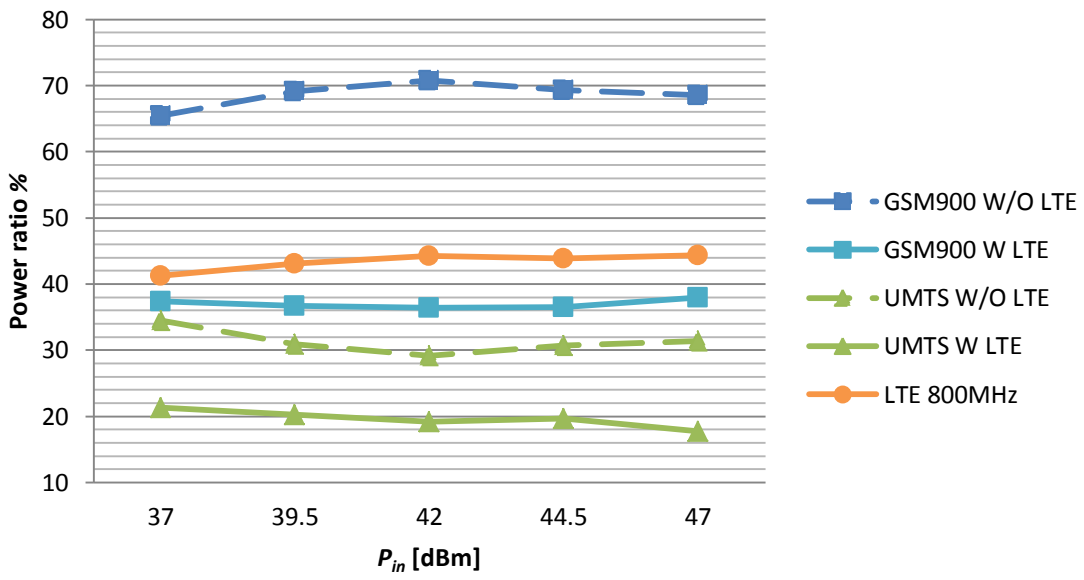

Figure D.29 - Power ratio results with the variation of input power for SRural-1.a (2/1).

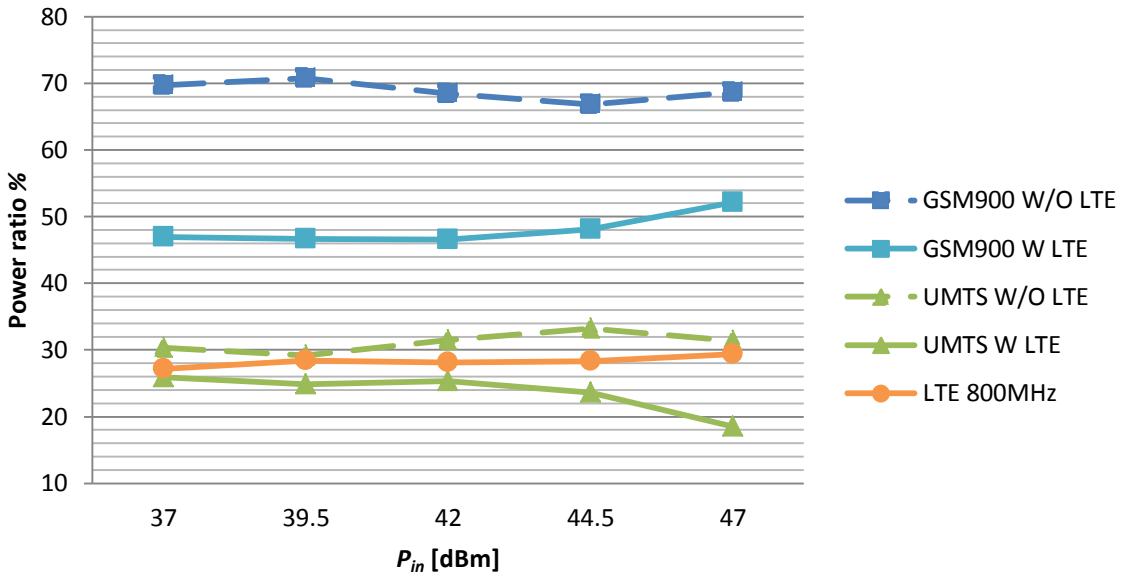

Figure D.30 - Power ratio results with the variation of input power for SRural-1.a (4/2).

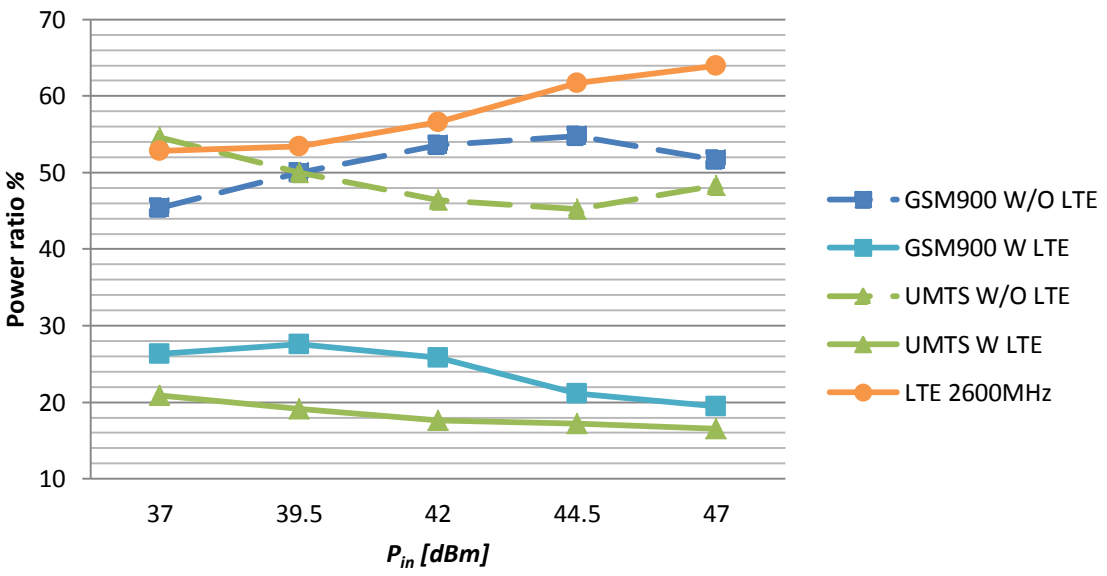

Figure D.31 - Power ratio results with the variation of input power for SUrban-1.a (1/1).

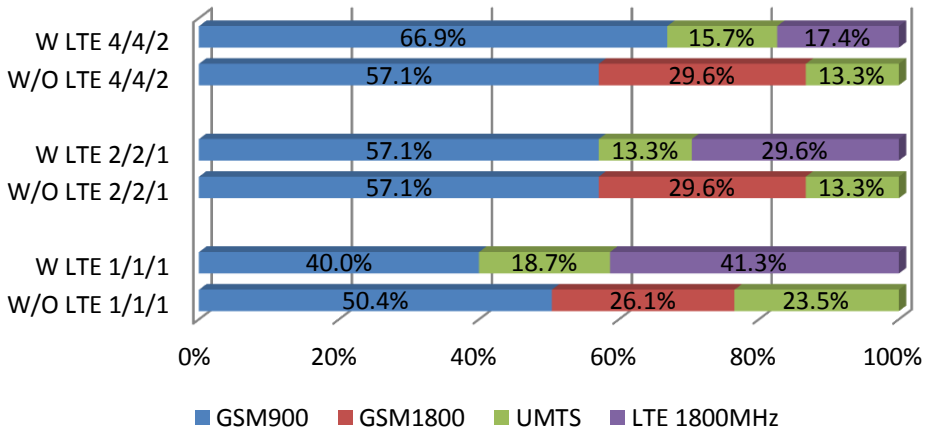

Figure D.32 - Power ratio with the variation of input power for IPanel-1 and ICeiling-1 (W MIMO).

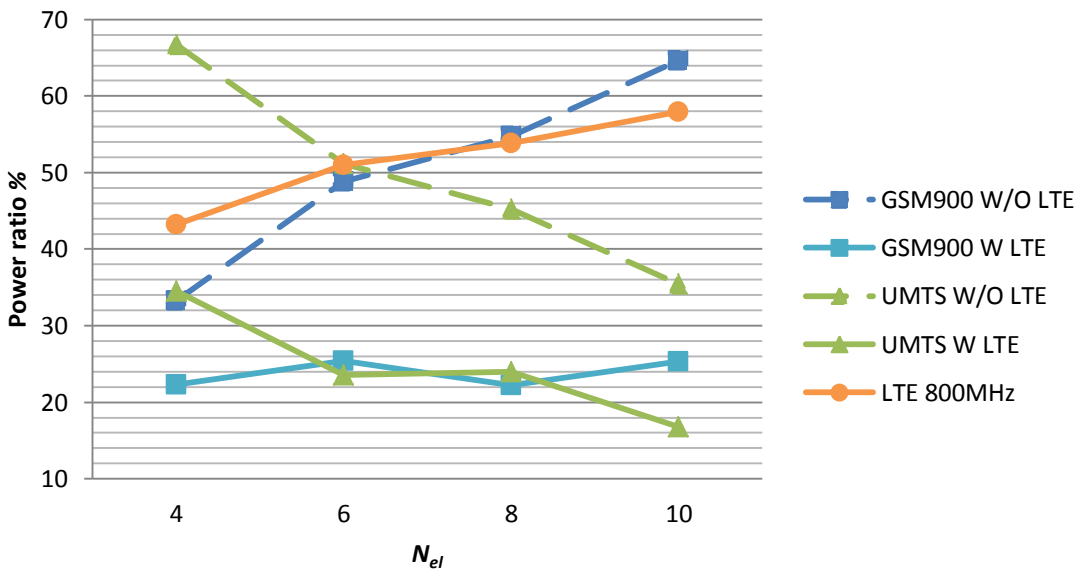

Figure D.33 - Power ratio results with the variation of N_{el} for SRural-1.a (1/1).

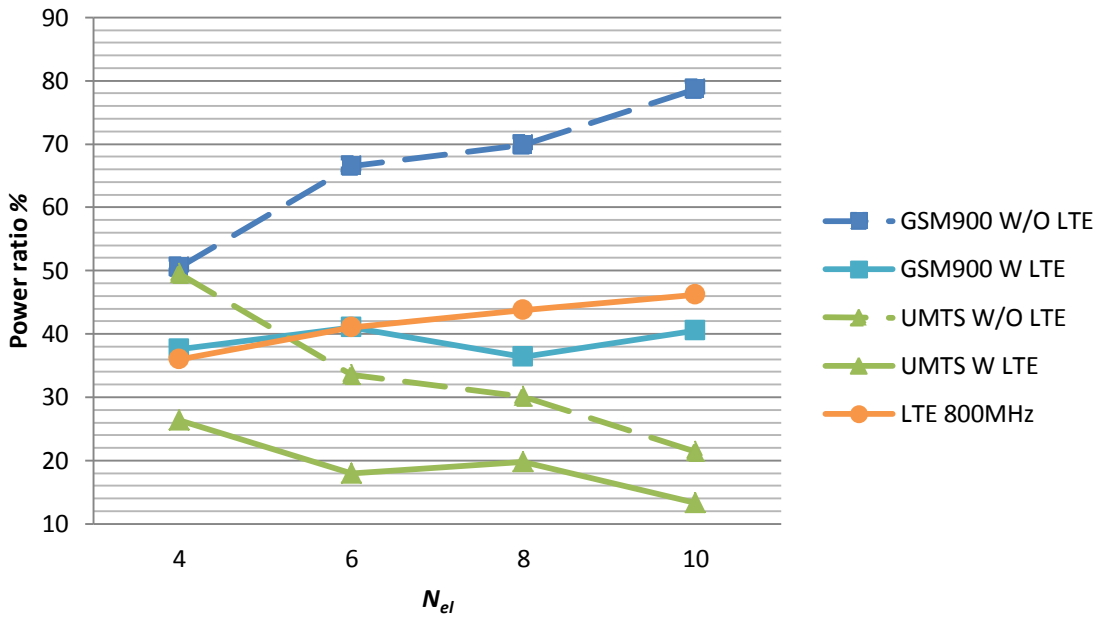

Figure D.34 - Power ratio results with the variation of N_{el} for SRural-1.a (2/1).

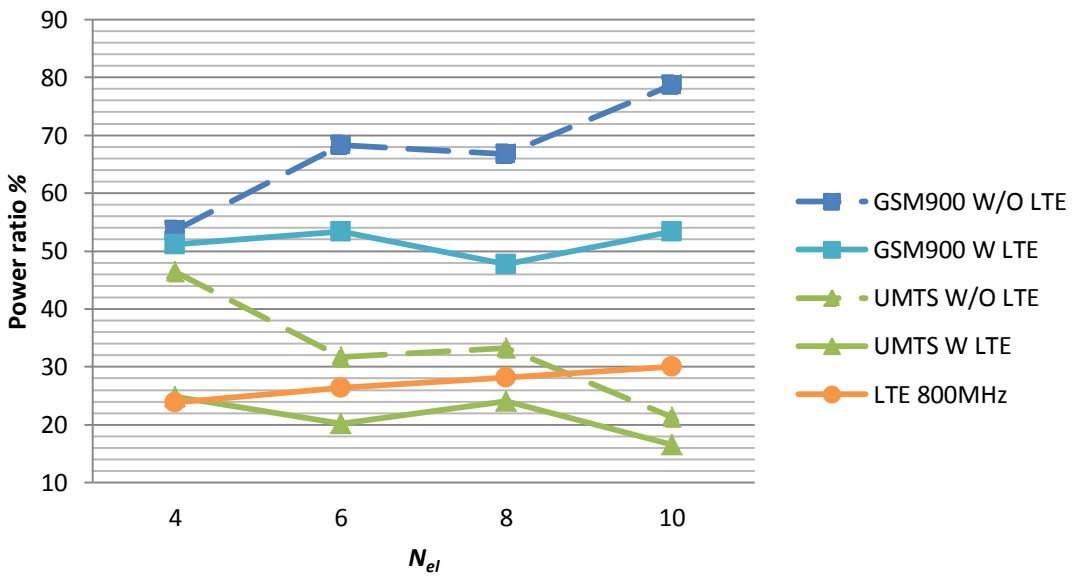

Figure D.35 1- Power ratio results with the variation of N_{el} for SRural-1.a (4/2).

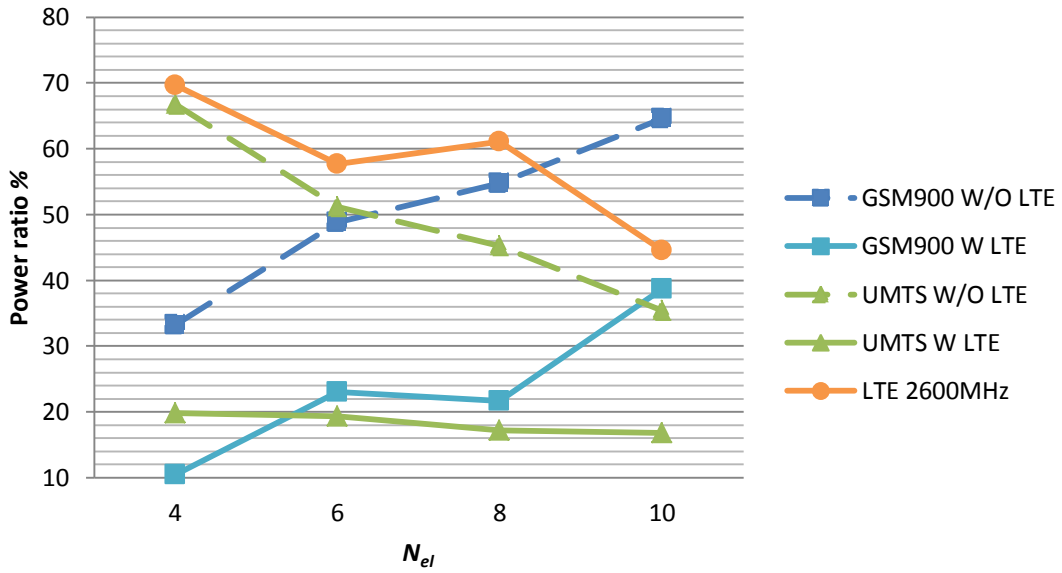

Figure D.36 - Power ratio results with the variation of N_{el} for SUrban1.a (1/1).

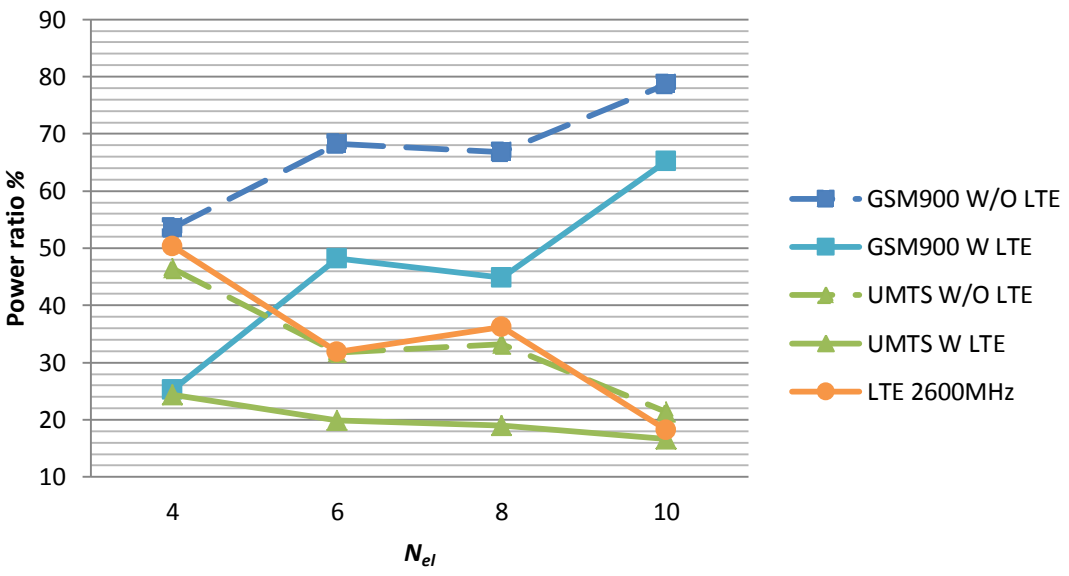

Figure D.37 - Power ratio results with the variation of N_{el} for SUrban1.a (4/2).

D.3 Qualitative Analysis for the Outdoor Scenarios

The study results of the definition of physical barriers in order to protect the public from EM exposure are shown, for the outdoor scenario results described in Section 4.1 and Section D.1. The BS antennas of the analysed scenarios have a downtilt equal to 12° and the inclination of the exclusion zone is taken into account from two parameters: D'_{front} and h_a, Figure 4.4. The minimum height to which a BS antenna should be of a person with 1.8 m high in order to be protected from potentially dangerous radiation is also presented for the outdoor scenarios, h_{min}.

Table D.18 - Barrier definition in front of BS for SRural-1.a scenario with downtilt of 12º.

	$N_{c,GSM900}/N_{c,GSM1800}/N_{c,UMTS}$		D_{front} [m]	D'_{front} [m]	h_a [m]	h_{min} [m]
SRural-1.a	2/2/1	W/O LTE	**6.73**	6.58	1.40	3.20
		W LTE	**10.28**	10.06	2.14	3.94
	4/4/2	W/O LTE	**11.75**	11.49	2.44	4.24
		W LTE	**14.35**	14.04	2.98	4.78

Table D.19 - Barrier definition in front of BS for SRural-1.b scenario with downtilt of 12º.

	$N_{c,GSM900}/N_{c,GSM1800}/N_{c,UMTS}$		D_{front} [m]	D'_{front} [m]	h_a [m]	h_{min} [m]
SRural-1.b	**2/2/1**	**W/O LTE**	**10.16**	9.94	2.11	3.91
		W LTE	**13.48**	13.19	2.80	4.60
	4/4/2	**W/O LTE**	**16.35**	15.99	3.40	5.20
		W LTE	**16.57**	16.21	3.45	5.25

Table D.20 - Barrier definition in front of BS for ORural-1 scenario with downtilt of 12º.

	$N_{c,GSM900}/N_{c,GSM1800}/N_{c,UMTS}$		D_{front} [m]	D'_{front} [m]	h_a [m]	h_{min} [m]
ORural-1	**2/2/1**	**W/O LTE**	**2.10**	2.05	0.44	2.24
		W LTE	**7.59**	7.42	1.58	3.38
	4/4/2	**W/O LTE**	**3.39**	3.32	0.70	2.50
		W LTE	**8.13**	7.95	1.69	3.49

Table D.21 - Barrier definition in front of BS for SUrban-1.a scenario with downtilt of 12º.

	$N_{c,GSM900}/N_{c,UMTS}$		D_{front} [m]	D'_{front} [m]	h_a [m]	h_{min} [m]
SUrban-1.a	**2/2/1**	**W/O LTE**	**6.73**	6.58	1.40	3.20
		W LTE	**11.51**	11.26	2.39	4.19
	4/4/2	**W/O LTE**	**11.75**	11.49	2.44	4.24
		W LTE	**15.16**	14.83	3.15	4.95

Table D.22 - Barrier definition in front of BS for SUrban-1.b scenario with downtilt of 12º.

	$N_{c,GSM900}/N_{c,GSM1800}/N_{c,UMTS}$		D_{front} [m]	D'_{front} [m]	h_a [m]	h_{min} [m]
SUrban-1.b	**2/2/1**	**W/O LTE**	**10.16**	9.94	2.11	3.91
		W LTE	**13.21**	12.92	2.75	4.55

Table D.22 (cont.) - Barrier definition in front of BS for SUrban-1.b scenario with downtilt of 12º.

	4/4/2	**W/O LTE**	**16.35**	15.99	3.40	5.20
		W LTE	**16.07**	15.72	3.34	5.14

Table D.23 - Barrier definition in front of BS for SUrban-2.a scenario with downtilt of 12º.

	$N_{c,GSM900}/N_{c,UMTS}$		D_{front} [m]	D'_{front} [m]	h_a [m]	h_{min} [m]
SUrban-2.a	**2/2/1**	**W/O LTE**	**4.89**	4.78	1.02	2.82
		W LTE	**8.46**	8.28	1.76	3.56
	4/4/2	**W/O LTE**	**8.37**	8.19	1.74	3.54
		W LTE	**11.98**	11.72	2.49	4.29

Table D.24 - Barrier definition in front of BS for SUrban-2.b scenario with downtilt of 12º.

	$N_{c,GSM900}/N_{c,GSM1800}/N_{c,UMTS}$		D_{front} [m]	D'_{front} [m]	h_a [m]	h_{min} [m]
SUrban-2.b	**2/2/1**	**W/O LTE**	**7.93**	7.76	1.65	3.45
		W LTE	**13.58**	13.28	2.82	4.62
	4/4/2	**W/O LTE**	**15.10**	14.77	3.14	4.94
		W LTE	**16.28**	15.92	3.38	5.18

Table D.25 - Barrier definition in front of BS for OUrban-1 scenario with downtilt of 12º.

	$N_{c,GSM900}/N_{c,GSM1800}/N_{c,UMTS}$		D_{front} [m]	D'_{front} [m]	h_a [m]	h_{min} [m]
OUrban-1	**2/2/1**	**W/O LTE**	**2.10**	2.05	0.44	2.24
		W LTE	**10.39**	10.16	2.16	3.96
	4/4/2	**W/O LTE**	**3.39**	3.32	0.70	2.50
		W LTE	**11.07**	10.83	2.30	4.10

Annex E

Cylindrical Model

In this annex, the results of the back, bottom, top and side border of the exclusion region are presented for the study scenarios according to the model of the cylindrical exclusion region, as well as the correction factors used for this purpose.

E.1 Correction Factors of the Scenarios of this Study

This section presents the correction factors (CFs) of each scenario for the dimensions of the exclusion zone: D_{back}, D_{bottom}, D_{top} and D_{side}. These factors were obtained by the method explained in Section 3.6, analysing the antennas installed in each scenario (Table 4.1) and their respective normalised gains (Table A.17).

Table E.1 - Correction factors of the SRural-1.a scenario.

SRural-1.a	CF	Bottom		Top		Back		Side	
		dB	linear u.	dB	linear u.	dB	linear u.	dB	linear u.
	W/O LTE	-30	0.001	-30	0.001	-27.8	0.0017	-6.4	0.23
	W LTE	-20	0.01	-20	0.01	-20	0.01	-5.8	0.26

Table E.2 - Correction factors of the SRural-1.b scenario.

SRural-1.b	CF	Bottom		Top		Back		Side	
		dB	linear u.	dB	linear u.	dB	linear u.	dB	linear u.
	W/O LTE	-30	0.001	-30	0.001	-26.1	0.0025	-5.1	0.31
	W LTE	-20	0.01	-20	0.01	-20	0.01	-5	0.32

Table E.3 - Correction factors of the ORural-1 scenario

ORural-1	CF	Bottom		Top		Back		Side	
		dB	linear u.	dB	linear u.	dB	linear u.	dB	linear u.
	W/O LTE	-30	0.001	-30	0.001	-*		-*	
	W LTE	-20	0.01	-20	0.01	-29.3**	0.0012	-5.7**	0.27

*Omni-directional BS: $D_{side} = D_{back} = D_{front}$.

**For sector antennas.

Table E.4 - Correction factors of the SUrban-1.a scenario.

SUrban-1.a	CF	Bottom		Top		Back		Side	
		dB	linear u.	dB	linear u.	dB	linear u.	dB	linear u.
	W/O LTE	-25	0.0032	-30	0.001	-30	0.001	-4.5	0.35
	W LTE	-25	0.0032	-30	0.001	-28	0.0016	-4.5	0.35

Table E.5 - Correction factors of the SUrban-1.b scenario

SUrban-1.b	CF	Bottom		Top		Back		Side	
		dB	linear u.	dB	linear u.	dB	linear u.	dB	linear u.
	W/O LTE	-25	0.0032	-30	0.001	-26.1	0.0025	-4.5	0.35
	W LTE	-30	0.001	30	0.001	-25.6	0.0028	-5	0.32

Table E.6 - Correction factors of the SUrban-2.a scenario.

SUrban-2.a	CF	Bottom		Top		Back		Side	
		dB	linear u.	dB	linear u.	dB	linear u.	dB	linear u.
	W/O LTE	-30	0.001	-30	0.001	-27.8	0.0017	-6.4	0.23
	W LTE	-30	0.001	-28	0.0016	-27	0.002	-4	0.40

Table E.7 - Correction factors of the SUrban-2.b scenario.

SUrban-2.b	CF	Bottom		Top		Back		Side	
		dB	linear u.	dB	linear u.	dB	linear u.	dB	linear u.
	W/O LTE	-30	0.001	-30	0.001	-26.1	0.0025	-5.1	0.31
	W LTE	-30	0.001	-30	0.001	-27.8	0.0017	-5	0.32

Table E.8 - Correction factors of the OUrban-1 scenario.

OUrban-1	CF	Bottom		Top		Back		Side	
		dB	linear u.	dB	linear u.	dB	linear u.	dB	linear u.
	W/O LTE	-30	0.001	-30	0.001	-*		-*	

Table E.8 (cont.) - Correction factors of the OUrban-1 scenario.

	W LTE	-20	0.01	-20	0.01	-28**	0.0016	-5**	0.32

*Omni-directional BS: $D_{side} = D_{back} = D_{front}$.

**For sector antennas.

Table E.9 - Correction factors of the IPanel-1 and IPanel-2 scenario.

IPanel-1 and IPanel-2	**CF**	**Bottom**		**Top**		**Back**		**Side**	
		dB	**linear u.**	**dB**	**linear u.**	**dB**	**linear u.**	**dB**	**linear u.**
	W/O LTE	*		*		-20	0.01	-3	0.50
	W LTE **W/O MIMO**								
	W LTE **W MIMO**								

* Without access to the data.

Table E.10 - Correction factors of the ICeiling-1 and Ceiling-2 scenario.

ICeiling-1 and ICeiling-2	**CF**	**Bottom**		**Top**		**Back**		**Side**	
		dB	**linear u.**	**dB**	**linear u.**	**dB**	**linear u.**	**dB**	**linear u.**
	W/O LTE	*		*		-**		-**	
	W LTE **W/O MIMO**								
	W LTE **W MIMO**								

* Without access to the data.

**Omni-directional BS: $D_{side} = D_{back} = D_{front}$.

E.2 Results of the Back, Bottom, Top and Side Border

With the results of the previous section and the results obtained for D_{front} for each scenario (shown in Chapter 4.2 and Annex D.1), values of the back, bottom, top and side border of the exclusion zone were obtained according to the cylindrical exclusion region model described in Section 3.6.

Table E.11 - Back, bottom, top and side border of the exclusion zone for SRural-1.a.

	$N_{c,GSM900}/N_{c,UMTS}$		D_{front} [m]	D_{bottom} [m]	D_{top} [m]	D_{back} [m]	D_{side} [m]
SRural-1.a	1/1	W/O LTE	4.59	$< 2\lambda_{GSM900}$			1.06
		W LTE	8.61	$< 2\lambda_{LTE\ 800MHz}$			2.24
	2/1	W/O LTE	6.73	$< 2\lambda_{GSM900}$			1.55
		W LTE	10.28	$< 2\lambda_{LTE\ 800MHz}$			2.67
	4/2	W/O LTE	11.75	$< 2\lambda_{GSM900}$			2.70
		W LTE	14.35	$< 2\lambda_{LTE\ 800MHz}$			3.73

Table E.12 - Back, bottom, top and side border of the exclusion zone for SRural-1.b.

	$N_{c,GSM900}/N_{c,GSM1800}/N_{c,UMTS}$		D_{front} [m]	D_{bottom} [m]	D_{top} [m]	D_{back} [m]	D_{side} [m]
SRural-1.b	1/1/1	W/O LTE	6.20	$< 2\lambda_{GSM900}$			1.92
		W LTE	12.03	$< 2\lambda_{LTE\ 800MHz}$			3.85
	2/2/1	W/O LTE	10.16	$< 2\lambda_{GSM900}$			3.15
		W LTE	13.48	$< 2\lambda_{LTE\ 800MHz}$			4.31
	4/4/2	W/O LTE	16.35	$< 2\lambda_{GSM900}$			5.07
		W LTE	16.57	$< 2\lambda_{LTE\ 800MHz}$			5.30

Table E.13 - Back, bottom, top and side border of the exclusion zone for ORural-1.

	$N_{c,GSM900}/N_{c,GSM1800}/N_{c,UMTS}$		D_{front} [m]	D_{bottom} [m]	D_{top} [m]	D_{back} [m]	D_{side} [m]
ORural-1	1/1/1	W/O LTE	1.50	$< 2\lambda_{GSM900}$			1.50*
		W LTE	7.44	$< 2\lambda_{LTE\ 800MHz}$		1.13**	2.01
	2/2/1	W/O LTE	2.10	$< 2\lambda_{GSM900}$			2.10*
		W LTE	7.59	$< 2\lambda_{LTE\ 800MHz}$		1.47**	2.05
	4/4/2	W/O LTE	3.39	$< 2\lambda_{GSM900}$			3.39*
		W LTE	8.13	$< 2\lambda_{LTE\ 800MHz}$			2.24**

*Omni-directional BS: $D_{side} = D_{back} = D_{front}$.

**D_{front} of the Omni GSM900/UMTS antenna.

Table E.14 - Back, bottom, top and side border of the exclusion zone for SUrban-1.a.

	$N_{c,GSM900}/N_{c,UMTS}$		D_{front} [m]	D_{bottom} [m]	D_{top} [m]	D_{back} [m]	D_{side} [m]
SUrban-1.a	1/1	W/O LTE	4.59	$< 2\lambda_{GSM900}$			1.61
		W LTE	9.75				3.41
	2/1	W/O LTE	6.73				2.36
		W LTE	11.51				4.03
	4/2	W/O LTE	11.75				4.11
		W LTE	15.16				5.31

Table E.15 - Back, bottom, top and side border of the exclusion zone for SUrban-1.b.

	$N_{c,GSM900}/N_{c,GSM1800}/N_{c,UMTS}$		D_{front} [m]	D_{bottom} [m]	D_{top} [m]	D_{back} [m]	D_{side} [m]
SUrban-1.b	1/1/1	W/O LTE	6.20	$< 2\lambda_{GSM900}$			2.17
		W LTE	12.07				3.86
	2/2/1	W/O LTE	10.16				3.56
		W LTE	13.21				4.23
	4/4/2	W/O LTE	16.35				5.72
		W LTE	16.07				5.14

Table E.16 - Back, bottom, top and side border of the exclusion zone for SUrban-2.a.

	$N_{c,GSM900}/N_{c,UMTS}$		D_{front} [m]	D_{bottom} [m]	D_{top} [m]	D_{back} [m]	D_{side} [m]
SUrban-2.a	1/1	W/O LTE	3.72	$< 2\lambda_{GSM900}$			0.86
		W LTE	7.15				2.86
	2/1	W/O LTE	4.89				1.12
		W LTE	8.46				3.38
	4/2	W/O LTE	8.37				1.93
		W LTE	11.98				4.79

Table E.17 - Back, bottom top and side border of the exclusion zone for SUrban-2.b.

	$N_{c,GSM900}/N_{c,GSM1800}/N_{c,UMTS}$		D_{front} [m]	D_{bottom} [m]	D_{top} [m]	D_{back} [m]	D_{side} [m]
SUrban-2.b	1/1/1	W/O LTE	5.09	$< 2\lambda_{GSM900}$			1.58
		W LTE	12.75				4.08
	2/2/1	W/O LTE	7.93				2.46
		W LTE	13.58				4.35
	4/4/2	W/O LTE	15.10				4.68
		W LTE	16.28				5.21

Table E.18 - Back, bottom, top and side border of the exclusion zone for OUrban-1.

	$N_{c,GSM900}/N_{c,GSM1800}/N_{c,UMTS}$		D_{front} [m]	D_{bottom} [m]	D_{top} [m]	D_{back} [m]	D_{side} [m]
OUrban-1	1/1/1	W/O LTE	1.50	$< 2\lambda_{GSM900}$		1.50*	
		W LTE	10.21			1.13**	3.27
	2/2/1	W/O LTE	2.10			2.10*	
		W LTE	10.39			1.47**	3.32
	4/4/2	W/O LTE	3.39			3.39*	
		W LTE	11.07			2.24**	3.54

*Omni-directional BS: $D_{side} = D_{back} = D_{front}$.

**D_{front} of the Omni GSM900/UMTS antenna.

In IPanel-1 and IPanel-2 scenarios, regardless of the conditions studied, D_{back} and D_{side} are always smaller than λ_{GSM900} since $D_{front} < \lambda_{GSM900}$ and $CF < 1$. Although data are not available to determine the CF's of bottom and top border of the exclusion zone, D_{bottom} and D_{top} must have values lower than λ_{GSM900} because the CFs studied of the other scenarios/antennas do not exceed -20 dB. For ICeiling-1 and ICeiling-2, it is not necessary to apply CFs, because the BS is omnidireccional, with circular exclusion zone around the antenna and radius equal to D_{front}. In accordance to the order of magnitude of D_{bottom} and D_{top}, the introduction of tilt will not significantly affect these two regions, remaining below the limit of the used models.

Annex F

Measurement Data

This annex presents the data from the measurements and characteristics of the BSs and the surrounding environment.

F.1 Measurement Data of the BS1

Figure F.1 shows a sketch of the measurement site while a photograph of analysed BS is presented in Figure F.2. The data from the measurements and the $R(d)$ obtained from them are presented in Table F.1.

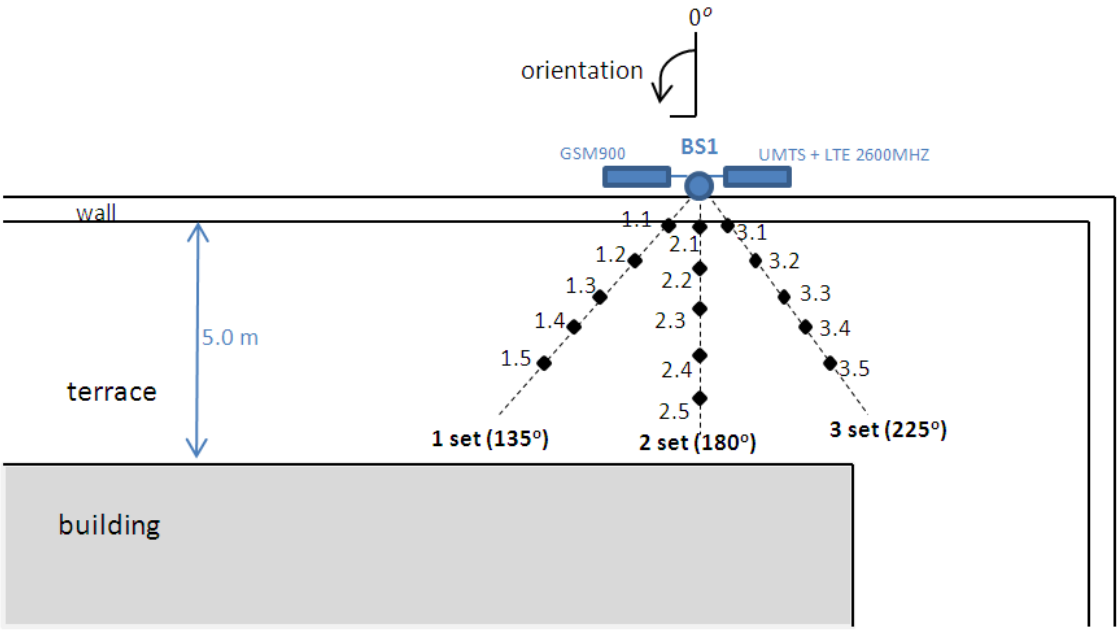

Figure F.1 - Sketch of the BS1 measurement site.

Figure F.2 - Point of view from the terrace access of the BS1.

Table F.1 - Results of the BS1 measurements.

Observation Point	Distance [m]	E_{med} [mV/m]						$R(d)$ [$\times 10^{-3}$]
		GSM 900	σ_{GSM}	UMTS	σ_{UMTS}	LTE 2600MHz	σ_{LTE}	
1.1	0.7	178.8	30.3	165.2	104.3	56.8	18.8	0.247
1.2	1.2	167.1	34.5	164.0	103.1	44.2	14.2	0.218
1.3	1.7	173.1	32.9	57.7	35.3	23.3	7.3	0.212
1.4	2.2	98.73	21.7	63.8	39.2	29.1	9.1	0.072
1.5	2.7	126.1	26.5	62.7	38.8	30.4	9.8	0.115
2.1	0.7	163.6	34.0	159.3	100.8	64.8	21.2	0.210
2.2	1.2	146.3	29.9	63.5	38.8	51.8	16.7	0.154
2.3	1.7	132.1	26.9	94.7	58.8	33.1	10.4	0.130
2.4	2.2	160.8	31.9	74.1	46.0	34.7	11.5	0.185
2.5	2.7	96.0	18.6	74.4	46.2	41.4	13.5	0.070
3.1	0.7	155.3	31.5	104.2	64.7	93.4	31.9	0.184
3.2	1.2	118.25	22.2	87.6	54.9	83.1	27.3	0.109
3.3	1.7	151.4	29.2	102.0	63.8	59.4	19.9	0.171
3.4	2.2	116.1	23.2	94.6	58.8	66.2	22.3	0.105
3.5	2.7	154.9	27.2	60.4	37.3	41.5	13.9	0.171

F.2 Measurement Data of the BS2

Figure F.3 shows a sketch of the measurement site while a photograph of analysed BS is presented in Figure F4. The data from the measurements and the $R(d)$ obtained from them are presented in Table F.2.

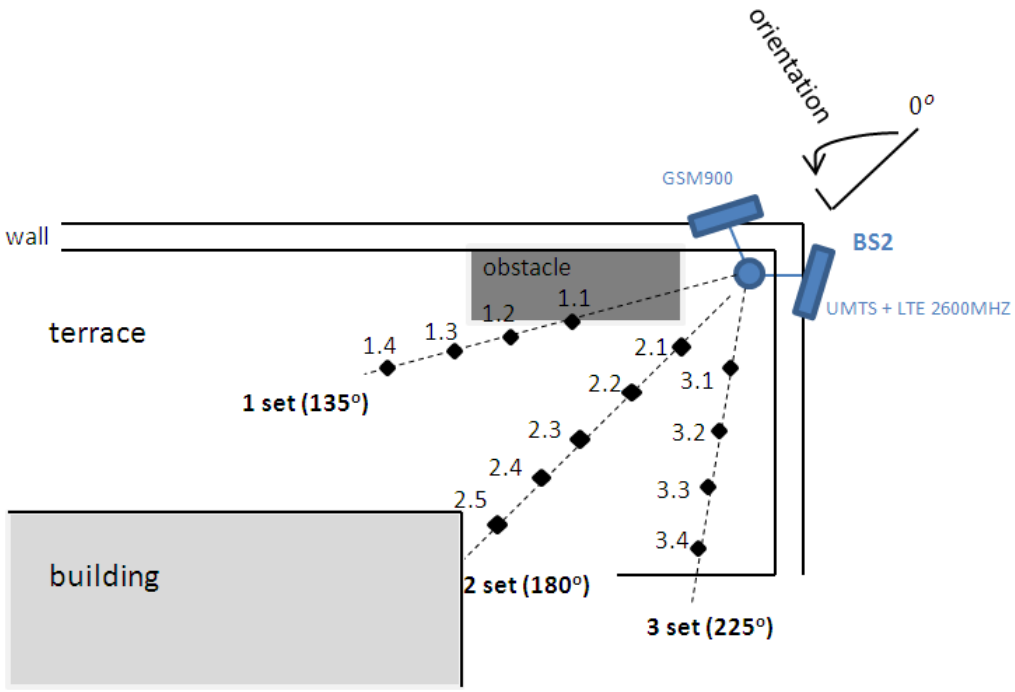

Figure F.3 - Sketch of the BS2 measurement site.

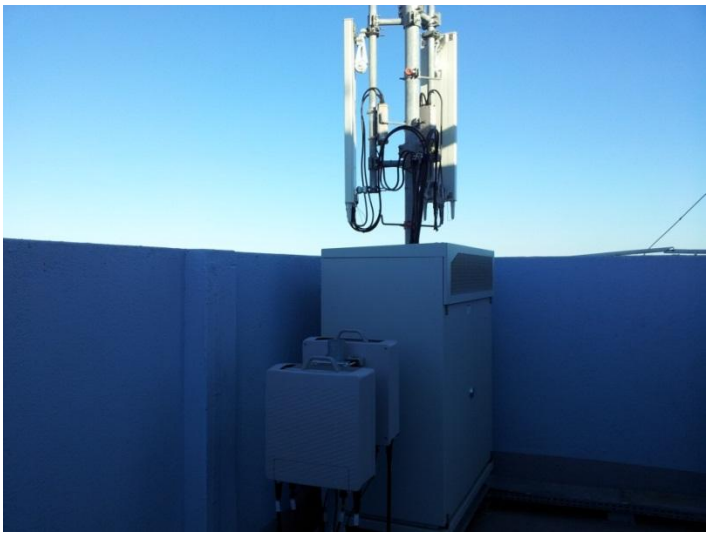

Figure F.4 - Point of view from the terrace access of the BS2.

Table F.2 - Results of the BS2 measurements.

Observation Point	Distance [m]	E_{med} [mV/m]						$R\ d$ [$\times 10^{-3}$]
		GSM 900	σ_{GSM}	UMTS	σ_{UMTS}	LTE 2600MHz	σ_{LTE}	
1.1	1.2	556.3	251.7	118.6	75.1	86.0	28.0	2.170
1.2	1.7	373.3	170.0	95.2	60.0	88.0	28.1	0.983
1.3	2.2	315.7	141.1	106.4	67.3	54.0	17.0	0.705
1.4	2.7	328.8	149.2	88.8	56.3	74.1	23.9	0.763
2.1	0.7	15.4	1.6	294.9	127.3	224.3	73.4	0.113
2.2	1.2	12.4	1.4	126.8	80.8	175.9	61.0	0.039
2.3	1.7	13.1	1.80	157.2	99.8	145.7	48.3	0.039
2.4	2.2	11.4	1.9	183.6	116.3	135.6	43.7	0.043
2.5	2.7	9.4	1.4	159.4	101.4	90.9	29.1	0.028
3.1	0.7	7.7	0.8	177.8	112.8	148.3	48.7	0.044
3.2	1.2	27.1	3.4	192.4	122.9	201.4	65.3	0.068
3.3	1.7	18.2	3.1	134.8	85.5	98.0	31.8	0.025
3.4	2.2	20.8	3.2	187.0	119.1	140.3	46.2	0.047

F.3 Measurement Data of the BS3

Figure F.5 shows a sketch of the measurement site while in Table F.3, the data from the measurements and the $R(d)$ obtained from them are presented. The normalised gains in V plane used in model are shown in Table F.4, for a downtilt of 3° and 4.1 m height.

Table F.3 - Results of the BS3 measurements.

Observation Point	Distance [m]	E_{med} [mV/m]						$R(d)$ [$\times 10^{-3}$]
		GSM 900	σ_{GSM}	UMTS	σ_{UMTS}	LTE 800MHz	σ_{LTE}	
1.1	4.8	28.6	6.3	25.5	1.6	37.4	3.8	0.009
1.2	5.3	59.0	17.1	37.9	2.7	38.0	3.1	0.028
1.3	5.8	64.5	19.1	65.0	4.1	60.7	6.5	0.039
1.4	6.3	63.1	19.0	72.6	4.4	106.9	9.9	0.054
1.5	6.8	75.0	22.2	38.0	2.5	81.4	11.6	0.053
1.6	7.3	88.3	24.6	55.9	3.3	50.2	6.6	0.062
1.7	7.8	43.7	12.3	40.8	2.4	82.4	11.9	0.027
1.8	8.3	76.0	21.6	40.7	2.7	107.5	12.1	0.063
1.9	8.8	65.2	19.0	65.7	4.0	126.9	14.1	0.063
1.10	9.3	51.2	15.6	56.5	3.3	125.2	14.4	0.050
1.11	9.8	67.5	20.3	35.9	2.1	139.3	13.3	0.069
1.12	10.3	99.4	30.4	63.0	3.8	144.6	12.8	0.111
1.13	10.8	129.3	36.6	89.1	5.5	146.1	19.5	0.163
1.14	11.3	187.6	52.8	78.8	4.4	165.9	15.5	0.302

Table F.4 - Normalised gains in V plane for downtilt of 3º and 4.1 m height [KATH12a].

Distance [m]	4.8	5.3	5.8	6.3	6.8	7.3	7.8	8.3	8.8	9.3	9.8	10.3	10.8	11.3
Normalised Gain [-dB]	20	18.8	20	21	22	23	15	10	6	5	4	3	2	1.7

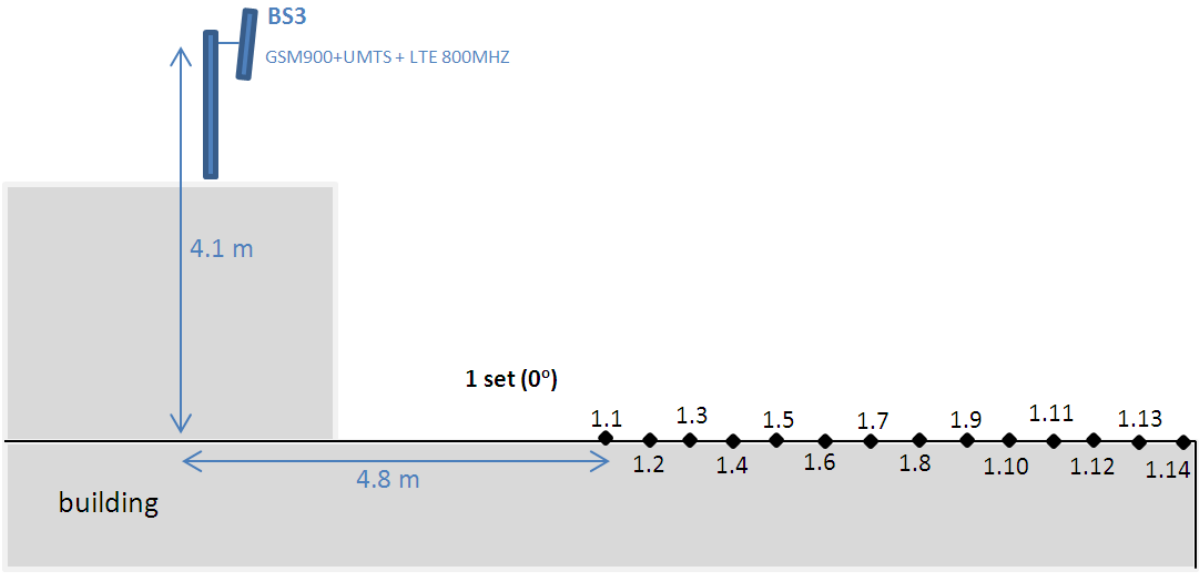

Figure F.5 - Sketch of the BS3 measurement site.

F.4 Measurement Data of the BS4

Figure F.6 shows a sketch of the measurement site while a photograph of analysed BS is presented in Figure F7. The data from the measurements and the $R(d)$ obtained from them are presented in Table F.5.

Table F.5 - Results of the BS4 measurements.

Observation Point	Distance [m]	E_{med} [mV/m]						$R(d)$ [$\times 10^{-6}$]
		GSM 900	σ_{GSM}	UMTS	σ_{UMTS}	LTE 1800MHz	σ_{LTE}	
1.1	1.0	10.8	4.1	4.7	0.9	3.5	0.6	0.840
2.1	1.0	9.3	3.3	3.5	0.5	2.4	0.4	0.617
2.2	1.6	8.9	3.1	4.2	0.7	2.5	0.4	0.571
2.3	2.2	14.5	5.1	4.8	0.8	2.9	0.4	1.489
2.4	2.7	6.4	2.3	4.5	0.8	2.5	0.3	0.307
2.5	3.3	6.3	2.3	4.2	0.7	3.0	0.5	0.298
3.1	1.0	13.5	5.2	4.7	1.2	2.7	0.3	1.292
3.2	1.6	10.1	3.7	4.9	0.8	4.0	0.5	0.743
3.3	2.2	5.6	2.0	4.2	0.7	3.6	0.6	0.244
4.1	1.0	14.1	5.1	4.9	0.8	2.5	0.4	1.408
4.2	1.6	10.6	3.9	4.3	0.8	2.3	0.3	0.801
4.3	2.2	8.2	2.8	4.9	1.3	2.3	0.2	0.492
4.4	2.7	11.0	3.8	5.0	0.9	2.2	0.3	0.866
4.5	3.3	7.8	2.7	3.7	0.5	2.2	0.3	0.439

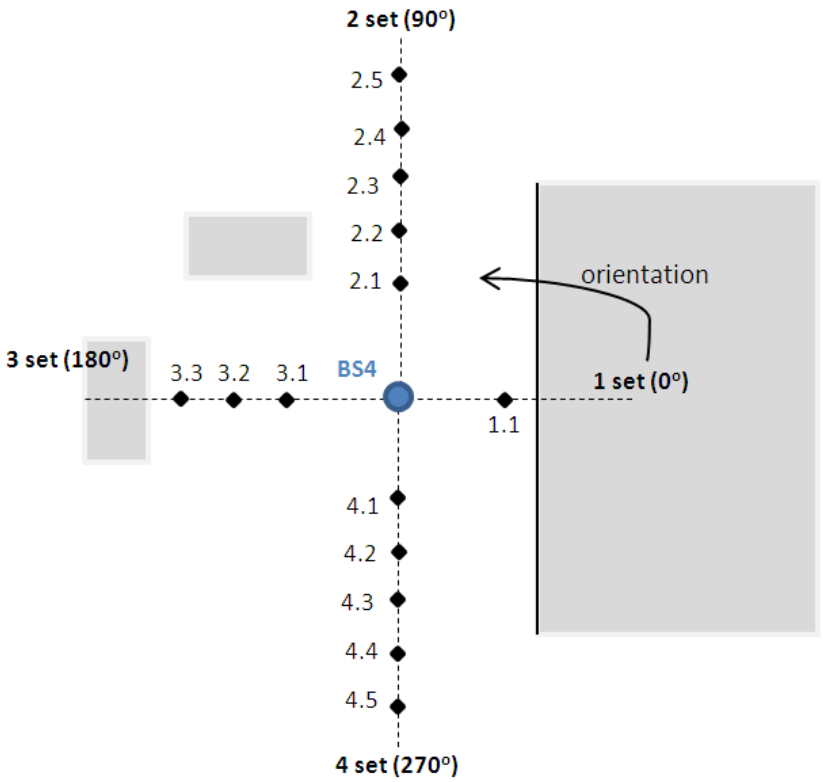

Figure F.6 - Sketch of the BS4 measurement site.

Figure F.7 - Point of view from the area access of the BS4.

F.5 Measurement Data of the BS5

Figure F.9 shows a sketch of the measurement site while a photograph of analysed BS is presented in Figure F8. The data from the measurements and the $R(d)$ obtained from them are presented in Table F.6.

Figure F.8 - Point of view from the area access of the BS5.

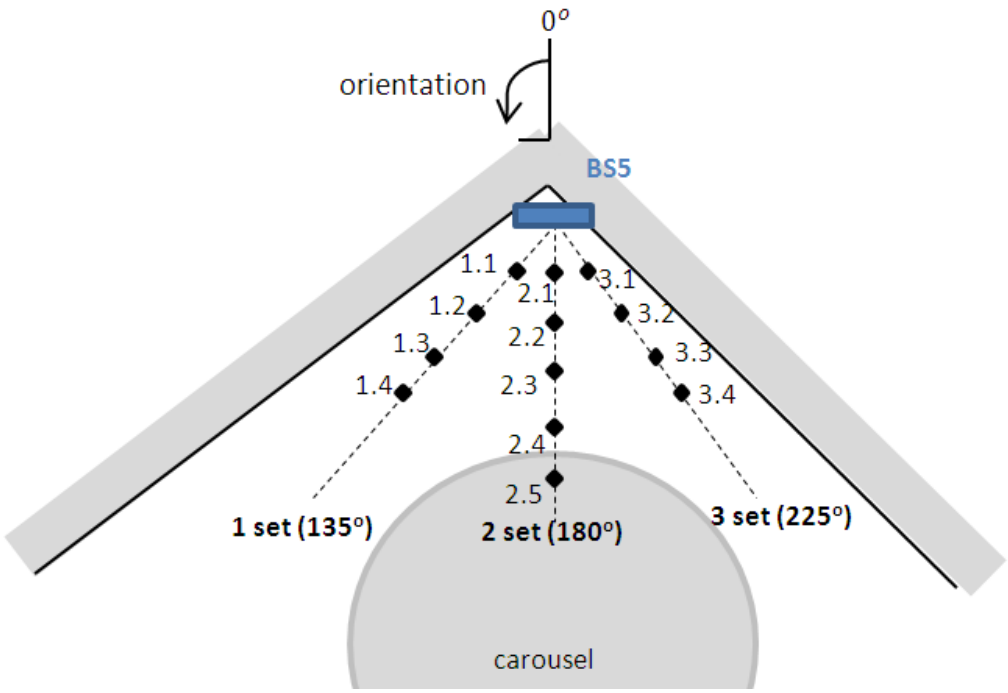

Figure F.9 - Sketch of the BS5 measurement site.

Table F.6 - Results of the BS5 measurements.

Observation Point	Distance [m]	E_{med} [mV/m]						$R(d)$ [$\times 10^{-6}$]
		GSM 900	σ_{GSM}	UMTS	σ_{UMTS}	LTE 1800MHz	σ_{LTE}	
1.1	0.5	20.8	6.1	9.9	1.0	10.2	1.6	3.182
1.2	1.1	25.2	7.5	13.4	1.5	8.8	1.3	4.633
1.3	1.7	33.2	8.8	14.8	1.5	11.0	1.5	7.953
1.4	2.2	24.5	6.8	13.5	1.6	8.7	1.6	4.391
2.1	0.5	24.1	6.3	13.4	1.6	16.3	2.8	4.425
2.2	1.1	54.0	9.3	15.6	1.7	12.0	1.7	20.610
2.3	1.7	53.5	14.6	19.3	2.1	11.3	2.0	20.326
2.4	2.2	39.3	11.3	21.6	2.5	15.6	2.0	11.341
2.5	2.8	45.8	13.6	*				-
3.1	0.5	24.9	7.2	9.13	1.0	8.4	1.9	4.444
3.2	1.1	11.0	3.2	10.0	1.0	7.9	1.3	0.979
3.3	1.7	34.8	10.6	10.9	1.3	5.4	0.8	8.546
3.4	2.2	22.0	6.4	*				-

* The records of measurements were deleted by mistake.

References

[3GPP09a] 3GPP, *Technical Specification Group Radio Access Network; Evolved Universal Terrestrial Radio Access (E-UTRA) and Evolved Universal Terrestrial Radio Access Network (E-UTRAN), Overall description (Release 8)*, Report TS 36.300, V8.10.0, Sep. 2009 (http://www.3gpp.org/ftp/Specs/html-info/36300.htm).

[ABDK02] Altman,Z., Begasse,B., Dale,C., Karwowski,A., Wiart,J., Wong,M.-F. and Gattoufi,L., "Efficient Models for Base Station Antennas for Human Exposure Assessment", *IEEE Transactions on Electromagnetic Compatibility*, Vol. 44, No. 4, Nov. 2002, pp. 588-592.

[ABOM09] Ahmed,M.B, Bouhorma,M., Ouaai,F.E, Mamouni,A., "A new miniaturized patch antenna for wireless systems: GSM, UMTS, HIPERLAN", *2009 IEEE International Conference on Wireless and Mobile Computing, Networking and Communications*, Marrakech, Morocco, Oct. 2009.

[Allg12] Allgon, Power Wave, http://www.powerwave.com /allgon, Fev. 2012.

[ANAC07] ANACOM, "86/2007 Regulation: Procedures for monitoring and measurement of electromagnetic field strength levels originated by radiocommunication stations" (in Portuguese), *Diário da República, Series 2, No. 98*, May 2007, pp. 13650-13659.

[ANAC12] ANACOM, *Final report of auction* (in Portuguese), Ver. 18.01.12, Portugal, Jan. 2012 (http://www.anacom.pt/render.jsp?categoryId=344542).

[Andr12] Andrew, CommScope, http://www.commscope.com/andrew, Fev. 2012.

[Bala05] Balanis,C.A., *Antenna Theory - Analysis and Design*, John Wiley, New Jersey, United States of America, 2005.

[BCDF02] Barbiroli,M., Carciofi,C., Degli-Esposti,V. and Faciasecca,G., "Evaluation of Exposure Levels Generated by Cellular Systems: Methodology and Results", *IEEE Transactions on Vehicular Technology*, Vol. 51, No. 6, Nov. 2002, pp.1322-1329.

[BCFF99] Barbiroli,M., Carciofi,C., Falciasecca,G. and Frullone,M., "Analysis of field strength levels near base station antennas", in *Proc. of VTC'99 - IEEE International Conference on Vehicular Technology*, Houston, Texas, USA, May 1999.

[Bena02] Benabdallah, N., *Technical Specification Group Radio Access Networks - RF System Scenarios (Release 1999)*, 3GPP Technical Specification, No. 25.942, Ver. 3.3.0, June 2002 (http://www.3gpp.org).

[BFHM02] Bergqvist,U., Friedrich,G., Hamnerius,Y., Martens,L., Neubauer,G., Thuroczy,G., Vogel,E. and Wiart,J., *Mobile telecommunication base stations – exposure to electromagnetic field,* Report of a Short Term Mission within COST 244bis, COST 244bis, Europe, 2002 (http://www.elettra2000.it/phocadownload/archivi/docymenti/cost244bis.pdf).

[BiGi99] Bizzi,M. and Gianola,P., "Electromagnetic fields radiated by GSM antennas, Electronic Letters", *Electronic Letters*, Vol. 35, No. 11, May 1999, pp. 855-857.

[Capp01] Capps,C., "Near field or far field?", *Electronics Design Network,* Edition Aug. 16 2001*,* August 2001, pp. 95-102 (http://www.edn.com/article/486198Near_field_or_far_field_.php).

[CENE02] CENELEC, *Basic standard for the calculation and measurement of electromagnetic field strength and SAR related to human exposure from radio base stations and fixed terminal*

stations for wireless telecommunication systems (110 MHz – 40 GHz), Ref. No. EN 50383:2002 E, Central Secretariat, Brussels, Belgium, July 2002.

[CGLM99] Carli,E., Gianola,P., Lombardi,G., Mama,L. and Vescovo,R., "Antenna models for field level evaluation in proximity of GSM Base stations", in *Proc. of EPMCC'99 – 3rd European Personal and Mobile Communications Conference*, Paris, France, Mar. 1999.

[Chen89] Cheng,D.K, *Field and Wave Electromagnetics*, Addison-Wesley, Roseville, Minnesota, United States of America, 1989.

[CoEU04] Council of the European Union, "Corrigendum to Directive 2004/40/EC of the European Parliament and of the Council of 29 April 2004 on the minimum health and safety requirements regarding the exposure of workers to the risks arising from physical agents (electromagnetic fields) (18th individual Directive within the meaning of Article 16(1) of Directive 89/391/EEC)", *Official Journal of the European Communities L 184/1*, Brussels, Belgium, May 2004.

[CoEU99] Council of the European Union, "Council Recommendation of 12 July 1999 on the limitation of exposure of the general public to electromagnetic fields (0 Hz to 300 GHz)", *Official Journal of the European Communities L 199/59*, Brussels, Belgium, July 1999.

[CoFe04] Correia,L.M., Fernandes,C., Carpinteiro,G., Oliveira,C., *A Procedure for Measurement of Electromagnetic Radiation in the Presence of Multiple Base Stations*, monIT Project, Report Ext_Tec_0147_03_COST281Paris, Ver. 3, Instituto de Telecomunicações, Lisbon, Portugal, Aug. 2004.

[Corr12a] Correia,L.M., *Antennas for Bases and Mobiles*, Notes of Mobile Communication Systems, Instituto Superior Técnico, Lisbon, Portugal, 2012.

[Corr12b] Correia,L.M., *Propagation Models*, Notes of Mobile Communication Systems, Instituto Superior Técnico, Lisbon, Portugal, 2012.

[COST00] COST 244 bis, *Biomedical Effects of Electromagnetic Fields*, Final report, COST 244 bis, Nov. 2000.

[ECCC07] Electronic Communications Committee (ECC) European Conference of Postal and Telecommunications Administrations (CEPT), *Measuring Non-Ionizing Electromagnetic Radiation (9 kHz – 300 GHz),* ECC Recommendation (02)04, Edition 060207, Helsinki, Finland, 2007.

[ETSI00] ETSI, *Digital cellular telecommunications system (Phase 2+); Radio transmission and Reception*, ETSI GSM 05.05, European Telecommunications Standards Institute, Sophta-Antipolis, France, Nov. 2000 (http://www.etsi.org).

[ETSI06] ETSI, *User Equipment (BS) radio transmission and reception (FDD)*, Report 3GPP TS 25.101, Ver. 3.19.0 (Release 1999), Dec 2006 (http://www.etsi.org).

[ETSI11a] ETSI, *Base Station (BS) radio transmission and reception (FDD)*, Report 3GPP TS 25.104, Ver. 8.13.0 (Release 8), June 2011 (http://www.etsi.org).

[ETSI11b] ETSI, *User Equipment (BS) radio transmission and reception (FDD)*, Report 3GPP TS 25.101, Ver. 10.3.0 (Release 10), Oct 2011 (http://www.etsi.org).

[Gree90] Green, E., "Radio link design for microcellular systems," *Brit. Telecom Technol. J.*, Vol. 8, No. 1, Jan. 1990, pp. 85–96.

[HoTo04] Holma, H., Toskala, A., *WCDMA FOR UMTS – Radio Access for Third Generation Mobile Communications*, John Wiley, Chichester, United Kingdom, 2004.

[HoTo06] Holma, H., Toskala, A., *HSDPA/HSUPA for UMTS*, John Wiley, Chichester, United Kingdom, 2006.

[HoTo07] Holma,H. and Toskala,A., *WCDMA for UMTS - HSPA Evolution and LTE*, John Wiley, Chichester, United Kingdom, 2007.

[HoTo09] Holma, H., Toskala, A., *LTE for UMTS: OFDMA and SC-FDMA Based Radio Access*, John Wiley, Chichester, United Kingdom, 2009.

[ICNI01] ICNIRP, “Review of the Epidemiologic Literature on EMF and Health”, *Environ Health Perspect*, Vol. 109, Supplement 6, pp. 911-934, Dec. 2001 (http://www.icnirp.de).

[ICNI04] ICNIRP, “Review of the Epidemiology of Health Effects of Radio Frequency Exposure”, *Environmental Health Perspectives*, Vol. 112, Supplement 17, pp. 1741-1754, Dec. 2004 (http://www.icnirp.de).

[ICNI09] ICNIRP, “Statement on the “Guidelines for Limiting Exposure to Time-Varying Electric, Magnetic, and Electromagnetic Fields (up to 300 GHz)””, *Health Physics*, Vol. 97, Supplement 3, pp. 257-258, 2009 (http://www.icnirp.de).

[ICNI11] ICNIRP, “Review of the Mobile Phones, Brain Tumours and the iInterphone Study: Where Are We Now?”, *Environmental Health Perspectives*, Vol. 119, Supplement 11, pp. 1534-1538, July 2011 (http://www.icnirp.de).

[ICNI98] ICNIRP, “Guidelines for Limiting Exposure to Time-Varying Electric, Magnetic, and Electromagnetic Fields (up to 300 GHz)”, *Health Physics Society*, Vol. 74, No. 4, pp. 494-522, 1998 (http://www.icnirp.de).

[IEEE05] IEEE, *C95.1-2005, IEEE Standard for Safety Levels with Respect to Human Exposure to Radio Frequency Electromagnetic Fields, 3 kHz to 300 GHz*, IEEE-SA Standards Board, USA, Apr. 2005.

[JAYB12] Amphenol JAYBEAM, http://www.amphenol-jaybeam.com, Fev. 2012.

[KATH12a] KATHREIN, http://www.kathrein.de, Fev. 2012.

[KATH12b] KATHREIN-Werke KG, *Summary of Technical Information*, 2012 (http://www.kathrein.de/en/mcs/techn-infos/download/technical_information.pdf).

[KATH12c] KATHREIN-Werke KG, *Basic Antenna Principles for Mobile Communications*, 2012 (http://www.kathrein.de/en/mcs/techn-infos/download/basicantenna.pdf).

[Krau88] Kraus,J.D., *Antennas*, McGraw-Hill, New York, United States of America, 1988.

[LeSu09] Lee,Y.C., Sun,J.S., “A New Printed Antenna for Multiband Wireless Applications”, *Antennas and Wireless Propagation Letters, IEEE*, Vol. 8, , May 2009, pp. 402-405.

[MFRL02] Martínez-González,A.M., Fernández-Pascual,A., Reyes,E., Loock,W.V., Gabriel,C. and Sánchez-Hernández,D., “Practical procedure for verification of compliance of digital mobile radio base stations to limitations of exposure of the general public to electromagnetic fields”, *IEE Proceedings Microwaves*, Antennas and Propagation, Vol. 149, No. 4, Aug. 2002, pp. 218-228.

[MNMV02] Martínez-Burdalo,M., Nonídez,L., Martín,A. and Villar,R., “On the calculation of safety distances for human exposure to electromagnetic fields from base-station antennas”, *Microwave and Optical Technology Letters*, Vol. 43, No. 5, Sep. 2002, pp. 364-367.

[Moli11] Molisch, A.F., *Wireless Communications*, John Wiley, Chichester, United Kingdom, 2011.

[More12] Moreira,A.M., *Microstrip Antennas* (in Portuguese), Notes of Antennas, Instituto Superior Técnico, Lisbon, Portugal, 2012.

[MSPS01] Ministère de la Santé et de la Protection Sociale, *Interdepartmental circular of October 16, 2001 relating to radiotelephony mobile antennas* (in French), France, Oct. 2001.

[Nard07] Narda Safety Test Solutions, “SRM-3000 Selective Radiation Meter - Operating Manual”, Narda Safety Test Solutions, Pfullingen, Germany, 2007.

[OFRC05] Oliveira,C., Fernandes,C., Reis,C., Carpinteiro,G., Ferreira,L., Correia,L.M. and Sebastião,D., *Definition of Exclusion Zones around Typical Installations of Base Station Antennas*, monIT Project, Report Int_Tec_0102_15_BSExclZones, Ver. 15, Instituto de Telecomunicações, Lisbon, Portugal, Fev. 2005.

[OlCa02] Oliveira,C.S., Carpinteiro,G., *Electromagnetic radiation exposure of GSM and UMTS Base Station Antennas* (in Portuguese), Final Graduation Project, Instituto Superior Técnico, Technical University of Lisbon, Lisbon, Portugal, 2002.

[Oliv06] Oliveira,C.S., *Estimation of Exclusion Zones for Base Station Antennas in Wireless Communication Systems*, Master D. Thesis, Instituto Superior Técnico, Technical University of Lisbon, Lisbon, Portugal, 2006.

[OPTI11] OPTIMUS, *Results of 4G auction strengthen the optimus bet on mobile data* (in Portuguese), Report 2011_11_30_Press_Release_LTE, Porto, Portugal, Nov. 2011 (http://other.static.sonaecom.pt/mediagallery.clix.pt/2011/11/30/2011_11_30_Press_Release_LTE.vf/2011_11_30_Press_Release_LTE.vf.pdf).

[Opti12] Private Communication, Optimus, 2012.

[OSLA08] Oliveira,C., Sebastião,D., Ladeira,D., Antunes,M., and Correia,L.M., *Report of 5 years of measurements* (in Portuguese), monIT Project, Report monIT_Ext_Tec_0520_02_Rel5anos, Ver. 2, Instituto de Telecomunicações, Lisbon, Portugal, Jan. 2008.

[PaPH12] Paul,D.L., Paterson,M.G., and Hilton,G.,S., "A Low-Profile Textile Antenna for Reception of Digital Television and Wireless Communications", *Radio and Wireless Symposium (RWS), IEEE*, Santa Clara, CA, Apr. 2012.

[Pars92] Parsons, J. D., *The Mobile Radio Propagation Channel*, Pentech, London, 1992.

[RaWh98] Ramsdale,P. and Whetstone,R., *Summary of Oral Evidence presented to IEGMP*, One 2 One, UK, Oct. 1998 (http://www.iegmp.org.uk/evidence/ramsdale.htm).

[RFSy12] RFS, Radio Frequency Systems, http://www.rfsworld.com, June 2012.

[SBCo12] Sebastião,D., Branco,M., and Correia,L.M., *Measures in nearby areas of antennas* (in Portuguese), monIT Project, Report monIT_1084_05_Ext_Tec_ReportNearFields, Ver. 5, Instituto de Telecomunicações, Lisbon, Portugal, Jan. 2012.

[Sche43] Schelkunoff,S.A., *Electromagnetic Waves*, D. van Nostrand, New York, New York, USA, 1943.

[STAT09] Statistics Portugal (INE), "Construction and Housing Statistics 2009" (in Portuguese), Statistics Portugal (INE), Lisbon, Portugal, 2010.

[STAT10] Statistics Portugal (INE), "Construction and Housing Statistics 2010" (in Portuguese), Statistics Portugal (INE), Lisbon, Portugal, 2011.

[StuT98] Stutzman,W.L. and Thiele,G.A., *Antenna Theory and Design*, John Wiley, Maryland, United States of America, 1998.

[Tuan10] Tuan,T.M., "Design Dual Band Microstrip Antenna For Next Generation Mobile Communication", *The 2010 International Conference on Advanced Technologies for Communications*, Ho Chi Minh City, Vietnam, Oct. 2010.

[Vile12] Vilela, J., "Small Cells and Heterogeneous Networks", *19th of June 2012 –IEEE ComSoc Portugal Chapter and Instituto Superior Técnico Seminar*, Instituto Superior Técnico, Technical University of Lisbon, Lisbon, Portugal, June 2012 (http://chapters.comsoc.org/Portugal/).

[WaSe03] Walke, B., Seidenberg, P., Althoff, M.P., *The UMTS: The Fundamentals*, John Wiley, Chichester, United Kingdom, 2003.

[WoHO02] World Health Organization (WHO), *Establishing a dialogue on risks from electromagnetic fields* , Radiation and Environmental Health, Department of Protection of the Human Environment, WHO, Geneva, Switzerland 2002.